Reviews in Mineralogy & Geochemistry
Vol. 89 pp. 1-51, 2023

Recent Exploration of the Moon: Science from Lunar Missions Since 2006

Lisa R. Gaddis[*,1], Katherine H. Joy[2], Ben J. Bussey[3], James D. Carpenter[4], Ian A. Crawford[5], Richard C. Elphic[6], Jasper S. Halekas[7], Samuel J. Lawrence[8], Long Xiao[9]

[1]Lunar and Planetary Institute, 3600 Bay Area Boulevard
Houston, Texas, 77058, USA
lgaddis@lpi.usra.edu

[2]Department of Earth and Environmental Sciences, University of Manchester
Oxford Road, Manchester, M13 9PL, UK
katherine.joy@manchester.ac.uk

[3]The Johns Hopkins Applied Physics Laboratory, 11100 Johns Hopkins Road
Laurel, Maryland, 20723, USA
ben.bussey@jhuapl.edu

[4]European Space Agency, European Space Research and Technology Centre
Keplerlaan 1, Postbus 299, 2200 AG Noordwijk, The Netherlands
james.carpenter@esa.int

[5]Dept. of Earth and Planetary Sciences, Birkbeck, University of London
Malet St, Bloomsbury, London, WC1E 7HX, UK
i.crawford@ucl.ac.uk

[6]NASA Ames Research Center, Planetary Systems Branch, Code SST
Moffett Field, Mountain View, California, 94043, USA
richard.c.elphic@nasa.gov

[7]Dept. Physics and Astronomy, 414 Van Allen Hall, University of Iowa
Iowa City, Iowa, 52242, USA
jasper-halekas@uiowa.edu

[8]NASA Lyndon B. Johnson Space Center, Mail Code XI3, 2101 NASA Parkway
Houston, Texas, 77058, USA
samuel.j.lawrence@nasa.gov

[9]China University of Geosciences, Planetary Science Institute
388 Lumo Road, Wuhan, Hubei, 430074, People's Republic of China
longxiao@cug.edu.cn

1529-6466/23/0089-0001$10.00 (print)
1943-2666/23/0089-0001$10.00 (online)
http://dx.doi.org/10.2138/rmg.2023.89.01

1. INTRODUCTION

Exploration of the Moon has been a goal of humankind for millennia, and in recent decades enormous advances in lunar knowledge have resulted from orbital, landed, robotic, and human exploration and sample return (Spudis 2001; National Research Council 2007; Jaumann et al. 2012; Crawford and Joy 2014; Lunar Exploration Analysis Group 2016a). The Moon still retains the marks of human footprints, and these and other artifacts can now be seen with amazing clarity in images returned from the NASA Lunar Reconnaissance Orbiter Cameras (LROC; Robinson et al. 2010). The six U.S. Apollo missions to the Moon, from 1969 to 1972, mark the first and only time thus far that humans have walked and driven upon another planetary body. These missions returned ~382 kg of lunar samples (Vaniman et al. 1991), along with ~0.3 kg of regolith from three Soviet Luna missions (16, 20, and 24), and these have been augmented by recognition of a significant volume of lunar samples in the terrestrial meteorite collection. Humankind has now mapped the lunar surface in high detail (e.g., ~50 cm/pixel, LROC) and at a variety of wavelengths, including measurements of subsurface and interior properties. Analyses of new datasets from missions and lunar samples in this century have transformed our view of the Moon with regard to the chronology of formation and differentiation, tectonic and geochemical processes, the exosphere, radiation environment, volatile reservoirs, and potential resources. Studies of lunar datasets have shown, for example, that the collection of Apollo and meteorite samples are not representative of all lithologies on the Moon (see also Elardo et al. 2023; Hiesinger et al. 2023, both this volume), that the crust is thinner than our view immediately following Apollo (see Andrews-Hanna et al. 2023; Wieczorek et al. 2023, both this volume), and that there are volatile cycles that follow various periodicities (see Hurley et al. 2023, this volume).

Since the publication of two seminal books on lunar science, *The Lunar Sourcebook, A User's Guide to the Moon* (Heiken et al. 1991) and especially the first *New Views of the Moon* volume (Jolliff et al. 2006), there have been 13 science-focused missions to the Moon. Each of these missions explored different aspects of the Moon's geology, environment, and resource potential. Lunar science has greatly advanced because of international (USA, Europe, Japan, India, China) missions to the Moon. Analyses of data from these new missions, coupled with lunar and meteorite sample analysis using new tools and methods, revealed many undiscovered characteristics of the Moon not even imagined just a few years earlier. These discoveries range from phenomenally low temperatures in permanently shadowed regions (PSRs) at lunar poles, ephemeral surface volatile reservoirs both inside and outside PSRs (see Hurley et al. 2023, this volume), new crustal lithologies and processes (see Andrews-Hanna et al. 2023; Plescia et al. 2023, both this volume), endogenous lunar volatile reservoirs (see McCubbin et al. 2023, this volume), relatively recent dynamic processes (see Gaffney et al. 2023; Shearer et al. 2023, both this volume), and the potential for the elusive lunar mantle to reside near or at the surface.

This chapter introduces the planetary community to the array of missions that have explored the Moon in the years since 2006. Because other chapters in this volume will address the discoveries and results of these missions, we focus here on a short summary of science goals for each mission and a description of instruments and their capabilities.

2. HISTORIC LUNAR MISSIONS

A summary of the most important spacecraft to have visited the Moon before 2006 is listed in Table 1. A brief summary of the objectives and major accomplishments is provided below.

Table 1. Historic lunar missions as described by the US National Space Science Data Center

Mission	Origin	Launch Year	Objectives
Luna 2, 3	USSR	1959	First lunar impact; Lunar flyby, first far side images
Ranger 4, 6 to 9	USA	1962–1965	Descent images to lunar surface, impact
Zond 4, 5 to 8	USSR	1965–1970	Lunar flyby & circumlunar, second far side images, surface mapping
Luna 9 to 13	USSR	1966	First soft lander, surface images
Surveyor 1, 3, 5 to 7	USA	1966–1968	Soft landers, surface properties
Lunar Orbiter 1 to 5	USA	1966–1967	Orbiters, surface images, near-global mapping
Apollo 8, 10	USA	1968, 1969	Crewed lunar orbiters, surface images
Luna 14	USSR	1968	Lunar orbiter, lunar geophysical measurements
Apollo 11, 12, 14 to 17	USA	1969–1972	Crewed landings, surface mapping, soil and surface properties, subsurface measurements, gravity mapping, sample return
Lunokhod 1, 2 (Luna 17, 21)	USSR	1970, 1973	Surface rovers, surface properties
Luna 16, 20, 24	USSR	1970, 1972, 1976	Surface rovers, sample return
Galileo	USA	1989	Orbiter, surface remote sensing, first color mapping
Hiten (Muses-A)	Japan	1990	Lunar orbiter with satellite Hagoromo
Clementine	USA	1994	Orbiter, surface remote sensing, global mapping
Lunar Prospector	USA	1998	Orbiter, surface remote sensing, global mapping
Small Missions for Advanced Research in Technology (SMART-1)	Europe	2003	Orbiter, surface remote sensing, global mapping, south polar imaging

2.1. Early lunar missions (1959–1972): Luna, Zond, Ranger, Surveyor, Apollo

The first spacecraft to reach the Moon was the Soviet ***Luna 2***, which impacted the lunar surface on 12th September 1959. ***Luna 3***, in October 1959, completed a flyby of the Moon and obtained the first images of the far side. These first observations were very low resolution but sufficient to show that the surface of the far side is different to that of the near side, with extensive cratering and few of the large, dark expanses of basaltic lava that dominate the latter. In 1966, two more successful Soviet space probes were launched: on February 3, ***Luna 9*** successfully soft-landed on the Moon and obtained the first surface images, and on April 3, ***Luna 10*** became the first spacecraft to enter lunar orbit.

The U.S. lunar exploration program then began, initially with the ***Ranger*** series (1962–1965) of 'hard landers' and followed by the ***Surveyor*** program (1966–1968), which soft-landed five static robotic landers on the lunar surface to investigate regolith properties and composition. Then between 1966 and 1967, the US flew the highly successful series of ***Lunar Orbiter*** spacecraft that obtained near-global coverage and high-resolution images of the lunar surface to identify potential landing sites for the future Apollo missions. In parallel, the Soviet Union flew the Mars-bound ***Zond 3*** (1965) past the Moon, and ***Zond 4*** (1968) through ***Zond 8*** (1970) as un-crewed lunar flyby and Earth return missions.

The Soviet robotic program included two 'Lunokhod' rovers (***Luna 17 and 21***) that landed on the Moon in November 1970 and January 1973, respectively. These were the first

tele-operated robotic rovers to operate on another planetary body. ***Lunokhod 1*** operated for 322 days and traversed a total distance of 10.5 km, while ***Lunokhod 2*** operated for 115 days and drove 37 km. The Lunokhods made traverse measurements of regolith properties and composition, as well as the surface radiation environment. They also carried laser reflector panels which, similar to those deployed by the Apollo 11, 14 and 15 missions, have been used to measure the Earth–Moon distance and the Moon's physical librations (from which internal structure can be inferred). [Note: ***Lunokhod 1*** was effectively "lost" for laser ranging as its final resting location was poorly documented. The camera on the Lunar Reconnaissance Orbiter accurately located the rover in 2010 (Murphy et al. 2011).] Three successful Soviet robotic sample return missions also occurred during this time: ***Luna 16*** (1970), ***Luna 20*** (1972), and ***Luna 24*** (1976). These collected and returned to Earth a total of 320 g from three sites near the eastern limb of the lunar near side. The geographical separation of these samples from the Apollo landing sites makes them important for our understanding of lunar geological diversity and the calibration of remote sensing measurements.

The height of early lunar exploration culminated with the U.S. first human landing on the Moon at Mare Tranquillitatis with ***Apollo 11*** in July 1969. Another five Apollo crewed missions visited the southeast Oceanus Procellarum (***Apollo 12***, Nov. 1969), the Fra Mauro region (***Apollo 14***, Feb. 1971), Hadley Rille region to the east of Mare Imbrium (***Apollo 15***, July 1971), the Descartes-Cayley highlands (***Apollo 16***, April 1972), and the Taurus-Littrow valley to the southeast of Mare Serenitatis (***Apollo 17***, Dec. 1972) (Fig. 1). In addition to returning ~382 kg of lunar rock and soil sampled from over 2000 localities, the Apollo missions acquired orbital photography and mapping at X-ray and gamma-ray wavelengths for surface mapping of geochemistry and composition. An array of Apollo Lunar Surface Experiment Packages (ALSEPs) also was deployed by Apollo astronauts, for geophysics, heat flow measurements, and atmosphere and ionosphere experiments (see Table 2 of Crawford and Joy 2014 for a full list). The Apollo program and its scientific achievements has been documented in the "Apollo Lunar Surface Journal" (Jones and Glover 2017), discussed in many earlier reviews (Taylor 1975; Heiken et al. 1991; Jolliff et al. 2006; Crawford and Joy 2014), and aspects are described within other chapters of this volume.

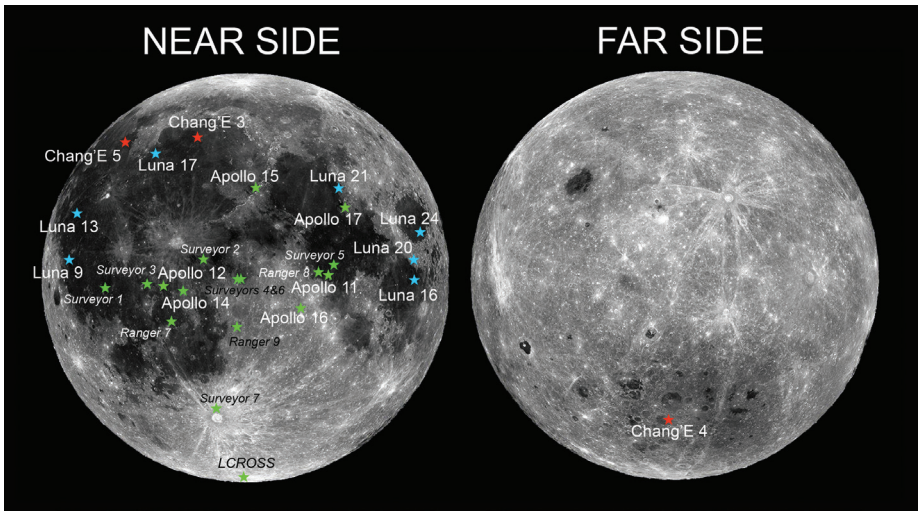

Figure 1. The Moon's near and far side hemispheres as viewed by NASA's Lunar Reconnaissance Orbiter Cameras (LROC) Wide Angle Camera (WAC; NASA/GSFC/ASU). The locations of international landed or intentionally crashed (in **italics**) exploration missions are marked with **stars** on this WAC mosaic (USA in **green**, Soviet Union in **blue**, China in **red**). Accidental crash sites are not shown.

2.2. Later lunar missions (1989–2003): Galileo, Hiten, Clementine, Lunar Prospector, SMART-1

The nearly twenty-year gap in lunar exploration was broken in the 1990's when the Galileo, Hiten, Clementine and Lunar Prospector spacecraft flew by or to the Moon and began an era of renewed lunar exploration (Crawford and Joy 2014). The U.S. ***Galileo*** mission orbited Jupiter for eight years, and on the way obtained the first detailed color images of the lunar far side using a solid-state imaging camera (SSI, 0.375–1.1 microns; Belton et al. 1992a) and a near-infrared mapping spectrometer (NIMS) (0.7–5.2 microns; Carlson et al. 1992). Additional instruments included an ultraviolet spectrometer (UVS), photopolarimeter radiometer, magnetometer, energetic particles detector, plasma investigation, plasma wave subsystem, dust detector, and heavy ion counter (Russell 1992). Galileo mission results included a series of color mosaics (1.1 to ~5 km/pixel) that highlighted both very mature and fresh lunar soils at craters (McEwen et al. 1993), the iron-rich compositions of the lunar maria (Greeley et al. 1993), and the huge extent of the South Pole–Aitken basin on the far side (Belton et al. 1992b).

The Japanese ***Hiten*** mission, known before launch as MUSES-A, launched in 1990 and entered into lunar orbit in 1992 to measure the ambient dust density using the Munich Dust Counter (Uesugi 1993). After successful swing by with cis-lunar aerobraking, Hiten impacted the lunar surface. The Hiten satellite carried a small probe called Hagoromo, designed to enter lunar orbit. Although transmission from the probe was lost, the fact that it reached lunar orbit was confirmed by visual inspection from Earth. The Hiten–Hagoromo mission became the first non-U.S. or Soviet mission to enter lunar orbit.

The U.S. ***Clementine*** mission was launched on 25th January 1994, and lunar mapping occurred in two parts: the first month-long part had a 5-hour elliptical polar orbit with a periapse of about 400 km at 28° S latitude; during the second month, the orbit was rotated to a periapse of 29° N latitude. Clementine was designed to enter lunar orbit, map the Moon's surface, and then travel to a near-Earth asteroid (Nozette 1994). The spacecraft successfully completed two months of lunar mapping, but upon leaving lunar orbit on 3rd May 1994, a software failure resulted in the firing of the altitude-control thrusters, causing the spacecraft to spin uncontrollably (Sorensen and Spudis 2005). Although the further mission was abandoned and Clementine did not rendezvous with its asteroid target, the global color lunar mapping was considered a great success. Clementine carried a suite of instruments designed to investigate the mineralogy and topography of surface soils and rocks. There was a multispectral camera operating in the ultraviolet-visible (5-band UV-VIS, 0.415, 0.75, 0.90, 0.95 and 1.0 microns) and another in the near-infrared (6-band NIR, 1.1, 1.25, 1.5, 2.0, 2.6 and 2.78 microns) spectral ranges. With over 2.8 million images of the Moon acquired, near-global multi-spectral mapping was completed at an average resolution of 100 m/pixel (UV-VIS) and 200 m/pixel (near-IR, NIR). Long-wave-infrared (LWIR, 1.5-micron band centered at 8.75 micron, 55 m/pixel at the equator, 200 m/pixel near the poles; Lawson et al. 2000) and high-resolution (HiRes, 0.415, 0.56, 0.65, 0.75 microns and broadband 0.4–0.80 microns, 13–30 m/pixel) cameras also obtained significant imaging data. A laser ranging detector system mapped lunar topography from about −75° to +75° latitude (Spudis et al. 1994).

The global Clementine color mapping provided the first hemispheric views of lunar rock types, and studies showed that the Moon's crust is complex and diverse, with evidence for heavy early bombardment, large basin formation, and extensive periods of mare basalt flooding (e.g., McEwen and Robinson 1997; Jolliff et al. 2000; Rajmon and Spudis 2004). Lucey et al. (1994, 1995, 1998, 2000, 2006) presented a method for using the UVVIS data to determine the concentration of iron in the lunar surface using empirical calibrations of the relationship between sample maturity, FeO wt% concentration and spectral reflectance ratios, using ground truths from the Apollo landing sites. Global maps of FeO wt% abundance and other surface

properties allowed us to study in detail the geology of Apollo landing sites and their regional contexts (Robinson and Jolliff 2002; Lucey 2004), and characterize the history of the lunar far side (e.g., Gillis and Spudis 2000). The relationship between UV/VIS color ratios and the Ti content of silicate minerals, glasses and opaque phases (Hapke et al. 1975) was also exploited and used to produce maps of lunar Ti content (Blewett et al. 1997; Lucey et al. 1998, 2000).

The Clementine laser altimeter successfully mapped lunar topography at a resolution of 1–2 km along track with 40 m height resolution (Smith et al. 1997). This was the first accurate lunar topographic map to be obtained and, among other things, it revealed the true extent of many lunar craters and basins, including the giant (~2400 × 2000 km diameter and ~13 km deep) far-side South Pole–Aitken basin (Spudis et al. 1994). Clementine also viewed the lunar poles in detail, and studies showed that there were both permanently shadowed regions (Nozette et al. 2001) and also regions of near-permanent illumination (Bussey et al. 1999). The Clementine bi-static radar experiment aimed radio signals at the lunar surface, which were reflected and collected back on Earth by ground-based radio telescopes. Scattered reflections from the lunar poles suggested the presence of icy materials within some permanently shadowed craters (Nozette et al. 2001).

The NASA ***Lunar Prospector*** (LP) mission was launched on 7th January 1998, and orbited the Moon for a year in a polar orbit at an altitude of 100 km before being dropped into two lower orbits of 30 km and 10 km. The satellite was crashed into a south polar crater in a controlled experiment on 31st July 1999 in an attempt to see if ejected material was ice-rich (Goldstein et al. 1999), although the results were inconclusive. Lunar Prospector carried five experiments (Binder 1998), including a Gamma Ray Spectrometer (GRS), a Neutron Spectrometer (NS), a Magnetometer, an Electron Reflectometer, and an Alpha Particle Spectrometer (damaged at launch); Earth-based spacecraft tracking also provided gravity data.

The Lunar Prospector Gamma Ray Spectrometer detected gamma rays emitted from the top meter of the lunar surface. Gamma ray production is initiated by the interaction of galactic cosmic rays (GCR) colliding with a planetary surface or from the decay of naturally occurring radioactive elements. LP gamma ray spectra were used to map the abundance of major elements (O, Mg, Al, Si, Ca, Ti and Fe) and radioactive elements (K, Th and U) across the lunar surface at variable spatial resolutions (0.5° to 20° per pixel) (Lawrence et al. 1998, 1999, 2000, 2002, 2003, 2004; Feldman et al. 1999; Prettyman et al. 2002, 2006; Gillis et al. 2004) (see Electronic Annex [EA] 1-1). In particular, the Th distribution showed that the north-west nearside of the Moon around the Imbrium Basin is compositionally unusual, with an enhanced abundance of Th and other incompatible trace elements. This region was dubbed the Procellarum KREEP Terrane (PKT) (Jolliff et al. 2000) (see EA-1-2). As KREEP is the dominant carrier of radioactive elements, this suggests that a large portion of the Moon's heat-producing elements may be concentrated in this region of the Moon (Wieczorek and Phillips 2000).

The Lunar Prospector Magnetometer made detailed investigations of lunar crustal remanent magnetization (Lin et al. 1998), confirming the presence of isolated magnetic anomalies discovered by earlier missions, and suggesting a relationship between large near side basins and magnetized antipodal materials (Hood et al. 2001). Combined with electron reflectometer measurements, these observations indicate that lunar crustal magnetic anomalies create mini-magnetospheres that give some protection to the underlying surface from the solar wind (see Gaffney et al. 2023, this volume).

The Lunar Prospector Neutron Spectrometer provided independent evidence for ice at the lunar poles (Feldman et al. 2001). Neutrons are produced by cosmic ray interaction with nuclei in the top few meters of regolith. Neutrons encountering significant hydrogen concentrations will be moderated; the leakage flux of epithermal neutrons in particular will be reduced. Such a signal was observed by Lunar Prospector and interpreted to provide evidence of near-surface

hydrogen, inferred to support the Clementine bi-static radar results that water ice may be present at the lunar poles. However, the data lacked sufficient spatial resolution to confirm that the areas of attenuated neutron flux correspond to permanently shadowed craters, and it is still an area of active debate whether these regions represent water ice or concentrations of hydrogen from solar wind implantation (see Hurley et al. 2023, this volume).

The European Space Agency's (ESA) Small Missions for Advanced Research in Technology-1 (***SMART-1***) mission launched on the 27th September 2003 (Foing et al. 2001). The mission used an innovative solar-electric propulsion (ion) drive to travel to the Moon, arriving in an operational elliptical lunar orbit (~300 km periapse, ~3000 km apoapse; Foing et al. 2006) on 15th November 2004. SMART-1 spent almost two years orbiting the Moon before being crashed onto its surface on 3rd September 2006, when it impacted into Lacus Excellentiae (34.262° S, 46.193° W; Stooke and Foing 2017) on the near side. SMART-1 was primarily a technology demonstration mission for solar electric propulsion in deep space. Science goals were secondary, and instrument selection was driven primarily by various instrument technology demonstration objectives. The spacecraft carried seven miniaturized technology demonstration instruments, including the Advanced Moon micro-Imager Experiment (AMIE) camera that obtained intermediate-resolution images of the lunar surface (about 250 m/pixel globally, but better than 50 m/pixel at periapse). The highest resolution images were of the south polar region and these proved to be valuable in mapping surface mineralogy in the South Pole–Aitken basin (Borst et al. 2012) and the changing illumination conditions at the pole over the course of nearly two years. SMART-1 also carried two instruments designed to investigate the chemical and mineralogical composition of the lunar surface. These were the SMART-1 Infrared Spectrometer (SIR, 0.9–2.4 microns, 300 m/pixel) (Basilevsky et al. 2004) and Demonstration of a Compact X-ray Spectrometer (D-CIXS) (Grande et al. 2007) for mineralogical and chemical mapping of the Moon. Major results of the latter instrument included a measurement of Ti concentration in lunar soils (Swinyard et al. 2009), and although discrepancies existed between these and earlier results from Clementine and Lunar Prospector, lessons learned from this instrument later were applied to the X-Ray Spectrometer on Chandrayaan-1 (C1XS; see below).

2.3. New results from older lunar data

Several avenues of research using data returned from lunar missions have proven very fruitful since 2006, and many of these are outlined in a study report on Advancing Science of the Moon (Lunar Exploration Analysis Group 2018a). For example, the Apollo seismic data remain the only direct source of information about the thickness of the lunar crust. Several recent studies have addressed the earlier uncertainties in measured seismic arrival times from the Apollo data, and also in quantifying the effects of scatter in those data (Lognonné et al. 2009; Blanchette-Guertin et al. 2012; Gillet et al. 2017). A recent reanalysis of seismic data from the Apollo 17 Lunar Seismic Profiling Experiment have resulted in a refinement of the subsurface structure at this landing site (Heffels et al. 2017). Use of laser ranging data from Apollo retroflectors continues, and these data suggest the lunar core is liquid (e.g., Barkin et al. 2014; Williams and Boggs 2015) and the deep mantle is at least partially molten (Harada et al. 2014), although combining more recent gravity, topography and laser ranging data to model the deep interior of the Moon (Matsuyama et al. 2016) results in a solid inner and fluid outer core with total core size akin to the core modeled using Apollo seismic data (Weber et al. 2011; Andrews-Hanna et al. 2023, this volume). Paleomagnetic studies of Apollo samples have demonstrated that the Moon had surface magnetic fields of ~30–100 μT between at least 4.2 and 3.56 Ga (Weiss and Tikoo 2014; Garrick-Bethell et al. 2017), possibly from an ancient core dynamo (see Wieczorek et al. 2023, this volume).

Analysis of Apollo samples with more modern methods since 2008 has revealed the presence of water and other magmatic volatiles in pyroclastic glasses and apatite minerals from several landing sites (Saal et al. 2008; Hauri et al. 2011, 2015, 2017; McCubbin et al.

2011, 2015; Tartèse et al. 2013; Anand et al. 2014), and these have completely revised our understanding of the formerly anhydrous Moon and its geologic history (see McCubbin et al. 2023 and Crawford et al. 2023, both this volume).

3. LUNAR MISSIONS SINCE 2006

The last 14 years have seen **13** additional missions to the Moon (Table 2), and a variety of advanced instrumentation and methodologies have been brought to bear on different aspects of the Moon's geology, geophysics, environment, and resource potential. Launched between 2007 and 2009, the China National Space Administration (CNSA) began the ***Chang'E*** spacecraft series (Zheng et al. 2008a), Japanese Space Agency's (JAXA) SELenological and ENgineering Explorer (SELENE) or ***Kaguya*** mission (Kato et al. 2008, 2010), the Indian ***Chandrayaan-1*** mission (Goswami et al. 2006; Pieters et al. 2009a), the U.S. ***Lunar Reconnaissance Orbiter*** (LRO) mission (Chin et al. 2007), and the U.S. ***Lunar Crater Observation and Sensing Satellite*** (LCROSS) mission (Ennico et al. 2012) carried instruments to map and characterize the Moon, its evolution, and its environment. These missions were later complemented by the U.S. ***Gravity Recovery and Interior Laboratory*** (GRAIL) mission (Zuber et al. 2013a), designed to map the gravity field of the Moon, and the ***Lunar Atmosphere and Dust Environment***

Table 2. Recent lunar missions as described by the US National Space Science Data Center.

Mission	Origin	Launch Date	Objectives
SELENE/Kaguya	Japan	14/09/2007	Orbiter, surface remote sensing, global mapping
Chang'E 1	China	24/10/2007	Orbiter, surface remote sensing, global mapping
Chandrayaan-1	India	22/10/2008	Orbiter, surface remote sensing, global mapping
Lunar Reconnaissance Orbiter	USA	18/06/2009	Orbiter, surface remote sensing, global mapping
Lunar Crater Observation and Sensing Satellite (LCROSS)	USA	18/06/2009	Impactor, subsurface probe, polar volatile detection
Chang'E 2	China	01/10/2010	Orbiter, surface remote sensing, global mapping
Acceleration, Reconnection, Turbulence and Electrodynamics of Moon's Interaction with the Sun (ARTEMIS)	USA	17/02/2007 (reprogrammed 01/01/2009)	Two orbiters, solar wind measurements (far and near)
Gravity Recovery and Interior Laboratory (GRAIL)	USA	10/09/2011	Orbiter, gravity mapping
Lunar Atmosphere and Dust Environment Explorer (LADEE)	USA	06/09/2013	Orbiter, exospheric gas and dust measurements
Chang'E 3	China	02/12/2013	Soft lander with rover, global mapping
Chang'E 4	China	07/12/2018	Soft lander with rover, surface and subsurface properties; Lunar far side
Beresheet	Israel	21/02/2019	Soft lander, magnetic field measurement, laser retroreflector, digital time capsule
Chandrayaan-2	India	22/07/2019	Orbiter, soft lander, rover; south pole region
Chang'E 5	China	24/11/2020	Sample Return: Mons Rümker, Oceanus Procellarum

Explorer (LADEE) mission (Elphic et al. 2014), designed to characterize the lunar exosphere and dust environment. Science highlights of these missions include the discovery of both long-lived far side (Haruyama et al. 2009a) and possibly recent volcanism (Braden et al. 2014), the discovery of lunar water and hydroxyl (Pieters et al. 2009b; Sunshine et al. 2009) (see EA-1-3) and, building upon Apollo observations (Hörz 1986; Coombs and Hawke 1992), new lava tubes and skylights have been found that might serve as future habitats (Haruyama et al. 2009b; Robinson et al. 2012; Wagner and Robinson 2014), evidence for a lunar dynamo (Harada et al. 2014) and new lunar rock types (e.g., Pieters et al. 2011), and high-precision measurements of the topography of the Moon (Smith et al. 2010a,b). In addition, LADEE results include discovery of an asymmetric dust cloud around the Moon (Horányi et al. 2015) and a map of the lunar exosphere (Benna et al. 2015a,b; Halekas et al. 2015). Finally, GRAIL revolutionized our knowledge of the lunar interior with its high-quality mapping of the lunar gravitational field (Zuber et al. 2013b). The combination and cross-validation of data from these various missions has enabled new lunar science (Besse et al. 2013a,b; Pieters et al. 2013; Wieczorek et al. 2013; Barker et al. 2016), and the discovery of new rock types not represented in the current sample collections (Pieters et al. 2011; Ohtake et al. 2013).

As outlined below, significant advances in lunar science have been made because of the capabilities of and data returned from these international (U.S.A., China, Europe, India, Japan) missions to the Moon. For example, in 2007 the CNSA launched the first of the successful ***Chang'E*** series of spacecraft, starting with orbital reconnaissance and including surface landing, imaging and roving (e.g., Huang et al. 2018; Jia et al. 2018). During the writing of this chapter, the ***Chang'E-5*** spacecraft landed at 43.06° N, 51.92° W, about 170 km east-northeast of Mons Rümker, a location selected because it was expected to host basalt lavas younger than those return by the Apollo and Luna missions. Analyses of basalt fragments yielded Pb–Pb ages of 1963 ± 57 million years (Che et al. 2021) and 2,030 ± 4 million years (Li et al. 2021). Interestingly, there is no evidence for high concentrations of heat-producing elements in the deep mantle of the Moon that generated these lavas. Work continues on these new lunar samples.

3.1. SELENE/Kaguya

The SELENE mission, nicknamed ***Kaguya***, launched on September 14, 2007, consisted of three spacecraft: one main satellite and two small sub-satellites. The main satellite carried a total of 11 science instruments, augmented by a radio science experiment and a high-definition camera for public outreach (Kato et al. 2010). The instruments (Table 3) included X-ray and gamma-ray spectrometers, a multi-band imager, a spectral profiler, a terrain camera, a lunar radar sounder, a laser altimeter, a magnetometer, a charged particle spectrometer and a plasma analyzer and plasma imager. The sub-satellites were part of the gravity experiment. The instruments on the main satellite were designed to address several areas of study: the elemental distribution, mineralogical distribution, the topography of the lunar surface and subsurface structure, and the plasma environment (Kato et al. 2008).

Kaguya's primary mission lasted from October 20, 2007 until October 31, 2008, and the extended mission lasted from November 1, 2008 until the controlled crash of the main satellite on the lunar surface on June 10, 2009 (Kato et al. 2010). The average altitude during the primary mission was kept at 100 km and it was lowered to an average of 50 km during the extended mission (Araki et al. 2013). In June 2009, the Kaguya spacecraft was put into orbits as low as 8 km to perform more science and engineering measurements (e.g., for magnetic observations, Tsunakawa et al. 2015) (see EA-1-4), and the spatial resolution of data from instruments such as the TC improved from 20 to 5 m/pixel. Due to the use of improved gravity field data from GRAIL and the availability of multiple tracking data types (such as radio links and LALT altimetric crossovers), the derived orbits for Kaguya during the primary mission have a precision of 10–30 m and these have been improved further (Goossens et al. 2011, 2018), along with those for the extended mission data (Goossens et al. 2019).

Table 3. Kaguya science instruments (after Kato et al. 2008).

Instrument	Spatial Resolution	Measurements & Capabilities
Multiband Imager (MI)	20–60 m/pixel	UV–VIS–NIR CCD & InGaAs imager, spectral bandwidth from 0.4 to 1.6 microns, 9 bands at 0.415, 0.75, 0.90, 0.95, 1.0 microns (UVVIS) and 1.0, 1.05, 1.10, 1.25 microns (NIR), spectral resolution 20–30 nm
Terrain Camera (TC)	10 m/pixel	High resolution stereo camera, monochrome (430–850 nm)
Spectral Profiler (SP)	500 m/pixel	Continuous spectral profile ranging from 0.5 to 2.6 microns, spectral resolution 6–8 nm
Laser Altimeter (LALT)	1400 m	Nd:YAG laser altimeter, 100 mJ output power, height resolution 5 m, pulse rate 1Hz, Beam divergence 3 mrad
X-ray Spectrometer (XRS)	20 km	Global mapping of Al, Si, Mg, Fe distribution using 100 cm2 CCD, Energy range 0.7–8 keV, 5 micron Be film, Solar X-ray monitor
Gamma-ray Spectrometer (GRS)	160 km	Global mapping of U, Th, K, major elements distribution using 250 cm^2 large pure Ge crystal, Energy range 0.1–10 MeV
Lunar Radar Sounder (LRS)	~	Mapping of subsurface structure using active sounding, frequency 5 MHz, echo observation range 5 km, detection of radio waves (10k–30MHz) from the Sun, the Earth, Jupiter and other planets; 150 m range resolution
Differential VLBI Radio Source (VRAD)	~	Differential VLBI observation from ground stations, selenodesy and gravitational field, onboard two sub-satellites, 3 S-bands and 1 X-band
Relay Satellite Transponder (RSAT)	~	Far side gravimetry using 4-way range rate measurement from ground station to orbiter via relay satellite, periapse 100 km, apoapse 2400 km in altitude, Doppler accuracy 1 mm/s
Lunar Magnetometer (LMAG)	~	Magnetic field measurement using flux-gate magnetometer, accuracy 0.5 nT
Charged Particle Spectrometer (CPS)	~	Measurement of high-energy particles, 1–14 MeV(LPD), 2–240 MeV(HID), alpha particle detector, 4–6.5 MeV
Plasma Analyzer (PACE)	~	Charged particle energy, angle and composition measurement, 5 eV/q–28 keV/q
Radio Science (RS)	~	Detection of the tenuous lunar ionosphere using S- and X-band carriers
Plasma Imager (UPI)	~	Observation of terrestrial plasmasphere from lunar orbit, XUV(304A) to VIS

Among the major products of the Kaguya mission are several high-quality, high-resolution monochrome mosaics from the TC (at ~10 m/pixel at morning, evening, and simulated 'ortho' or directly-above illumination; Haruyama et al. 2008; Isbell et al. 2014), MI-derived high-resolution multiband images and map mosaics (Ohtake et al. 2008), as well as topographic products derived from laser altimeter data (Araki et al. 2009, 2013) and stereo imaging (Barker et al. 2016). The global TC mosaics are well registered to the Apollo Lunar Retroreflector array and LOLA data (Haruyama et al. 2012). With their low-sun illumination, the TC data

provide excellent complements to high-illumination (often color) data such as those from the Clementine global mosaics at Ultraviolet/Visible (UVVIS; Eliason et al. 1999), the Lunar Reconnaissance Orbiter Narrow Angle Camera (NAC) and Wide Angle Camera (WAC) mosaics (Robinson et al. 2010), and the hyperspectral data from Chandrayaan-1's Moon Mineralogy Mapper (Pieters et al. 2009a) for geologic studies, mapping, and morphologic and structural analyses of the lunar surface.

Availability of the global TC derived high-resolution (approx. 10 m/pixel), monochrome, tiled frames and mosaics (Haruyama et al. 2008; Isbell et al. 2014) have greatly facilitated a wide variety of lunar studies, including relative and absolute chronology (e.g., crater counting), geologic mapping, structural analyses, and detailed surface characterization to better understand the Moon's geologic record. These TC data have enabled discoveries of relatively small lunar features such as lava-tube skylights (Haruyama et al. 2009b), evidence for a double peak in volcanic activity near the Aristarchus plateau (Morota et al. 2011), lack of an exposed ice sheet at the south polar Shackleton crater (Haruyama et al. 2013), and characterization of mare eruption ages (Cho et al. 2012). Using TC stereo observations, a global DEM was produced with vertical accuracy of 10 m or better (Haruyama et al. 2012, 2014). A more recent hybrid topographic model (dubbed the SELENE LOLA Digital Elevation Model or SLDEM2015) has been developed using LOLA and TC stereo data, and it covers latitudes within ±60° at a horizontal resolution of 512 pixels per degree (~60 m at the equator) and a typical vertical accuracy ~3 to 4 m (Barker et al. 2016).

The MI data have been used to determine the global distributions of purest anorthosite (PAN) sites (Ohtake et al. 2009) and pyroxene-rich sites in highland fresh craters (Ogawa et al. 2011). Detailed geologic analyses of the South Pole–Aitken basin are also reported (Uemoto et al. 2017). When calibrated with Apollo samples, the MI data can be used to derive mineral maps of lunar surface composition, including maps of olivine, plagioclase, orthopyroxene, and clinopyroxene derived using Hapke's radiative transfer equations, FeO, OMAT, submicroscopic iron, the plagioclase grain size, and the weighted criteria calculated to identify the best spectral match between each MI spectrum and a spectral library (Lemelin et al. 2016, 2019). Cross-calibrations among the MI, SP, M^3, and the Robotic Lunar Observatory (ROLO, an Earth-based lunar radiance calibration standard; Stone 2008) data have also been conducted (Besse et al. 2013a; Ohtake et al. 2013; Pieters et al. 2013*)*.

The LALT collected 6.77×10^6 range measurements globally with an along-track shot spacing of ~1.6 km, a cross-track equatorial spacing of ~15 km, a radial uncertainty of ~4 m, and a horizontal uncertainty of ~77 m (Araki et al. 2009). From these data, the first polar topographic maps with complete coverage were produced (Araki et al. 2009), and improved estimates of the lunar figure from a spherical harmonic model complete to degree and order 359 on a quarter-degree grid were made.

Spectral Profiler (SP) data from Kaguya have been used to identify new rock lithologies (Matsunaga et al. 2008), discover magnesian anorthosites on the lunar far side (Ohtake et al. 2012) (see EA-1-5), complete global mineral surveys of the Moon (Matsunaga et al. 2011; Hareyama et al. 2017) (see EA-1-6) and to provide evidence for an impact origin of the Moon's Procellarum Basin (Nakamura et al. 2012). SP data also enabled more detailed surface characterization, such as for identifying olivine of possible mantle origin (Yamamoto et al. 2010), and mapping olivine in South Pole–Aitken basin (Yamamoto et al. 2012). Online databases are also available for accessing the SP spectral data (Hayashi et al. 2016; Haugaard et al. 2017).

Discoveries were also made using data from other Kaguya instruments. For example, data from the radar sounder instrument were used to identify sub-surface layers within lava units in the Serenitatis and western Procellarum basins (Ono et al. 2009; Oshigami et al. 2009), suggestive of ancient palaeoregolith layers trapped between lava flow units.

Such measurements have also assisted in estimation of the thickness of surface regolith layers (Kobayashi et al. 2010) and thickness of mare basalt lava units across the Moon (Oshigami et al. 2014). Two types of basin structure (Namiki et al. 2009) were identified from relay satellite tracking data, and new global maps of calcium oxide were developed through analyses of GRS data (e.g., Yamashita et al. 2012) (see EA-1-7).

The Kaguya Data Archive, maintained by JAXA (see http://l2db.selene.darts.isas.jaxa.jp/) serves data from all instruments at a variety of processing levels, and ancillary spacecraft data such as attitude kernels and clock parameters are also available at this archive. Kaguya acquired many new, high-quality datasets that paved the way for a renewed scientific examination of the Moon.

3.2. Chang'E 1

Chang'E 1 (***CE1***) was the first lunar satellite for the initial (orbiting) stage of the Chinese lunar exploration project of the China National Space Administration (CNSA). It was launched on 24th October 2007, entered lunar orbit on 7th November 2007, worked for 495 days, and ended its mission on 1st March 2009 with a controlled impact in Mare Fecunditatis at 52.36° E, 1.5° S (Ouyang et al. 2010). As an orbiter, Chang'E-1 successfully accomplished the first of the goals of the three-pronged Chang'E lunar exploration project, with the next goals to include soft landing and roving and then sample return. There were eight scientific instruments on board the Chang'E-1 (CE1) satellite (Table 4; Zuo et al. 2014).

Table 4. Chang'E 1 instruments (Ouyang et al. 2010).

Instrument	Spatial Resolution	Measurements & Capabilities
Stereo camera, charge-coupled device (CCD)	120 m/pixel	Global high-quality images
Laser altimeter (LAM)	7 km	Global topography data (1064 nm, 150 mJ laser; range resolution 1 m)
Interference imaging spectrometer (IIM)	200 m/pixel	Mineral detection, 0.5 to 1.0 micron
Gamma-ray spectrometer (GRS)	300 km^2	Elemental mapping (U, Th, K, Fe, Ti), 0.3–9 MeV
X-ray spectrometer (XRS)	170 km^2 (at 200 km altitude)	Elemental mapping (Mg, Al, Si), 1–10 keV
Microwave radiometer (MRM)	56 km (3 GHz), 30 km for other 3 channels	Regolith thickness and brightness temperature, ^{3}He mapping, 1° × 1°
High-energy particle detector (HPD)	~	Detection of high-energy particles, lunar plasma environment
Solar wind ion detector (SWID)	Instantaneous field of view: 6.7° × 180° Acceptance angle: 6.7° × 15°	Energy spectra of primary solar wind, 40 eV–20 keV

Scientific products from CE1 include global high resolution image maps [positioning accuracy better than 240 m, location accuracy is 100 m to 1.5 km (Li et al. 2010a; Ouyang et al. 2010); global DEM models (3 km resolution, plane positioning accuracy 445 m, height measurement accuracy is 60 m; Li et al. 2010b), with a recent version that improves vertical accuracy from 127.3 m to 48.7 m (Huang et al. 2018); and elemental distribution maps (major elements at 200 m/pixel: SiO_2, Al_2O_3, CaO, FeO, MgO, TiO_2, trace elements: Th, U and K (5° × 5° or ~215 km/pixel; Ling et al. 2011; Zou et al. 2011; Wang and Niu 2012; Wu 2012; Wu

et al. 2012; Yan et al. 2012; Wang and Zhu 2013; Sun et al. 2016). The solar wind ion particles phenomenon and the plasma physics process reveals the interaction process of the solar wind with the Moon (Ouyang et al. 2010). Digital data access was made available online at http://moon.bao.ac.cn/index.jsp (in Chinese) and http://moon.bao.ac.cn/index_en.jsp (in English).

Data from the Microwave Radiometer were used to produce brightness temperature maps of the whole Moon under different illumination conditions and identified variations caused by surface topography and mineralogy (Zheng et al. 2012) (see EA-1-8). These data were used to derive thickness estimates of the lunar regolith and assess the distribution of potential ^{3}He reserves (Zheng et al. 2008b; Fa and Jin 2010a), and for measurements of the temperature of the lunar soil (Fa and Jin 2010b) and throughout the lunar day–night cycle.

3.3. Chandrayaan-1

Chandrayaan-1 (Ch-1) was the first planetary exploration mission of the Indian Space Research Organization (ISRO), and it was designed to perform remote sensing observations of the Moon to further our understanding about its origin and evolution. Ch-1 launched on 22 October 2008 carrying 11 instruments and an impactor (Table 5**;** five instruments from ISRO, two from NASA-funded teams, three from institutions in the European Space Agency (ESA), one from the Bulgarian Academy of Sciences). After orbiting 3400 times operations were completed on 29 August 2009 (Bhandari 2005; Goswami and Annadurai 2009; Planetary Data System 2009). Hyper-spectral studies in the 0.4–3μm region using three imaging spectrometers, combined with analyses of data from a low energy X-ray spectrometer, a sub-keV atom analyzer, a 3D terrain mapping camera and a laser ranging instrument provided information on mineralogical and chemical composition and topography of the lunar surface (Goswami and Annadurai 2009; Chauhan et al. 2012). A low energy gamma ray spectrometer and a miniature imaging radar investigated volatile transport on lunar surface and water ice at the poles (Spudis et al. 2009). A radiation dose monitor provided an estimation of energetic particle flux between Earth and the Moon as well as in lunar orbit. An impact probe carrying a mass spectrometer was also carried to study the lunar atmosphere and view the surface and measure any possible volatiles prior to impact (Kumar 2009).

After five Earthbound maneuvers, lunar insertion maneuver, and circularizing maneuvers at the Moon, on 12 November 2008, the Ch-1 spacecraft reached its intended 100 km circular polar orbit for chemical, mineralogical, and photo-geologic mapping of the Moon; scientific observations were scheduled to continue at this altitude for two years. These plans changed soon after orbit was achieved because of loss of one of the redundant bus management units and one of two star-trackers (Boardman et al. 2011). Because of thermal issues with the instruments and the loss of the second star tracker (and resulting limited knowledge of spacecraft attitude), the Chandrayaan-1 spacecraft was raised to a 200 km orbit between 16 to 19 May 2009. Although imaging instrument spatial resolutions were reduced after this maneuver, this change enabled further studies of orbital perturbations and gravitational field variations and imaging of more of the lunar surface with a wider swath. After completing more than 3400 orbits of the Moon in 312 days and providing a large volume of data from its suite of sensors that met most mission objectives, communication with the spacecraft was abruptly lost around 20:00 UT on 28 August 2009. ISRO officially terminated the mission on 31 August 2009, after operating for nearly 10 months in lunar polar orbit.

During Ch-1 primary mission operations at 100 km, the ***TMC*** (Kumar and Chowdury 2005) and ***HySI*** instruments acquired data for the equatorial region (±30°) and parts of the southern hemisphere (−60°) and Mini-SAR operated at both poles. At 200 km altitude, more systematic global mapping was performed by TMC (Sivakumar et al. 2012) and HySI, starting with the poles and mid-latitude regions, and polar imaging by Mini-SAR began on 17 August 2009 and continued until the spacecraft was lost on 28 August 2009. On 14th November 2008, the Moon Impact Probe (***MIP***) carrying the ***CHACE*** instrument suite was separated from

Table 5. Chandrayaan-1 instruments (e.g., Goswami and Annadurai 2009).

Instrument	Resolution at 100 km	Goal & Capability
Terrain Mapping Camera (TMC)	5 m/pixel	Global mapping, stereo-derived topography (base/height = 1 m); Panchromatic, 0.5–0.85 microns, 20 km swath
Hyper Spectral Imager (HySI)	80 m/pixel	Mineralogy, lithology; 64 bands, 0.42–0.96 microns, 15 nm spectral resolution, 20 km swath
Moon Mineralogy Mapper (M3; US)	140–280 m/pixel (Global Mode)	Mineralogy; 85 bands, 0.42 to 3.0 microns, pushbroom imager, 10 nm spectral resolution
Sub-Infrared Spectrometer (SIR-2; MPI)	80 m/pixel	Mineralogy; 0.9–2.4 microns, 256 channels, 6 nm spectral resolution
Lunar Laser Ranging Instrument (LLRI)	5 m height	Lunar topography, gravity field; Nd:Yag laser with energy 10 mJ and 20 cm optics receiver operating at 10 Hz, 5 m range resolution
Chandrayaan-1 X-ray Spectrometer (C1XS; RAL) with the Solar X-ray monitor (SIXS)	25 km/pixel	Elemental abundance (Mg, Fe, Al, Si, Ca, Ti); 0.5–10 keV, 140 eV resolution
Sub-keV Atom Reflecting Analyzer (SARA; SISP): Chandrayaan-1 Energetic Neutrals Analyser (CENA)	~	Lunar surface chemistry (H, O, Na/Mg/Si/Al, K/Ca groups and Fe atoms) via mass spectrometry; 10 eV–3.3 keV
Sub-keV Atom Reflecting Analyzer (SARA; SISP): Solar Wind Monitor (SWIM)	~	Radiation environment (Ions H, He, O); 10 eV–15 keV
High Energy X-ray Spectrometer (HEX)	33 km^2/pixel	Volatile transport; 30–270 keV
Mini-Synthetic Aperture Radar (Mini-SAR; US)	150 m/pixel	Near-surface water abundance at the poles; S-band, 13-cm wavelength, 2.38 GHz
Radiation Dose Monitor (RADOM; BAS)	~	Radiation environment, cosmic particle detector; 1–256 MeV, Silicon detector with pulse analyzer
Moon Impact Probe (MIP)	~	Lunar atmosphere and exosphere; Package: imager, C-band radar altimeter, mass spectrometer
Chandra's Altitudinal Composition Explorer (CHACE)	~	Lunar atmosphere; 1–100 amu, mass spectrometer on MIP

Notes: MPI = Max-Planck Institute, Lindau, Germany; RAL = Rutherford Appleton Laboratory, UK; SISP = Swedish Institute of Space Physics, Kiruna, Sweden; BAS = Bulgarian Academy of Sciences

Chandrayaan-1 lunar craft at an altitude of about 100 km and it took nearly 3000 descent images of the lunar surface and 650 mass spectra of lunar atmospheric constituents, covering the latitudinal range of 20 °N to the South Pole (Bhandari and Srivastava 2014). The TMC and HySI datasets and derived products such as TMC mosaics and DEMs from Chandrayaan-1 mission are available at the Indian Space Science Data Centre (ISSDC) website (http://www.issdc.gov.in). A Chandrayaan-1 Lunar Science Atlas highlighting many of the derived products is also available (Kumar et al. 2015). The two ESA instruments on board, ***CIXS*** and ***SIR-2***, delivered regional chemical (Narendranath et al. 2011; Weider et al. 2012, 2014) and spectral maps (Mall et al. 2009; Bugiolacchi et al. 2013) of the lunar surface.

Among the major science results of the Ch-1 mission was the discovery that the lunar atmosphere was denser than expected, with an atmospheric pressure of ~6.7×10^{-5} Pa as measured by CHACE (Sridharan et al. 2010a,b). Mass spectrometer data showed an increase in H_2O and CO_2 as the probe descended toward the south pole. These have been interpreted as earlier results of the presence of water at or near the lunar surface and of possible degassing from the lunar interior (Sridharan et al. 2013, 2015).

MiniSAR transmitted circular polarization and received two orthogonal linear polarizations coherently, supporting reconstruction of the four Stokes parameters and the derivation of maps in circular polarization. Mini-SAR mapped the lunar poles and collected data on the scattering properties of sun-lit and permanently shadowed areas (Spudis et al. 2009). From February to April 2009, Mini-SAR covered 95% of the lunar poles (latitude > 80°) at 150 m resolution, and these data were the first to provide a look inside the very dark lunar polar craters where evidence for water ice was discovered at the north pole (Spudis et al. 2010a,b). Subsequent studies have questioned this discovery and have presented evidence for alternate explanations for the Mini-SAR elevated polar radar signatures (e.g., Fa and Eke 2018).

Moon Mineralogy Mapper (***M³***) data were acquired in two modes and over two operating periods: Global Mode (GM) and Targeted Mode, acquired in Optical Periods (OP) 1 and 2. M^3 data acquired in Global Mode have 85 channels covering the spectral range from 460 to 2976 nm; the spatial resolution of GM M^3 data was 140 m/pixel from 100 km altitude (decreased to 280 m/pixel when the spacecraft climbed to a 200 km orbit beginning 5/13/09 until the end of the mission on 8/16/09). GM data covered >95% of the Moon. M^3 data are available from the PDS in the form of Level 2 products (e.g., calibrated to reflectance, thermally and photometrically corrected; Clark et al. 2011; Besse et al. 2013a,b).

Studies using M^3 hyperspectral data, particularly identification of absorption features near 3 μm, spectra have indicated the presence of hydrated minerals [and/or adsorbed water (H_2O) or hydroxyl (OH) molecules or both] in the lunar regolith (Pieters et al. 2009b) (see Crawford et al. 2023, McCubbin et al. 2023, both this volume). These results were independently confirmed with analysis of data from the Cassini Visible Mapping Spectrometer (VIMS; Clark 2009) and instruments on the Deep Impact/EPOXI spacecraft (Sunshine et al. 2009). Pieters et al. (2009b) estimated a water abundance of 10 to 1000 ppm with the highest values observed at high latitudes where it is cold enough to ensure volatile retention (see EA-1-3). The M^3 data also supported identification and mapping of the abundance and distribution of lunar indigenous water (Klima et al., 2013; Milliken and Li 2017) and provided evidence for exposed water ice at the lunar poles (Li et al. 2018) (see Crawford et al. 2023, McCubbin et al. 2023 , both this volume).

3.4. Lunar Reconnaissance Orbiter (LRO)

The Lunar Reconnaissance Orbiter (***LRO***) mission was conceived by NASA in 2004 as an exploration mission, with the goal of reconnaissance of resources and the radiation environment, and identifying safe landing sites for future human and robotic missions to be supported by NASA's Exploration Systems Mission Directorate (NASA 2004; Chin et al. 2007).

Table 6. LRO instruments (Vondrak et al. 2010; Keller et al. 2016).

Instrument	Resolution at 50 km	Goal & Capability
Lunar Orbiter Laser Altimeter (LOLA)	25 m horizontal, 10 cm vertical	Topography, slopes, roughness (5-spot altimeter) (see EA-1-9, Smith et al. 2010)
Lunar Reconnaissance Orbiter Cameras (LROC): Wide Angle Camera (WAC)	100 m/pixel	Global imaging, lighting, lunar resource mapping (7-band UV-VIS); stereo topography
Lunar Reconnaissance Orbiter Cameras (LROC): Narrow Angle Camera (NAC)	50 cm/pixel	Targeted imaging, hazards (2 NACs, 5 km combined swath); stereo topography
Laser Ranging (LR)	~	Precision orbit determination (LOLA detector from Earth to LRO)
Diviner Lunar Radiometer	170 m across track, ~500 m along track,	Thermal state, volatile stability, rocks, regolith, composition (0.35–400 μm in 9 channels)
Synthetic Aperture Radar (Mini-RF)	150 × 150 m/pixel, 15 × 30 m/pixel zoom (S-band); 150 × 150 m/pixel (X-band)	Resources, topography, hazards (bistatic radar, S- & X-bands)
Cosmic Ray Telescope (CRaTER)	~	Radiation spectra, tissue effects (LET spectra, 0.9 keV/μm to 2.2 MeV/μm)
Lunar Exploration Neutron Detector (LEND)	10 km/pixel	Neutron albedo, hydrogen maps (thermal, epithermal, energetic neutrons)
Lyman-Alpha Mapping Project (LAMP)	~300 m/pixel	Water-frost, permanently shadowed regions

Instruments were selected competitively to address these objectives (Table 6; Vondrak et al. 2010). LRO was launched on June 18, 2009 and entered lunar orbit on June 23, 2009. After spacecraft commissioning in lunar orbit, the Exploration Mission began on September 15, 2009; this reconnaissance mission was completed on September 15, 2010 when operations were transferred to NASA's Science Mission Directorate for a two-year Primary Science Mission. LRO is currently operating in a fourth extended mission phase.

LRO was initially placed into a 30 × 200 km polar orbit with periapse over the south pole during commissioning (Keller et al. 2016). At the beginning of the exploration phase, LRO was moved to a quasi-circular mapping orbit, maintained at 50 km altitude with frequent station-keeping propulsive maneuvers. To obtain high resolution imaging of the Apollo landing sites and other locations of high scientific interest, the periapse was lowered to 21 km in August and November of 2011. To conserve fuel and permit extended operations for several more years, on December 11, 2011 the LRO spacecraft was returned to a 30 km × 200 km quasi-stable polar orbit, requiring minimal annual station-keeping maneuvers.

LRO operations included several special events, both to obtain new views of surface artifacts and features and to respond to events such as eclipses, coordinated observations with other spacecraft, and spacecraft impacts. These events included targeting slews to obtain

off-nadir (oblique) views, the impact of the Lunar Crater Observation and Sensing Satellite (LCROSS, see below) in Cabeus crater near the lunar south pole on October 9, 2009 (Colaprete et al. 2010), and the impact of the two Gravity Recovery and Interior Laboratory (GRAIL, see below) into a northern sunlit peak on December 17, 2012 (Robinson et al. 2015).

Science objectives of LRO focused on a variety of topics, and several discoveries related to these have resulted from the mission. For example, possible evidence for lunar polar water was identified in data from the collimated epithermal neutron detector on the LEND instrument in maps of epithermal neutron flux at a spatial resolution of ~10 km (Mitrofanov et al. 2010a,b), indicating that there are local Neutron Suppression Regions (NSRs) near the poles. However, measurements of water content by LCROSS at Cabeus crater of 5.6 ±2.9 wt% (Colaprete et al. 2010) were higher than the estimated water content of 0.5–4 wt% from LEND. Similarly, in Shoemaker crater, LAMP data (Hayne et al. 2015) are consistent with small amounts of water frost on the surface, but LEND data support larger amounts of subsurface hydrogen (Sanin et al. 2017) (see EA-1-10). Results from analysis of data from Mini-RF (Nozette et al. 2010) also suggested that water ice may be present at Cabeus crater as a thin (~10 to 20 cm) layer, near the surface (Patterson et al. 2017). Using superposed crater density, analyses of LROC data support the determination of the relative and model ages of impact craters at a wide range of crater sizes, from a few meters to 100s of km in diameter. For example, use of both LROC and LOLA data indicate that basin and crater size distributions have changed such that older highland craters are preferentially larger than younger mare craters, indicating shifts in the impactor population characteristics over geologic time (Morbidelli et al. 2012; Kirchoff et al. 2013). New (< 5 years old) impact craters and were found to be widespread across the lunar surface (Speyerer et al. 2016). LROC images reveal a population of small contractional and extensional structures on the lunar near side and in the far side highlands (Watters et al. 2010, 2012; Banks et al. 2012), suggesting that the Moon is in a general state of relatively recent (< 1 Ga) contraction.

Science results from LRO also include a characterization of relatively young volcanic complexes, such as Ina (Braden et al. 2014), and revealed first direct evidence of the presence of highly silicic volcanic rocks on the Moon at sites such as Compton-Belkovich (Glotch et al. 2010; Jolliff et al. 2011; Wilson et al. 2015). Studies of CRaTer (Spence et al. 2010) data indicated that LRO measured galactic cosmic ray interactions with the Moon during a period with the largest cosmic ray intensities observed during the space age (Schwadron et al. 2012, 2013). Analyses of LAMP (Gladstone et al. 2010) data indicate that lunar surface water abundance varies with terrain type and local time and temperature (Hendrix et al. 2019).

The LRO data are archived and available in PDS formats online (http://pds-geosciences.wustl.edu/missions/lro/). Special interfaces have been developed for certain archives; for example, mosaics, landing site maps, and digital elevation models are all served at the LROC operations center (http://lroc.sese.asu.edu/). LRO has thus far produced a number of maps and datasets for both exploration and science, including high-resolution images of robotic and human exploration sites that showed hardware, the tracks of the astronauts, and surface disturbances from landing and ascent (e.g., Schmitt et al. 2017; Wagner et al. 2017) (see EA-1-11) and several major global products (i.e., 100 m/pixel spatial resolution, 7-color image and derived maps from LROC/WAC; Denevi et al. 2014; Sato et al. 2014, 2017; see EA-1-12); Diviner temperature at 0.5° (~20 km/pixel) and rock abundance at 4 pixels/degree spatial resolution; Paige et al. 2010a,b; Bandfield et al. 2011, 2017; Williams et al. 2017 (see EA-1-13); maps of roughness and radar scattering characteristics by Mini-RF at a resolution of ~250 m for the upper meter of the lunar surface; Cahill et al. 2014) (see EA-1-14). Polar products were of special interest for future exploration, and these included maps of illumination conditions near the poles (Mazarico et al. 2011; Speyerer and Robinson 2013), high resolution polar topographic maps (Zuber et al. 2010, 2012), and polar temperature products (Paige et al. 2010b).

3.5. Lunar Crater Observation Sensing Satellite (LCROSS)

The Lunar Crater Observation Sensing Satellite (***LCROSS***) mission was designed as a low-cost companion mission to LRO to provide direct evidence for water ice in permanently shadowed craters of the Moon (Colaprete et al. 2012). The intent was to crash the spent rocket stage (an Atlas V upper-stage Centaur rocket) from LRO into the Moon and observe the ejected debris, including hydrogen species, from instruments on a trailing spacecraft. Shortly after the LRO/LCROSS launch, LRO separated from the Centaur, the remaining fuel was vented, and the LCROSS Shepherding Spacecraft (SSc) then controlled the Centaur for 4 months while any residual volatiles baked off, calibrations were performed, and target the impacting site in Cabeus crater. On final approach to the Moon, about 9 hours before impact, the SSc separated from the Centaur, braked, and oriented its instruments toward the impact site. About 1 hour before impact, the nine LCROSS instruments were powered on and started collecting data (Ennico et al. 2012).

The LCROSS instrument suite consisted of nine science instruments (Table 7): one visible, two near infrared (NIR), and two mid-infrared cameras; one visible and two near-infrared spectrometers; and a photometer. Although the plume was smaller than expected and so could not be observed from Earth-based telescopes, observations from the near-infrared and ultraviolet/visible (UV/VIS) spectrometers indicated that near-infrared absorbance could be attributed to water vapor and ice and ultraviolet emissions could be attributable to hydroxyl radicals, both lines of evidence supporting the presence of water in the plume debris (Colaprete et al. 2010). The concentration of water ice in the regolith at the LCROSS impact site was estimated to be 5.6 ± 2.9% by mass. Spectral data also indicated that other volatile compounds also were observed, including light hydrocarbons, sulfur-bearing species, and carbon dioxide.

The LCROSS data (in the form of raw and calibrated images and spectra) are archived and available in PDS formats online (https://pds-imaging.jpl.nasa.gov/volumes/lcross.html).

Table 7. LCROSS instruments (Colaprete et al. 2010, 2012).

Instrument	Goal	Capability
Visible Camera (VIS)	Plume imaging	Analog video camera, CCD with f/1.2 lens for a 37.8° Field of View (FOV)
Near-Infrared Cameras × 2 (NIR1, NIR2)	Plume imaging	0.9-17 μm, InGaAs sensor, 320 × 240 pixels, 25 mm lens, f/1.4, 36° FOV; NIR1 had long-pass filter >1.4 μm, NIR2 had no filter
Mid-Infrared Cameras × 2 (MIR1, MIR2)	Plume imaging	6.0–13.5 μm, microbolometers, 164 × 128 pixels, 30 mm lens, f/1.6, 18.6° FOV; MIR1 had band-pass filter at 6-10 μm, NIR2 had no filter
Total Luminescence Photometer (TLP): Sensor Electronics Module (SEM) and Digital Electronics Module (DEM)	Brightness measurements	Visible light, 0.4–1.0 mm; SEM had 10° FOV
Visible Spectrometer (VSP)	Plume spectra	~0.263–0.65 μm slit spectrum is imaged onto a 1044 × 64 pixel CCD; resolving power is R~300, 500, and 850 at 0.30, 0.40 and 0.60 μm
Near-Infrared Spectrometers × 2 (NSP1, NSP2)	Plume spectra	Forward and rear facing, 1.2–2.4 μm spectra; NSP1 had 1° FOV, NSP2 had 130° FOV

3.6. Chang'E 2

Chang'E 2 (***CE2***) was China's second lunar orbital mission. It was essentially the backup satellite of Chang'E-1, but with additional technology improvement (see below). The main engineering goal of CE2 was to test key technologies for future lunar landed missions, and to enhance lunar scientific exploration (Ye et al. 2013). Scientific goals were extensions of those for CE1, including further mapping of element distribution in the lunar regolith, determination of the thickness of lunar regolith, and understanding the environment in near lunar space.

The CE2 satellite was launched on 1 October 2010, accomplished the primary lunar science mission (including flying at 100 km in a circular orbit and at a 100 × 15 km elliptical orbit for high-resolution surface imaging), and departed lunar orbit on June 9 2011. On the August 25 2011, the satellite was successfully captured into a Lagrange L2 point orbit, where it entered a Lissajous orbit (a low-energy, stable position in orbit around L2). On April 15 2012, the satellite departed lunar orbit to begin an extended mission in deep space. On December 13, 2012, the satellite flew by the 4179 asteroid Toutatis and obtained optical images with the highest resolution superior to 3 m (Huang et al. 2013; Zou et al. 2014; Zhu et al. 2014a).

CE2 has seven science instruments (Table 8), only lacking the interference imaging spectrometer that was used on CE1. The main differences from earlier instruments include: a Lanthanum Bromide (LaBr) crystal was used to replace Cesium Iodide (CeI) crystal for GRS and the detection accuracy was increased. The spectrum of the X-ray spectrometer was reduced from the original 10 keV–60 keV to 25 keV–60 keV to avoid high noise from 10 keV–25 keV detected by CE1 XRS.

Scientific achievements from Chang'E 2 include a global map of the Moon with 7 m/pixel spatial resolution (Zhao et al. 2012). In addition, stereo images with ~1.5 m spatial resolution were acquired from the Sinus Iridum area, for the purpose of planning for the subsequent soft-landing mission Chang'E 3 (see below). The stereo pair data were used to generate high

Table 8. List of Chang'E 2 instruments (Ye et al. 2013; Blewett et al. 2018).

Instrument	Resolution at 100 km	Goal & Capability
Stereo camera, charge-coupled device (CCD), 2-line pushbroom array	7 m/pixel (1.5 to 7 m/pixel in elliptical orbit)	Global high-quality images, monochrome global and stereo maps: 7 m/pixel at 100 km orbit (1.5 to 7 m/pixel in elliptical orbit)
Laser altimeter (LAM)	5 m vertical accuracy	Global topography data (instrument failed)
Gamma-ray spectrometer	150 km × 150 km	Elemental mapping, (U, Th, K, Fe, Ti), 4%@662 keV
X-ray spectrometer	240 km × 65 km	Elemental mapping, (Mg, Al, Si); low energy ≤ 300 eV@5.95 keV; high energy ≤ 10% @59.5 keV
Microwave radiometer	1° × 1°	Regolith thickness, surface temperature and brightness. Receiver frequencies: 3.0 GHz, 7.8 GHz, 19.35 GHz, 37 GHz
High-energy particle detector	~	Detection of high-energy particles, lunar plasma environment
Solar wind detectors	Instantaneous field of view: 6.7° × 180° Acceptance angle: 6.7° × 15°	Energy spectra of primary solar wind, 40 eV–20 keV

resolution lunar DEMs at 20 m/pixel (Wu et al. 2014). Additional elemental maps (e.g., Th, K) were generated at 2° × 2° or ~60 × 60 km (Zhu et al. 2013, 2014b, 2015; Chen et al. 2016; Wang et al. 2016) and regions of Oceanus Procellarum were chemically mapped in terms of Mg, A1, Si, Ca and Fe by the X-ray spectrometer (Ban et al. 2014). The full moon temperature mapping (Lian et al. 2015), the temperature of the lunar soil (Fang and Fa 2014) and the dielectric constant of the lunar soil (Lian et al. 2014) were obtained by the microwave radiometer.

The CE2 ground application system released archival products and advanced science data products; all data have been digitally released at http://moon.bao.ac.cn/index.jsp (in Chinese) and http://moon.bao.ac.cn/index_en.jsp (in English) (Zuo et al. 2014).

3.7. Acceleration, Reconnection, Turbulence and Electrodynamics of the Moon's Interaction with the Sun (ARTEMIS)

NASA's ***ARTEMIS*** mission (Acceleration, Reconnection, Turbulence and Electrodynamics of the Moon's Interaction with the Sun) repurposed two of five Earth-orbiting satellites to the Moon. These satellites were repurposed from the NASA Heliophysics constellation of satellites (THEMIS, Time History of Events and Macroscale Interactions during Substorms) that were launched on February 17, 2007 and successfully completed their mission in 2010 (Angelopoulos 2008, 2010; Angelopoulos et al. 2008). The ARTEMIS mission provides unprecedented two-point measurements over a range of altitudes from ~100 to 10,000 km, with a variety of orbital phasings and probe separations.

ARTEMIS utilized a complex trajectory design that leveraged transfer orbits through the "weak stability boundary" regions in the vicinity of Lagrange points (where the net gravitational force provides the centripetal force needed to allow an orbiting object to remain at rest with respect to a two-body system) to achieve the transfer of the two spacecraft from geocentric to selenocentric orbits (Broschart et al. 2009; Cosgrove et al. 2010; Folta et al. 2011, 2014). The two probes each conducted a combination of apoapsis-raise maneuvers, lunar flybys, and transfers through the vicinity of the Sun–Earth L1 Lagrange point to Lissajous orbits around the Earth-Moon Lagrange points to achieve their eventual insertion into lunar orbit. ARTEMIS conducted science throughout these maneuvers, which took almost two years to complete. The Lissajous orbit phase, during which the probes orbited the Earth–Moon (lunar) Lagrange points (LL1 and LL2), provided extended observations of the full three-dimensional lunar wake. The final lunar orbits, in which the probes still remain, lie nearly in the ecliptic and are highly elliptical, with apoapses of ~19,000 km and periapses that naturally vary from tens to hundreds of km in altitude. These orbits require little station keeping, and provide observations at a variety of distances from the Moon. One probe orbits prograde and the other probe orbits retrograde, so the orbits precess around the Moon at different rates, thereby providing a variety of different two-point perspectives on the lunar environment.

ARTEMIS is conducting a wide range of observations of the Moon's interaction with the solar wind and investigating clues about its planetary structure and evolution (Halekas et al. 2010; Sweetser et al. 2011). The original ARTEMIS mission goals (Sibeck et al. 2011) included both planetary science and heliophysics objectives. The planetary science objectives focused on measuring ions from the tenuous lunar exosphere, remotely sensing the near-surface electrostatic environment, utilizing electromagnetic sounding to investigate the lunar interior, and exploring the unique lunar magnetic fields and their interaction with the space environment. The heliophysics objectives focused on the structure and dynamics of the terrestrial magnetosphere and its boundaries at lunar distance (as observed during full Moon), the foreshock region upstream of the terrestrial bow shock, fundamental plasma physics processes in the solar wind, and the structure and dynamics of the lunar plasma wake. Each of the ARTEMIS probes maintains the same instrument complement as the original THEMIS constellation (Table 9), with all instruments still functional. Minor issues such as the loss

of one of the EFI booms and the failure of the SST attenuators have been compensated for operationally, and all sensors on both probes still return usable science data.

Table 9. ARTEMIS instrumentation (Angelopoulos 2008; Auster et al. 2008; Bonnell et al. 2008; Cully et al. 2008; Le Contel et al. 2008; Ludlam et al. 2008; McFadden et al. 2008a,b; Roux et al. 2008).

Instrument	Goal	Goal & Capability
Fluxgate Magnetometer (FGM)	Magnetic field	Vector magnetic field DC to 64 samples/s
Electrostatic Analyzer (ESA)	Charged particles	Ions and electrons 1 eV–30 keV
Solid-State Telescope (SST)	Charged particles	Ions 25 keV–6 MeV
Electrons 25 keV–900 keV	240 km × 65 km	Elemental mapping, (Mg, Al, Si); low energy ≤ 300 eV@5.95 keV; high energy ≤ 10% @59.5 keV
Search Coil Magnetometer (SCM)	Magnetic field	Vector magnetic field from 0.1–8192 samples/s

Analyses of the measurements made by the ARTEMIS mission have revealed the structure and dynamics of the lunar wake (Halekas et al. 2010; Tao et al. 2012; Zhang et al. 2012; Poppe et al. 2014), the characteristics of ions from the lunar exosphere (Halekas et al. 2012, 2013), the complex structure of the near-surface electrostatic environment (Halekas et al. 2011; Harada et al. 2017), the unique interaction between lunar magnetic fields and the space environment (Halekas et al. 2014; Harada et al. 2015; Howard et al. 2017; Poppe et al. 2017a), and the unusual behavior of the lunar environment inside the terrestrial magnetosphere (Poppe et al. 2012; Harada et al. 2013 Zhou et al. 2013). ARTEMIS measurements have also been used to study phenomena not originally envisioned, such as the outflow of matter from the Earth (Poppe et al. 2016), weathering of the lunar regolith (Poppe et al. 2017b), and the energetic particle environment at the Moon (Xu et al. 2017).

ARTEMIS has also played an important supporting role in lunar science, providing constant monitoring of the space environment around the Moon. These observations have proven important in providing the input conditions needed to organize measurements made by other orbiters around the Moon, including LADEE and LRO (Benna et al. 2015a; Halekas et al. 2015; Hurley et al. 2015). As more missions, including small satellites and landers, visit the Moon in the coming years, the environmental monitoring capability of ARTEMIS should prove invaluable in supporting further scientific investigations.

The ARTEMIS mission archives are publicly accessible through the mission web site (http://artemis.ssl.berkeley.edu) and at the NASA Space Physics Data Facility (https://spdf.gsfc.nasa.gov/). These data products include the basic measurements (vector field components, charged particle energy-angle distributions) and derived products such as charged particle moments (density, velocity, temperature, etc.) and Fourier transforms of the time series field data sets.

3.8. Gravity Recovery and Interior Laboratory (GRAIL)

The Gravity Recovery and Interior Laboratory (***GRAIL***) mission was a twin spacecraft system launched on 10 September 2011 (Zuber et al. 2013a,b). The spacecrafts (dubbed Ebb and Flow) were inserted into lunar polar orbit on 31 December 2011 and 1 January 2012. After lowering and circularizing the orbits to ~55 km mean altitude, GRAIL conducted a primary mapping mission of the lunar gravity field from 1 March through 30 May 2012, transmitting to Earth 637 MB of laser ranging science data.

The GRAIL payloads were nearly identical (Asmar et al. 2013; Zuber et al. 2013a), and they included Lunar Ka-band Lunar Gravity Ranging Systems (LGRS) and MoonKam (Moon Knowledge Acquired by Middle school students) cameras. The root mean square (RMS) range-rate residuals from the LGRS Ka-band (32 GHz) ranging system were generally on the order of 0.02 to 0.05 mm s^{-1}. The digital MoonKam system consisted of four cameras per spacecraft, three with 6 mm lenses (two pointing ± 60 degrees forward and backward, and one pointing down) and one with a 50 mm lens pointing down (Zuber et al. 2013a). Unfortunately, the MoonKam cameras were damaged by a solar flare event in November 2011, before they could acquire lunar data. Data from the GRAIL instruments is served by the NASA Planetary Data System's Geosciences Node (http://pds-geosciences.wustl.edu/missions/grail/default.htm), and the most recent maps are served by NASA's Goddard Space Flight Center (https://pgda.gsfc.nasa.gov/products/50).

The science goals of the GRAIL mission were to map the structure of the lunar crust and lithosphere, understand the Moon's asymmetric thermal evolution, determine the subsurface structure of impact basins and the origin of mascons, assess the temporal evolution of crustal brecciation and magmatism, constrain deep interior structure from tides, and place limits on the size of the possible inner core. GRAIL mapped the high-resolution lunar gravity field with unprecedented accuracy and resolution (Zuber et al. 2013b; Lemoine et al. 2014), most recently up to degree and order 1200 (Goossens et al. 2016), and the data returned supported analyses of crustal density and thickness (Wieczorek et al. 2013) (see EA-1-15), bulk Moon chemical composition (Taylor and Wieczorek 2014), numerical modeling of lunar mascon basins (Melosh et al. 2013), and the discovery of linear gravity features that appear to be from ancient intrusive magmatic dikes (Andrews-Hanna et al. 2013). More recent results used GRAIL data and Apollo lunar laser ranging (LLR) data to calculate models of the lunar interior with a fluid outer core with radius of 200 to 380 km, a solid inner core with radius of 0–280 km and mass fraction of 0–1%, and a deep mantle zone of low seismic shear velocity (Williams et al. 2014).

3.9. Lunar Atmosphere and Dust Environment Explorer (LADEE)

The Lunar Atmosphere and Dust Environment Explorer (***LADEE***) mission was launched on 6 September 2013, and entered lunar orbit on 6 October 2013 after using geocentric phasing loops to optimize arrival time and geometry (e.g., Elphic et al. 2014). After dropping into a 250 × 250 km orbit at 157º inclination (an Apollo-like retrograde, near-equatorial geometry), a 30-day period of science instrument checkout commenced. On 21 November 2013, LADEE was maneuvered into a ~50 × 150 km orbit, with periapsis over the sunrise terminator, and began the 100-day primary science operations phase. After successfully completing all primary mission requirements, an extended science phase was approved and began on 1 March 2014. After acquiring dust and exosphere measurements at unprecedented low altitudes (a few km), LADEE was deliberately decommissioned by impact into the eastern rim of Sundman V crater (11.85° N, 266.75° E) on the far side of the Moon on 18 April 2014.

LADEE carried three science instruments and a laser communications technology demonstration payload (Table 10). The LADEE instruments were operated with a duty cycle determined by spacecraft power balance and thermal management. Instrument operations, therefore, focused on acquiring data over strategic local times and altitudes, and with required cadence over the mission. The Lunar Dust Experiment (LDEX) operated throughout the entire mission, capturing measurements from slightly after noon local time around to nearly the dusk terminator. Measurements were made from a few km above the surface up to several hundred km. The Ultraviolet and Visible Spectrometer (UVS) instrument routinely measured Na and K emissions in the noon, dawn and sunset terminator local times. The Neutral Mass Spectrometer (NMS) measured helium, neon and argon in the exosphere over an altitude range of a few kilometers to several hundred km, at nearly all local times. NMS routinely measured neutral He, Ne, and ^{40}Ar, and other species seen include H_2^+, Na^+, K^+, as well as $^{12}C^+$, $^{14}N^+$.

The Lunar Laser Space Terminal (LLST) on LADEE was operated on dedicated orbits, when the science instruments were not operating (Elphic et al. 2014).

Table 10. LADEE Instruments (Boroson and Robinson 2014; Colaprete et al. 2014; Horányi et al. 2014; Mahaffy et al. 2014).

Instrument	Goal	Capability
Lunar Dust Experiment (LDEX)	Impact-ionization dust detector	Particles 0.7–5 μm in size
Ultraviolet and Visible Spectrometer (UVS)	Exosphere Na, K emissions	Point spectrometer, 250–800 nm wavelength, spectral resolution of <1 nm; Main telescope optic was 76.2 mm in diameter, with a 1° field-of-view
Neutral Mass Spectrometer (NMS)	Exosphere monitor	Ions 25 keV–6 MeV
Lunar Laser Communications Demonstration (LLCD) system: Lunar Laser Space Terminal (LLST) on LADEE, and the Lunar Laser Ground Terminals at White Sands, NM	Communications system	Downlink rates as high as 622 Mbits/sec, and uplinks of 20 Mbits/sec

Scientific results from the LADEE mission include details of the Moon's exosphere from surface through to several hundred km above surface. LDEX measurements revealed a permanent, asymmetric dust cloud over the morning side of the Moon (Horányi et al. 2015; Wooden et al. 2016). This dust cloud is clearly linked to the impact of micrometeoroids on the "upstream" side of the Moon, and varies on monthly and seasonal cycles, and particularly as the Earth–Moon system sweeps through cometary debris trails such as the Geminids. UVS measurements showed that the variable sodium and potassium lunar exospheres are controlled by both the solar wind (sputtering implicated), and orbit phase (Colaprete et al. 2016). When the Moon is in the magnetotail, production of sodium is reduced and the exosphere diminishes. NMS observations demonstrated that three noble gases, He, Ne and Ar, comprise the most dominant contribution to the exosphere (Benna et al. 2015a; Halekas et al. 2015). Helium definitely has a major solar wind source, but a small amount leaks out of the interior due to radiogenic decay. Neon also has its origins in the solar wind, where it is a very minor constituent; its very long lifetime against photoionization and loss allows the gas to build up to levels comparable to helium and argon. Argon is almost entirely ^{40}Ar, derived from decay of ^{40}K. Exospheric ^{40}Ar is seen to peak over the western maria, specifically the Procellarum KREEP Terrane, where potassium abundances are high. The mechanism of release is not well understood.

LADEE data were archived by the NASA Planetary Data System at two locations: LDEX data are at the PDS Asteroid/Dust archive (https://sbn.psi.edu/pds/resource/ldex.html) and UVS and NMS are available online at the PDS Planetary Atmospheres Node: (http://pds-atmospheres.nmsu.edu/data_and_services/atmospheres_data/LADEE/mainr.html). Details of the products and their calibrations can be found in the Software Interface Specification (SIS) for each instrument on the archive sites.

3.10. Chang'E 3

Chang'E 3 (***CE3***) was a robotic landing mission for the second, lunar surface operations stage of the Chinese lunar exploration project. CE3 included a lander (the Lunar Landing Vehicle or LLV) and the Yutu lunar rover, informally known as the Jade Rabbit. The mission was launched on 2 December 2013 and on 6 December 2013, CE3 entered a lunar circular orbit

with an altitude of 100 km. On 10 December 2013, the spacecraft was successfully entered into an elliptical orbit about 15 × 100 kilometers high in diameter, and it successfully landed on the northwestern part of the Imbrium basin on 14 December 2013 (340.49° E, 44.12° N; Xiao 2014; Xiao et al. 2015). The lander and the Yutu/Jade Rabbit rover were successfully separated on 15 December 2013 and the rover explored the geology of the local area before mobility was lost after several weeks on surface. Yutu was a six-wheeled vehicle powered by solar cells; mounted on top of the LLV, the rover was lowered on a ramp onto the lunar surface after landing. The rover continued to operate with some functionality through to 31 July 2016 at mission end. Powered by a radioisotope thermoelectric generator (RTG), the lander continues to operate.

CE3 had a total of 8 payloads, with the lander and the Yutu rover each with 4 payloads (Table 11). The science objectives of the CE3 mission include: (1) investigation of the morphological features and geological structures of and near the landing area; (2) integrated in-

Table 11. Chang'E 3 instruments (Chen et al. 2014; Fang et al. 2014; Feng et al. 2014; Fu et al. 2014; He et al. 2014 ; Liu et al. 2014; Ren et al. 2014; Su et al. 2014; Wang et al. 2014 ; Wen et al. 2014; Li et al. 2015).

Instrument	Goal	Capability
	Lander Instruments	
Moon-based Optical Telescope (MOT)	Optical astronomical science observations	0.2 to 0.4 μm; +6 to +15 Mv; energy concentration of diffuse speckle 80 (≤3 × 3 pixel)
Extreme Ultraviolet Camera (EUVC)	Image the entire ion layer of the Earth from lunar surface	30.4 nm; 15° field of view (FOV); 0.08 ang. resolution; 0.1 to 10 R; 0.1 counts/sec/R sensitivity
Landing Camera (LCAM)	Descent imaging of landing site, selection of smooth site for landing	3-Color RGB filter; 1024 × 1034 pixel CCD; 45° × 45° FOV; 10 frames/sec; 40 signal to noise ratio (SNR) at 9% albedo, 30° solar altitude angle
Terrain Camera (TCAM)	Topography, geological survey of landing site	3-color RGB filter; 2352 × 1728 pixel CCD; 22.9° × 16.9° FOV; 5 frames/sec; 36 signal to noise ratio (SNR) at 9% albedo, 30°solar altitude angle
	Rover Instruments	
Panoramic camera (PCAM)	Color imaging of landing site and rock samples	3-color RGB filter; 2352 × 1728 pixel CCD; 19.6° × 14.5° FOV; 5 frames/sec; 40 signal to noise ratio (SNR) at 9% albedo, 30°solar altitude angle
Lunar Penetrating Radar (LPR)	Subsurface structure	Channel 1: 0.5, 1, 2 kHz, >100 m detecting depth; 1 m thickness resolution; Channel 2: 5, 10, 20 kHz, >30 m detecting depth; 30 cm thickness resolution
Active Particle-induced X-ray Spectrometer (APXS)	Elemental mapping	0.3–25keV energy (140 eV@5.9 keV energy resolution); 25 mm work distance; 60 mm spot size
Visible and Near-infrared Imaging Spectrometer (VNIS)	Spectral and image data from visible light to shortwave infrared	Visible: 450–950 nm, 2–6 nm spectral resolution; 8.4° × 8.4° FOV; Shortwave: 900–2400 nm, 3–11 nm spectral resolution; 2° × 2° FOV; Both had SNR 31 at 9% albedo, 45°solar altitude angle

situ analysis of mineral and chemical composition of and near the landing area; and (3) exploration of the terrestrial–lunar space environment and lunar-based astronomical observations.

Major scientific achievements based on CE3 data included:

1. The Yutu rover drove 114 meters on the ejecta blanket and photographed the rough surface and the excavated boulders of a 450 m-diameter crater. The boulder contained a substantial amount of crystals, which are most likely plagioclase and/or other mafic silicate mineral aggregates similar to terrestrial dolerite;
2. The composition of regolith derived from olivine-normative basaltic rocks is high in FeO/(FeO_tMgO) and with abundant high-Ca ferropyroxene (augite and pigeonite) plus Fe-rich olivine, indicating a new mare basalt chemical type (Ling et al. 2015; Zhang et al. 2015a,b);
3. The LPR found the regolith thickness exceeded expectations and volcano eruption lasted until 2–3 Ga (Fa et al. 2015; Xiao et al. 2015; Zhang et al. 2015a);
4. The EUVC discovered the OH free radical upper limit of the outer atmosphere of the Moon (Wang et al. 2015); and
5. A causal relationship was observed between the substorms and the formation of three bulges on the plasmasphere (He et al. 2016).

The CE3 science data products (e.g., Tan et al. 2014; Zuo et al. 2016) were released online [at http://moon.bao.ac.cn/index.jsp (in Chinese) and http://moon.bao.ac.cn/index_en.jsp (in English)].

3.11. Chang'E 4

Chang'E 4 (***CE4***) was a robotic landing mission for the second lunar surface operations stage of the Chinese lunar exploration project, and it was designed to both back up and build on the success of CE3. Prior to launch of the CE4 lander, two microsatellites were launched (Longjiang-1 and -2) along with a relay satellite, with a student-built webcam (640×480 pixels) and a radio transmitter. While Longjiang-1 did not achieve orbit, Longjiang-2 did and has returned several lunar far side views. CE4 included a lander, the Yutu 2 robotic lunar rover, and a communications relay satellite (Queqiao) to orbit at the second Earth–Moon Lagrange point (L2) (Qin et al. 2019). Launched on 7 December 2018, the relay satellite carried a contributed instrument, the lander and rover each carried four instruments (Table 12; Jia et al. 2018). CE4 landed on 3 January 2019 within Von Kármán crater in the lunar South Pole–Aitken basin on the far side. The Yutu 2 rover was deployed about 12 hours after landing. Included in the lander payload was a "mini-biosphere" capsule experiment submitted by students, with a collection of seeds, water, a nutrient solution and air, and a small camera and data transmission system. Early in the CE4 mission images of sprouted seeds were widely circulated.

Science objectives of CE4 include: 1) Conducting low-frequency radio astronomy observations from the far side for Milky Way mapping, a Very Long Baseline Interferometry (VLBI) experiment with a ground array for studies of planetary low-frequency bursts, solar coronal studies, and space weather characterization; 2) Probing shallow lunar subsurface (likely crustal) structures and characterizing regolith thickness at up to 30 m depth; 3) Exploring landform morphology, topography and mineralogy at the landing site for crater and geologic studies, mapping pyroxene, olivine, plagioclase and other rock-forming minerals. The CE4 mission combined a variety of instruments to establish a comprehensive geological profile of a lunar far side site, with integrated analysis and mapping of topography, geological structure, material composition and shallow structures of Moon's far side, and focused on establishing a more complete model of the evolution of lunar geochemistry and tectonics. One early result was the preliminary spectroscopic identification of orthopyroxene and olivine in materials in

Table 12. Chang'E 4 instruments (Jia et al. 2018).

Instrument	Goal	Capability
	Lander Instruments	
Low-Frequency Spectrometer (LFS)	Solar electric fields	Antennas mounted on three five-meter-long booms. Bandwidth: 0.1–40 MHz
Lunar Lander Neutrons and Dosimetry (LND)	Lunar surface fast neutron spectrum and thermal neutron spectrum.	Fast neutrons (2–20 MeV), Thermal neutron flux (10–104/min), Proton energy spectrum (7–30 MeV), Electron spectroscopy (60–500 keV), Alpha particle energy (7–20 MeV/n), Heavy ion energy (10–30 MeV/n), LET (0.1–430 keV/μm)
Landing Camera (LCAM)	S/C mounted descent imager. Images first acquired at ~10 frames/s, at 12 km altitude, video stream of landing site acquired.	Complementary Metal Oxide Semiconductor or CMOS sensor; 419–777 nm, 1024 × 1024 pixels, 45° FOV
Terrain Camera (TCAM)	Lander mounted color imager with 360° viewing.	Complementary Metal Oxide Semiconductor (CMOS) sensor; 420–700 nm, 2352 × 1728 pixels, ~23° × 17° FOV
	Rover Instruments	
Panoramic camera PCAM)	Color imaging of landing site and rock samples.	Two mast cameras for 360° and stereo viewing; 420–700 nm, color and panchromatic modes, 19.7° × 14.5° FOV.
Lunar Penetrating Radar (LPR)	Subsurface structure and regolith thickness	Two bands at 40–80 MHz and 250–750 MHz
Advanced Small Analyzer for Neutrals(ASAN)	Backscattered energetic neutral atom fluxes from the lunar surface	10 eV–10 keV, Institute of Space Physics, Sweden
Visible and Near-infrared Imaging Spectrometer (VNIS)	Spectral and image data (visible light to short wave to infrared) for surface mineral mapping	Visible: 450–950 nm; Short wave: 900–2400 nm; Infrared: 0.4–2.4 μm
	Relay Satellite Instrument	
Netherlands-China Low-Frequency Explorer (NCLE)	Detect radio bursts from the Sun and planets	Work frequency/spectral resolution: 100 kHz–1MHz/1 kHz; 1 MHz–10 MHz/10 kHz; 10 MHz–80 MHz/100 kHz (Radboud University, Nijmegen, Netherlands)

the floor of Von Kármán crater that were suggested to have originated from the lunar mantle (Li et al. 2019). More recently, LPR data were used to map a lunar ejecta sequence, including its thickness and internal structure (Li et al. 2020).

CE4 is still operating on the Moon. Among its technical accomplishments thus far are the historic first lunar far side landing, the first communication between the lunar far side and an orbiting satellite, the first mapping of a far side landing site, and the first sprouting of a seed

on the Moon. The lander was designed for 12 months and the rover for 3 months of operation. Data from the CE4 archive were released online (http://moon.bao.ac.cn/), with data formats following PDS guidelines (Zhang et al. 2019).

3.12. Beresheet

Beresheet was a robotic lander and rover mission from the private, Israeli SpaceIL, a non-profit that began during the Google Lunar XPrize competition (GLXP; Aharonson et al. 2019; Russell et al. 2019). Launched on 21 February 2019, Beresheet was intended to land on the lunar surface on 11 April 2019, but the main engine cut off early due to gyroscope failure and it crashed. The Beresheet payload included a magnetometer (the SpaceIL Magnetometer or SILMAG; built at University of California, Los Angeles or UCLA), a laser Lunar Retroreflector Array (LRA; built by NASA Goddard Space Flight Center) for Moon–Earth distance measurements, and a digital "time capsule" with >30 million pages of data. The planned landing site was at northern Mare Serenitatis (Aharonson et al. 2020), and surface operations were planned for two days on the lunar surface; the retroreflector was expected to continue to operate for several decades. The goal of the SILMAG investigation was to measure the crustal magnetic field on the lunar surface and of the LRA was to help determine precise localization of the landing site and support orbiting lunar spacecraft in the future by initiating the setup of a surface navigation system. SILMAG data were expected to be recorded in two modes: 10 Hz and 0.625 Hz, the latter representing 16-measurement averages of the former. In addition, six 8-megapixel CCD cameras (5 panoramic cameras and a self-pointing camera) were integrated on the spacecraft, intended to acquire images for public engagement and scientific interpretation of the landing site. Data acquisition was planned during orbit and landing trajectory, providing a unique data set at low altitude. Although the likely velocity of the crash resulted in a total loss on impact with the lunar surface, there was hope that the retroreflector survived. The LRO NAC imaged the crash site and the LRO LOLA instrument directed lasers there, but the reflector was not found.

3.13. Chandrayaan-2

On July 22, 2019, ISRO launched a second lunar mission, ***Chandrayaan-2*** (***Ch-2***), which included an orbiter, lander and solar powered rover component (Mylswamy et al. 2012; Vanitha et al. 2020). The orbiter achieved orbital insertion on 20th August 2019, and was put into a 100 km polar orbit. The spacecraft carried eight orbital scientific packages (Table 13) to study surface geology via chemical mapping (the Chandrayaan-2 Large Area Soft X-ray Spectrometer: Narendranath et al. 2014; Radhakrishna et al. 2020), mineralogy mapping (the Imaging IR Spectrometer: Chowdhury et al. 2020a), and determination of regolith structure and surface geomorphology (the Dual Frequency L and S band Synthetic Aperture Radar: Putrevu et al. 2020, the Terrain Mapping Camera-2: Chowdhury et al. 2020b, and the Orbiter High Resolution Camera: Chowdhury et al. 2020c). Two other science packages were designed to look at the electron density (Dual Frequency Radio Science experiment: Choudhary et al. 2020) and chemistry (the Chandrayaan-2 Atmospheric Compositional Explorer 2: Das et al. 2020) of the lunar ionosphere and exosphere. The Ch-2 orbiter remains active at this time.

The lander and rover, called Vikram and Pragyan, were intended to land and operate near the south pole at ~70° S (Sinha et al. 2020). The lander was equipped with a seismometer package and a NASA-provided laser retroreflector unit to become part of the Moon-wide retroreflector network (Vanitha et al. 2020). The rover was intended to last for a 14-day traverse carrying two different instruments for mapping surface chemistry including a Laser induced Breakdown Spectroscope and an Alpha Particle Induced X-ray Spectroscope (Vanitha et al. 2020). However, both vehicles were lost during descent from the spacecraft on the 6th September 2019. Data from the LROC NAC camera (see above) were used to identify the lunar crash site and debris field at 70.8810° S, 22.7840° E (http://lroc.sese.asu.edu/posts/1131).

Table 13. Chandrayaan-2 orbiter instruments (Choudhary et al. 2020: Chowdhury et al. 2020a,b,c,d; Das et al. 2020; Radhakrishna et al. 2020; Vadawale et al. 2014; Vanitha et al. 2020).

Instrument	Goal	Capability
Chandrayaan-2 Large Area Soft X-ray Spectrometer (CLASS) and Solar X-ray monitor (XSM)	Elemental composition of the lunar surface	12.5 km/pixel; 6 swept charge devices (SCDs) operating in the energy range 0.8–15 keV
Dual Frequency L and S band Synthetic Aperture Radar (DFSAR)	Mapping lunar regolith and identification of water ice at poles	Silicon Drift Detector (SDD), energy range of 1–15 keV with energy resolution ~200 eV @ 5.9 keV
Imaging IR Spectrometer (IIRS)	Mapping of minerals and OH feature in regolith	~250 channels, 0.8 μm to 5 μm spectral resolution, 80 m/pixel
Chandrayaan-2 Atmospheric Compositional Explorer 2 (ChACE-2)	Lunar exosphere	Quadrupole Mass Analyzer, mass range 1–300 amu with mass resolution of 0.5 amu
Terrain Mapping Camera-2 (TMC-2)	Surface imaging, Stereo-derived topography of the lunar surface	Panchromatic, 0.4–0.85 microns; 5 m/pixel
Radio Anatomy of Moon Bound Hypersensitive Ionosphere and Atmosphere	Studies of electron density in the lunar ionosphere	Dual Frequency Radio Science experiment: 20 MHz evacuated miniaturized crystal oscillator source, ~10–11 stability, signals at X (8496 MHz) and S (2240 MHz) band radio frequencies
Orbiter High Resolution Camera (OHRC)	Surface imaging in detail, mapping	Panchromatic, 0.4-0.8 microns; 30 cm/pixel

3.14. Chang'E 5

On November 24, 2020, CNSA launched a fifth lunar mission, ***Chang'E 5*** (***CE5***), which was a sample return mission to target relatively young mare basalts (e.g., Ling et al. 2017; Qian et al. 2021a,b), and consisted of four components: orbiter, lander, ascender, and returner (Zhou et al. 2022). The lander-ascender combination touched down in the Mons Rümker region of Oceanus Procellarum (43.06° N, 51.92° W) on 1 December 2020. The lander contained a robotic arm with a sampling scoop and a drill to collect surface and subsurface samples, respectively. With sampling complete and the samples transferred to the ascender, launch from the lunar surface occurred on December 3, 2020. The ascender docked with the Earth-return vehicle in lunar orbit on December 5, 2020 and transferred the sample container. The components undocked on December 7, 2020, with the returner landing successfully in Mongolia on December 16, 2020 (Zhou et al. 2022); these were the first samples returned from the Moon since those of Luna 24 in 1976. The ***Chang'E 5*** orbiter was successfully captured at the Sun–Earth Lagrange point 1 (L1) on March 15, 2021. It made a lunar flyby on 9 September, 2021, and at the time of writing is thought to now be in a lunar distant retrograde orbit.

The main goals of the mission were to land on the lunar surface, collect ~2 kg of lunar regolith samples from depths up to ~2 m through gathering and drilling, return the samples back to Earth, and study the samples in terrestrial laboratories. A total of 1,731 g of sample were returned. Two science objectives were also identified (Zhou et al. 2022): i) Carry out in situ exploration in sample collection area, provide the evidence to selectively collect samples and establish the connection between the data acquired on the Moon and that analyzed in the ground laboratory. ii) Conduct systematic and long-term study of the lunar samples in terrestrial laboratories, analyze the structure, physical properties and substance composition of lunar samples and research the origin and evolution history of the Moon.

Four scientific payloads were on the lander: Landing Cameras (LCAM), Panoramic Camera (PCAM), a visible and near-infrared Lunar Mineralogical Spectrometer (LMS) and Lunar Regolith Penetrating Radar (LRPR). LCAM was a complementary metal oxide semiconductor (CMOS) descent imager operating at 1 image/second in two modes: mode 1 had a 2352 × 1728-pixel image and a compression ratio of 4:1, and mode 2 had a 1024 × 1024-pixel image and a compression ratio 8:1. PCAM consisted of two CMOS color imagers spaced 270 mm apart for stereo imaging; it operated over a visible wavelength (420–700 nm) color range with a 2352 × 1728-pixel sensor. The LRPR was an ultra-wideband ground penetrating radar array with 12 bow-tie antennas and a 1 to 3 GHz operating frequency, mounted around a drill ~90 cm above the ground. The LRPR had a vertical spatial resolution of ≤ 5 cm and a detection distance of ≥ 2m (Xiao et al. 2019). The LMS covered the spectral range of 480 to 3200 nm, with a spectral resolution of 5 to 25 nm, a 3° × 3° field of view, and acousto-optic tunable filters (Cai et al. 2019). Very long baseline interferometry (VLBI) and Unified X-band (UXB) was conducted using the lander to accurately determine the position of the lander on the Moon (Wang et al. 2021).

To date, basalt ages of 1963 ± 57 million years (Che et al. 2021) and 2,030 ± 4 million years (Li et al. 2021) have been reported. A variety of evolved basaltic materials have also been identified (He et al. 2022; Qi et al. 2022), including low- and relatively high-Ti basalts, and ~120 ppm water was detected by the LMS on the lunar surface attributed to solar wind implantation (Lin et al. 2022). However, the mantle source for the Chang'E 5 basalts is considered to be relatively dry (Hu et al. 2021) and relatively free of KREEP (Tian et al. 2021).

4. FUTURE LUNAR MISSIONS: 2020 AND BEYOND

The year 2020 marked a new resurgence of lunar exploration (Table 14), with more than 25 new missions planned by the U.S. and international teams. We present a snapshot of these plans at the time of writing, but it is important to note that plans for lunar exploration are changing rapidly, the dates noted below may be delayed, and missions may come and go as circumstances change. A variety of lunar orbital, landed robotic, and human space and surface exploration scenarios are envisioned (e.g., Crawford et al. 2012; Crawford and Joy 2014; Lunar Exploration Analysis Group 2016a, 2017, 2018a,b; International Space Exploration Coordination Group 2018a,b, 2020; National Aeronautics and Space Administration 2018, 2020). The NASA Lunar Reconnaissance Orbiter (LRO) spacecraft and instrument suite are the major dedicated lunar remote sensing mission currently operating. Its current extended mission is funded through 2025, but it has the fuel to run for several years beyond that and the plan (Petro et al. 2019) is to continue the mission to gather data in support of the next generation of lunar missions.

India has plans for a series of lunar expeditions as well and ISRO has announced a Chandrayaan-3 mission in ~2023 to demonstrate lunar landing and roving capabilities. ISRO intends to partner with Japan's JAXA on a future joint polar exploration mission called the Lunar Polar Exploration (LUPEX) Mission in ~2025.

China has an active, robust, and exciting plan of lunar exploration, called China's Lunar Exploration Program (CLEP) and nicknamed the Chang'E Project, that builds on earlier and current Chang'E missions and extending well into the future. The pioneering Chang'E-4 lander and rover are meeting major exploration goals such as landing for the first time on the lunar far side, surviving multiple lunar nights, and driving across the lunar surface. The next planned missions add logical challenges: Chang'E-6 will return far side samples, Chang'E-7 will explore for ice at the lunar south pole, and Chang'E-8 will help to advance technologies for a lunar base. (Note that the numbering of these missions will depend on the success of earlier spacecraft; new missions will simply repurpose backup spacecraft for later missions.) Sometime in the 2020's, CNSA plans to develop a lunar research station, and then to establish a lunar base in 2030's (e.g., Xu et al. 2018; Zhao and Wang 2019).

Japan's JAXA has plans for new missions to the Moon to take place over the next 5 years or so. In 2023, JAXA plans to launch the Smart Lander for Investigating the Moon (SLIM) mission, a demonstration of precision landing technology (with accuracy of ±100 m; Ohtake et al. 2018). The SLIM carries one scientific instrument (a multiband camera); it is planned to land near Shioli, a small crater located northwest of Mare Nectaris on the near side (Ohtake et al. 2019). JAXA is also planning the Lunar Polar Exploration Mission (LUPEX) jointly with ISRO, which consists of a lander and a rover operating at a polar site. LUPEX is scheduled to launch in 2025. JAXA is also studying the Demonstration and Experiment of Space Technology for INterplanetary voYage Phaethon fLyby dUSt science (DESTINY+) mission as a lunar flyby on the way to study asteroid 3200 Phaethon (e.g., Krüger et al. 2019).

NASA's plans for lunar exploration are changing rapidly. In one report (National Aeronautics and Space Administration 2018), NASA has five space exploration goals: to hand over low earth orbit (LEO) operations to commercial entities; build capabilities to support lunar surface operations; send prospecting robots to the Moon; establish a new human presence on the Moon; and demonstrate how humans might get to Mars. NASA recently released its Artemis Plan (NASA 2020) which describes the architecture by which it will return humans to the lunar surface. This includes a Lunar Gateway (formerly known as the Lunar Orbital Platform-Gateway, or the Deep Space Gateway), a robotic orbiting platform designed to support lunar surface exploration and involving participation from public and private partnerships and other nations, from which other exploration may extend to the Moon's surface, Mars, and asteroid targets (National Aeronautics and Space Administration 2018). The Artemis plan includes Artemis 1, flying an uncrewed Orion capsule to lunar orbit in 2022, and Artemis 2 in 2024 which will send a crewed Orion around the Moon. These are to be followed by Artemis 3 (2025) which will send "the first woman and next man" (e.g., National Aeronautics and Space Administration 2020) to the surface of the south polar region of the Moon.

In partnership with the German Aerospace Center (DLR) and the Israel Space Agency (ISA) (in conjunction with StemRad and Lockheed Martin) Artemis 1 will carry the Matroshka AstroRad Radiation Experiment (MARE; Gaza et al. 2018) on Orion, which will measure the effects of radiation on human tissue. Secondary payloads on the Space Launch System (SLS) for Artemis 1 include thirteen small satellites (CubeSats), four of which (Table 14) will involve lunar exploration (i.e., LunaH-Map, Hardgrove et al. 2020; Lunar Ice Cube, Clark et al. 2019; LunIR, Clark 2018, and JAXA's OMOTENASHI or Outstanding MOon exploration TEchnologies demonstrated by NAnoSemi-Hard Impactor, Hashimoto et al. 2017). Lunar Flashlight, a planned CubeSat lunar orbiter mission intended to find and characterize water ice deposits on the Moon (Cohen et al. 2017, 2020), is scheduled for launch in 2023. Another NASA program, Small Innovative Missions for Planetary Exploration (SIMPLEx), selected the Lunar Trailblazer mission concept that has a lunar orbiter with instruments designed to, among other things, detect and study water on the Moon (Ehlmann et al. 2020).

The Korea Aerospace Research Institute (KARI) of South Korea is planning to launch the Korea Pathfinder Lunar Orbiter (KPLO) in 2022 to orbit the Moon for one year (Korean National Committee for COSPAR 2020; Song et al. 2021) with a payload of South Korean instruments with one U.S. contributed instrument. Objectives of KPLO are to demonstrate a "space internet," conduct scientific investigations of the lunar environment, topography, and resources, and to identify potential landing sites for future missions. The KARI instruments include a Lunar Terrain Imager (LUTI), a Wide-Angle Polarimetric Camera (PolCam) (Jeong et al. 2020), a Magnetometer (KMAG) (Shin et al. 2019), a Gamma-Ray Spectrometer (KGRS), a Delay-Tolerant Networking experiment (DTNPL). NASA's instrument is the ShadowCam imager (Robinson et al. 2017, 2022), which is a focused investigation of the Moon's permanently shadowed regions (PSRs) that will provide information about the distribution and accessibility of volatiles in PSRs. The second phase of lunar exploration currently under study by KARI is expected to include a lunar orbiter, lander, and a rover.

Table 14. Recent agency lunar missions under development or under study (e.g., ISECG 2018a).

Mission	Origin	Target Launch	Objectives
		Recent	
Artemis 1	USA	2022	Launch 4 lunar Cubesats
Lunar Polar Hydrogen Mapper (LunaH-Map)	USA	2022	Polar hydrogen mapping (CubeSat)
Lunar Ice Cube	USA	2022	Map volatiles and water across the Moon (CubeSat)
LunIR	USA	2022	Flyby for spectral and thermal mapping (CubeSat)
OMOTENASHI	Japan	2022	CubeSat lunar impactor (spacecraft failure)
Korea Pathfinder Lunar Orbiter (KPLO)	Korea	2022	Lunar orbiter, 6 science payloads
Lunar Flashlight	USA	2022	Map South Polar volatiles in shadowed craters (CubeSat)
Chandrayaan-3	India	2023	Lunar rover, lander
Smart Lander for Investigating the Moon (SLIM)	Japan	2023	Precision landing, mineralogy of landing site
Luna 25	Russia	2023	Soft lander, south pole (failed)
		Under development	
Lunar TrailBlazer	USA	2024	Orbiter
Volatiles Investigating Polar Exploration Rover (VIPER)	USA	2024	Lunar polar water, drilling (CLPS)
Artemis 2	USA	2024	Test of Orion spacecraft on lunar trajectory (crewed)
Chang'E-6	China	2024	Soft lander (far side), sample return
DESTINY+	Japan–Germany	2025	Lunar flyby, solar electric propulsion demonstration
Lunar Gateway	USA	2025	Multipurpose orbiting platform to support lunar surface exploration
Lunar Polar Exploration Mission (LUPEX) or Chandrayaan-4	Japan/India	2026 (latest)	Lunar polar water
Artemis 3	USA	2025	Lunar landing (crewed)
Chang'E-7	China	2026	Soft lander (lunar south polar site), search for water ice
		Under study	
ISRU demonstration mission 1	ESA	2025?	Prospect for potential lunar resources
Luna 26	Russia/China	2027?	Orbiter
Luna 27	Russia/ESA	2028?	Soft lander (south pole)
Chang'E-8	China	2028?	Soft lander (far side, SPA site) to test technologies for base construction
ISRU demonstration mission 2	ESA	2028?	Demonstrate end to end production of oxygen or water
Orel	Russia	2029?	Lunar orbit (crewed)
Luna 28	Russia/ESA	2030? (earliest)	Soft lander (South Polar), sample return

Following the successful Luna 24 sample-return mission in 1976, Russia plans to launch a series of orbiters and landers starting in 2023 with Luna 25 (Mitrofanov et al. 2012: Djachkova et al. 2017), a lander designed to land at the lunar south pole and analyze regolith in situ. Reports from the Russian Space Research Institute indicate that Luna 26 will be an orbiter to study the Moon from a 50 to 100 km altitude, and Luna 27 will be a south polar lander that may involve a drill and sampling device. Luna 28 is planned to be a sample return mission from a south polar site. A new spacecraft, Orel, is also under development to support crew in space; a 2025 test flight is planned.

The Director General of the European Space Agency (ESA) has advocated for a "Moon Village" (Wörner and Foing 2016; Crawford 2017), a vision of collaborative activity at the Moon by diverse actors, including public and private, for multiple uses by multiple users. ESA's plans for human and robotic exploration activities at the Moon are focused on delivering science and societal benefits through international cooperation on missions with international and commercial partners. ESA is providing the European Service Module to NASA's Orion crewed vehicle and plans to contribute to the Lunar Gateway. ESA is providing the Package for Resource Observation and in-Situ Prospecting for Exploration, Commercial exploitation and Transportation (PROSPECT). This package to access and assess potential resources on the Moon and to prepare technologies that may be used to extract these resources in the future. PROSPECT's drill (ProSEED) will acquire samples from the subsurface that will be passed to the chemical laboratory (ProSPA) where they will be heated to extract any cold-trapped volatiles (Barber et al. 2019; Sefton-Nash et al. 2019). ESA is collaborating with Surrey Satellite Technologies to deliver a commercial communications relay service at the Moon, provide payloads to partner led missions and develop an ESA cargo lander capability in the late-2020s. An In Situ Resource Utilization (ISRU) preparation campaign (Carpenter et al. 2016; Binns et al. 2018) is also being studied, using commercially procured landers and rovers to prospect potential resources and test technologies to allow ISRU to be implemented in future human missions.

In 2018 NASA initiated the Commercial Lunar Payload Services (CLPS) program to spur the market for commercial delivery of payloads to the lunar surface. There are currently 14 companies on the CLPS catalog who can compete for a delivery when NASA releases a delivery task order. These task orders state the payload that NASA wants delivered as well as other pertinent information such as desired landing location, and instrument interfaces and operational requirements. NASA plans to conduct approximately two CLPS deliveries per year, beginning in 2021. To date, four CLPS delivery task orders have been awarded (Table 14). In 2021 Astrobotic will carry 11 payloads to Lacus Mortis on the central near side of the Moon, and Intuitive Machines will carry five payloads to Oceanus Procellarum on the western near side. In December 2022 Masten Space Systems is scheduled to deliver 9 payloads to lunar south pole. NASA's Volatiles Investigating Polar Exploration Rover (VIPER) rover will also be delivered by a CLPS company, with Astrobotic chosen to deliver VIPER to the lunar south pole in 2023.

In addition to CLPS, other companies have expressed an intention to offer customers the ability to have payloads delivered to the lunar surface. A Japanese company, iSpace, currently has two missions planned (Table 15).

5. NEXT STEPS TO THE MOON

We have outlined the instruments and capabilities of lunar missions operating since 2006, and briefly summarized their major exploration and scientific results. Details of these results can be found in the chapters to follow.

It is clear that the world's space agencies and many private engineering teams are serious about returning to the Moon and staying there. The 27 international space agencies/organizations participating in the International Space Exploration Coordination Group (ISECG) advanced a

Table 15. Private and/or agency partnership lunar missions, recent and under development

Lander / Mission	Origin	Target Launch	Objectives
	Recent		
Hakuto-R Mission 1	iSpace (Japan)	2022	Lunar lander
	Under development		
Peregrine	Astrobotic Technology (USA)	2023	CLPS Lander (Gruithuisen)
Griffin lander / VIPER	Astrobotic Technology (USA)	2024	CLPS South polar rover
Nova-C (IM1)	Intuitive Machines	2024	CLPS South Pole
Nova-C (IM2 or PRIME-1)	Intuitive Machines	2024	CLPS Lander (lunar south pole)
Nova-C (IM3)	Intuitive Machines	2024	CLPS Lander (Reiner Gamma)
Blue Ghost (M1)	Firefly Aerospace	2024	CLPS Lander (Mare Crisium)
Hakuto-R Mission 2	iSpace (Japan)	2024	Lunar lander, rover
Blue Ghost (M2)	Firefly Aerospace	2026	CLPS Lander

long-range international exploration strategy to expand human presence into the Solar System, as outlined in the Global Exploration Roadmap (GER; ISECG 2018a). To facilitate human and robotic exploration of destinations where humans may one day live and work, the roadmap lays out future exploration plans beginning with the International Space Station, proceeding to the Moon, and leads to human missions to explore Mars. In consultation with the Global Science Community, ISECG also prepared a report describing the science enabled by the Global Exploration Roadmap (ISECG 2018b) and in 2020 a supplement was issued as an update to the GER plan (ISECG 2020).

A widely acknowledged report prepared in the USA by the National Research Council (National Research Council or NRC 2007) described major scientific areas for research on the Moon and has been the basis of several more recent activities by the lunar science community, organized through the Lunar Exploration Analysis Group (LEAG 2016a,b, 2018a,b), to characterize our current understanding of lunar science and to outline the next logical steps for exploration of the Moon. These discussions addressed lunar science in 8 key areas:

1. Bombardment history of the inner Solar System;
2. Structure and composition of the lunar interior and lunar evolution;
3. Planetary surface processes and the nature of lunar crustal rocks;
4. The lunar polar environments and volatile flux in the Solar System;
5. Lunar volcanism and the compositional and thermal history of the Moon;
6. Impact processes, their manifestation, ages and evolution of planetary surfaces;
7. Regolith development and evolution; and
8. The lunar atmosphere and dust environment.

Many recent achievements in lunar science and exploration were recognized by a LEAG team in 2016 and remaining "strategic knowledge gaps" (SKGs) were identified (LEAG 2016b) as major near-term goals of a lunar human exploration strategy. The next follow-up LEAG report (LEAG 2018a) outlined the progress made towards achieving the goals of the 2007 NRC report. Although it was acknowledged that significant progress has been made in all key research areas (listed below), none of these goals are thought to be "complete" and so are not eligible to be retired.

1. Progress on understanding the bombardment history of the inner Solar System requires surface exploration, including in situ dating of samples and the return of samples for more sophisticated analysis. Comprehensive modeling is needed to tie data from such studies to specific lunar sites through compositional analysis of impact melts, petrology and geochemistry investigations, and detailed geochronology of impact melt samples.
2. Progress in expanding our knowledge of planetary differentiation can be made by the emplacement of instruments such as a simultaneous, globally distributed seismic and heat flow network and/or an expanded retroreflector network, as well as strategic collection of samples from terrains of different ages that can provide constraints on lunar geochemistry and new information on the history of the lunar dynamo.
3. Lunar crustal studies can be advanced through acquisition of compositional information at higher spatial resolutions, the return of samples from high-priority targets, in situ elemental and mineralogical analyses as well as regional seismic networks to determine vertical structure, and geologic fieldwork by astronauts.
4. The lunar polar environments are key to understanding the volatile flux over the latter part of Solar System history, but a better understanding volatile source(s), their detailed compositions, and the ancient solar environment, will require in situ analyses and the return of cryogenically preserved samples.
5. Advances in understanding planetary volcanism would come from subsurface sounding, sample return from deposits such as the youngest and oldest basalts and pyroclastic deposits, in situ elemental and mineralogical analyses, and astronaut field work that could include core drilling, active subsurface sounding, and sampling of a complete sequence of basalt flows.
6. Lunar impact processes could be addressed by studies of large-scale melt deposits at older basins, the establishment of regional seismic networks at multi-ringed basins, field studies and sample return from impact melt sheets and peak rings, and long-duration orbital observations.
7. Improved characterization of regolith processes and weathering on airless bodies would come from sounding to reveal the upper stratigraphy of the regolith, sample return from ancient stratigraphically preserved regoliths and from paleoregoliths, and by in situ analyses and targeted sample return from areas such as lunar swirls.
8. Investigations of the lunar atmosphere and dust environment identification of the sources of mid-latitude surface hydroxyl and water, determination of whether hydrogen products migrate poleward to the cold trap reservoirs, exploration of the near-surface electrostatic lofting of dust associated with plasma anomalies/voids in locations such as polar craters, magnetic anomalies, and the night-side terminator, systematic detection of trace volatile species (e.g., water, OH, hydrocarbon) in the exosphere.
9. Several new encompassing research concepts also were identified for future research, including the lunar volatile cycle, the origin of the Moon, and lunar tectonism and seismicity.
10. Finally, establishing a robust capability for lunar surface access and operations will enable advances in areas such as radio astronomy, through emplacement of a radio telescope on the lunar far side by robots and/or human explorers.

The second follow-up LEAG report (LEAG 2018b) expanded on the first report and addressed the next steps to be made to return to the Moon with robots in the next 5 years

and developed concepts for future lunar exploration missions. The same key lunar science questions provided an exploration focus, especially as they enable missions such as those addressing sample return (a theme that appears repeatedly), rover surface operations, and landed instrument packages. The opportunity for commercial synergies was also recognized, with several key contributions highlighted:

1. Providing communications relay services in support of surface exploration, surface delivery services, sample return missions, and base stations supporting communications, power, and other utilities to surface assets.

2. Utilization of the current orbiter, LRO, for supporting site selection and surface operations is vital.

3. New orbital missions would provide global compositional mapping at multiple wavelengths and at higher resolution than have previous missions, maps of major and minor elements via X-ray spectrometry and of hydrogen and other volatiles through bi-static radar and laser instruments, subsurface exploration through impactors, as well as relay satellites and navigational support.

4. Landed missions would support in situ studies of volatiles, plasma and electrical properties at the poles and, through a seismic network, a characterization of the lunar interior.

5. Missions with rovers and hoppers would contribute significantly to a host of lunar science and exploration objectives, through support of studies of features such as magnetic anomalies, lava tubes, the youngest basalts, thrust faults, and in situ age dating of key stratigraphic layers on the Moon.

In conclusion, the advances in scientific knowledge arising from recent lunar missions, reanalysis of older data, modeling, and sample analysis have produced dramatic results, leading to new questions about the nature, origin, and evolution of the Moon. As described in the pages that follow, the lunar science and exploration communities continue active research and analysis of data from these recent and legacy missions, the returns from Apollo and Luna samples, and those from lunar meteorites. Further progress will depend on the implementation of new robotic and human missions to the Moon as a new era of lunar exploration begins.

REFERENCES

Aharonson O, Garrick-Bethel I, Grosz A, Head JW, Russell CT, Smith DE, Weiss BP, Wieczorek M (2019) The science mission of the SpaceIL lunar lander. 50th Lunar Planet Sci Conf, abstract # 2290

Aharonson O, Russell CT, Head JW, Wieczorek M, Garrick-Bethel I, Weiss BP, Smith DE, Rowe K, Gomez A, Grosz A, Amrusi S, Novoselsky A, Nahaman N, Grossman Y, Shimoni Y (2020) The science mission of SpaceIL's Beresheet lander: Plans and results. 51st Lunar Planet Sci Conf, abstract # 1267

Anand M, Tartèse R, Barnes JJ (2014) Understanding the origin and evolution of water in the Moon through lunar sample studies. Phil Trans R Soc A 372:20130254

Andrews-Hanna JC, Asmar SW, Head JW, Kiefer WS, Konopliv AS, Lemoine FG, Matsuyama I, Mazarico E, McGovern PJ, Melosh HJ, Neumann GA, Nimmo F, Phillips RJ, Smith DE, Solomon SC, Taylor GJ, Wieczorek MA, Williams JG, Zuber MT (2013) Ancient igneous intrusions and the early expansion of the Moon revealed by GRAIL gravity gradiometry. Science 339:675–678

Andrews-Hanna JC, Weber RC, Garrick-Bethell I, Evans AJ, Kiefer WS, Grimm RE, Keane JT, Laneuville M, Ishihara Y, Kamata S, Matsuyama I (2023) The structure and evolution of the lunar interior. Rev Mineral Geochem 89:243–292

Angelopoulos V (2008) The THEMIS mission. Space Sci Rev 141:5–34

Angelopoulos V (2010) The ARTEMIS mission. Space Sci Rev 165:3–25

Angelopoulos V, Sibeck,D, Carlson CW, McFadden JP, Larson D, Lin RP, Bonnell JW, Mozer FS, Ergun R, Cully C, Glassmeier KH, Auster U, Roux A, LeContel O, Frey S, Phan T, Mende S, Frey H, Donovan,E, Russell CT, Strangeway R, Liu J, Mann I, Rae J, Raeder J, Li X, Liu W, Singer HJ, Sergeev VA, Apatenkov S, Parks G, Fillingim M, Sigwarth J (2008) First Results from the THEMIS Mission. Space Sci Rev 141:453–476

Araki H, Tazawa S, Noda H, Ishihara Y, Goossens S, Sasaki S, Kawano N, Kamiya I, Otake H, Oberst J, Shum C (2009) Lunar global shape and polar topography derived from Kaguya-LALT laser altimetry. Science 323:897–900

Araki H, Noda H, Tazawa S, Ishihara Y, Goossens S, Sasaki S (2013) Lunar laser topography by LALT on board the KAGUYA lunar explorer: Operational history, new topographic data, peak height analysis of laser echo pulses. Adv Space Res 52:262–271

Asmar SW, Konopliv AS, Watkins MM, Williams JG, Park RS, Kruizinga G, Paik M, Yuan D-N, Fahnestock E, Strekalov D, Harvey N, Lu W, Kahan D, Oudrhiri K, Smith DE, Zuber MT (2013) The scientific measurement system of the Gravity Recovery and Interior Laboratory (GRAIL) mission. Space Sci Rev 178:25–55

Auster HU, Glassmeier H, Magnes W, Aydogar O, Constantinescu D, Fischer,D, Fornacon KH, Georgescu E, Harvey P, Hillenmaier O, Kroth R, Ludlam M, Narita Y, Okrafka K, Plaschke F, Richter I, Schwarzi H, Stoll B, Valavanoglu A, Wiedemann M (2008) The THEMIS fluxgate magnetometer. Space Sci Rev 141:235–264

Ban C, Zhen Y, Zhang F, Zhu Y, Zou Y (2014) Element abundances in Oceanus Procellarum: Data analysis of Chang'E-2 X-ray spectrometry. Earth Sci Front 21:62–73 (in Chinese)

Bandfield JL, Ghent RR, Vasavada AR, Paige DA, Lawrence SJ, Robinson MS (2011) Lunar surface rock abundance and regolith fines temperatures derived from LRO Diviner Radiometer data. J Geophys Res 116:E00H02

Bandfield JL, Cahill JTS, Carter LM, Neish CD, Patterson GW, Williams J-P, Paige DA (2017) Distal ejecta from lunar impacts: Extensive regions of rocky deposits. Icarus 283:282–299

Banks ME, Watters TR, Robinson MS, Tornabene LL, Tran T, Ojha L, Williams NR (2012) Morphometric analysis of small-scale lobate scarps on the Moon using data from the Lunar Reconnaissance Orbiter. J Geophys Res 117:E00H11

Barber SJ, Wright IP, Abernethy F, Anand M, Dewar KR, Hodges M, Landsberg P, Leese MR, Morgan GH, Morse AD, Mortimer J, Sargeant HM, Sheard I, Sheridan S, Verchiovsky A, Goesmann F, Howe C, Morse T, Lillywhite N, Quinn A, Missaglia N, Pedrali M, Reiss P, Rizzi F, Rusconi A, Savoia M, Zamboni A, Merrifield JA, Gibson EK, Carpenter J, Fisackerly R, Houdou B, Sefton-Nash E, Trautner R (2019) ProSPA: Analysis of lunar polar volatiles and ISRU demonstration on the Moon. Lunar Planet Sci Conf 49:2172

Barker M, Mazarico E, Neumann G, Zuber M, Haruyama J, Smith DE (2016) A new lunar digital elevation model from the Lunar Orbiter laser altimeter and SELENE Terrain Camera. Icarus 273:346–355

Barkin YV, Hanada H, Matsumoto K, Sasaki S, Barkin MY (2014) Effects of a physical librations of the moon caused by a liquid core, and determination of the fourth mode of a free libration. Solar Syst Res 48:403–419

Basilevsky AT, Keller HU, Nathues A, Mall U, Hiesinger H, Rosiek M (2004) Scientific objectives and selection of targets for the SMART-1 Infrared Spectrometer (SIR). Planet Space Sci 52:1261–1285

Belton MJS, Klaasen KP, Clary MC, Anderson JL, Anger CD, Carr MH, Chapman CR, Davies ME, Greeley R, Anderson D, Bolef LK, Townsend TE, Greenberg R, Head JW III, Neukum G, Pilcher CB, Veverka J, Gierasch PJ, Fanale FP, Ingersoll AP, Masursky H, Morrison D, Pollack JB (1992a) The Galileo solid-state imaging experiment. Space Sci Rev 60:413–455

Belton MJS, Head JW III, Pieters CM, Greeley R, McEwen AS, Neukum G, Klaasen KP, Ander CD, Carr MH, Chapman CR, Davies ME, Fanale FP, Gierasch PJ, Greenberg R, Ingersoll AP, Johnson T, Paczkowski B, Pilcher CB, Veverka JP (1992b) Lunar impact basins and crustal heterogeneity: New western limb and far side data from Galileo. Science 255:570–576

Benna M, Mahaffy PR, Halekas JS, Elphic RC, Delory GT (2015a) Variability of helium, neon, and argon in the lunar exosphere as observed by the LADEE NMS instrument. Geophys Res Lett 42:3723–3729

Benna M, Hurley DM, Stubbs TJ, Mahaffy PR, Elphic RC (2015b) Observations of meteoroidal water in the lunar exosphere by the LADEE NMS instrument. Annual meeting of the Lunar Exploration Analysis Group, abstract # 2059

Besse S, Yokota Y, Boardman J, Green R, Haruyama J, Isaacson P, Mall U, Matsunaga T, Ohtake M, Pieters C, Staid M, Sunshine J, Yamamoto S (2013a) One Moon, many measurements II: Photometric corrections. Icarus 226:127–139

Besse S, Sunshine J, Staid M, Boardman J, Pieters C, Guasqui P, Malaret E, McLaughlin S, Yokota Y, Li J-Y (2013b) A visible and near-infrared photometric correction for Moon Mineralogy Mapper (M^3). Icarus 222:229–242

Bhandari N (2005) Chandrayaan-1: Science goals. J Earth Syst Sci 114:701–709

Bhandari N, Srivastava N (2014) Active Moon: evidences from Chandrayaan-1 and the proposed Indian missions. Geosci Lett 1:1–11

Binder AB (1998) Lunar Prospector: An overview. Science 281:1475–1476

Binns D, Hufenbach B, Borggräfe A, Carpenter J, Lindner R, Cipriano A, Landgraf M, Schonenberg R (2018) Lunar In-Situ Resource Utilisation (ISRU) demonstration mission activities in ESA's Exploration Envelop Programme (E3P). 69th Int Aeronaut Congress, paper 46742

Blanchette-Guertin J-F, Johnson CL, Lawrence JF (2012) Investigation of scattering in lunar seismic coda. J Geophys Res 117:E06003

Blewett DT, Lucey PG, Hawke BR, Jolliff BL (1997) Clementine images of the lunar sample return stations: Refinement of FeO and TiO_2 mapping techniques. J Geophys Res 102(E7):16319–16325

Blewett DT, Zheng Y-C, Chan KL, Hu G, Neish C, Tsang KT, Zhu Y-C (2018) Chang'E-2 microwave brightness temperature maps of the Moon. 49th Lunar Planet Sci Conf, abstract # 1228

Boardman JW, Pieters CM, Green RO, Lundeen SR, Varanasi P, Nettles J, Petro N, Isaacson P, Besse S, Taylor LA (2011) Measuring moonlight: An overview of the spatial properties, lunar coverage, selenolocation, and related Level 1B products of the Moon Mineralogy Mapper. J Geophys Res 116:E00G14

Bonnell JW, Mozer FS, Delory GT, Hull AJ, Ergun RE, Cully CM, Angelopoulos V, Harvey PR (2008) The Electric Field Instrument (EFI) for THEMIS. Space Sci Rev 141:303–341

Boroson DM, Robinson BS (2014) The lunar laser communication demonstration: NASA's first step toward very high data rate support of science and exploration missions. *In:* Elphic R, Russell C (eds) The Lunar Atmosphere And Dust Environment Explorer Mission (LADEE). Springer, Cham, p 115–128

Borst A, Foing BH, Davies GR, van Westenren W (2012) Surface mineralogy and stratigraphy of the lunar South Pole-Aitken basin determined from clementine UV/VIS and NIR data. Planet Space Sci 68:76–85

Braden SE, Stopar JD, Robinson MS, Lawrence SJ, van der Bogert CH, Hiesinger H (2014) Evidence for basaltic volcanism on the Moon within the past 100 million years. Nat Geosci 7:787–791

Broschart SB, Chung M-K J, Hatch SJ, Ma JH, Sweetser TH, Weinstein-Weiss SS, Angelopoulos V (2009) Preliminary trajectory design for the ARTEMIS lunar mission. 2009 AAS/AIAA Astrodynamics Specialists Meeting, Pittsburgh, PA. AAS Paper 09–382

Bugiolacchi R, Mall U, Bhatt M, McKenna-Lawlor S, Ullaland K (2013) From the Imbrium Basin to crater Tycho: The first regional spectral distribution map derived from SIR-2 near-infrared data. Icarus 223:804–818

Bussey DBJ, Spudis PD, Robinson MS (1999) Illumination conditions at the lunar south pole. Geophys Res Lett 26:1187–1190

Cahill JTS, Thomson BJ, Patterson GW, Bussey DBJ, Neish CD, Lopez NR, Turner FS, Aldridge T, McAdam M, Meyer HM, Raney RK, Carter LM, Spudis PD, Hiesinger H, Pasckert JH (2014) The Miniature Radio Frequency instrument's (Mini-RF) global observations of Earth's Moon. Icarus 243:173–190

Cai T, Chunlai L, He Z, Ren X, Liu B, Xu R (2019) Experimental ground validation of spectral quality of the Chang'E-5 lunar mineralogical spectrometer. Spectrosc Spectral Anal 39:257–262

Carlson RW, Weissman PR, Smythe WD, Mahoney JC (1992) Near-infrared mapping spectrometer experiment on Galileo. Space Sci Rev 60:457–502

Carpenter J, Fisackerly R, Houdou B (2016) Establishing lunar resource viability. Space Policy 37:52–57

Chauhan P, Kaur P, Prof A, Kumar ASK (2012) Lunar geosciences using Chandrayaan-1: Indian perspective. Proc Ind Nat Sci Acad 78:239–247

Che X, Nemchin A, Liu D, Long T, Wang C, Norman MD, Joy KH, Tartèse R, Head J, Jolliff B, Snape JF, Neal CR, Whitehouse MJ, Crow C, Bendix G, Jourdan F, Yang Z, Yang C, Liu J, Xie S, Bao Z, Fan R, Li D, Li Z, Webb SG (2021) Age and composition of young basalts on the Moon, measured from samples returned by Chang'e-5. Science 374:887–890

Chen B, Song KF, Li ZH, Wu QW, Ni QL, Wang XD (2014) Development and calibration of the Moon-based EUV camera for Chang'E-3. Res Astron Astrophys 14:1654–1663

Chen J, Ling Z, Li B, Sun L, Zhang J, Liu J (2016) The distribution of lunar iron revealed by Chang'E-2 gamma ray spectrometer. Scientia Sinica Phys Mech Astronom 46:029605 (in Chinese)

Chin G, Brylow S, Foote M, Garvin J, Kasper J, Keller J, Litvak M, Mitrofanov I, Paige D, Raney K, Robinson MS, Sanin A, Smith DE, Spence H, Spudis P, Stern SA, Zuber M (2007) Lunar Reconnaissance Orbiter overview: The instrument suite and mission. Space Sci Rev 129:391–419

Cho Y, Morota T, Haruyama J, Yasui M, Hirata N, Sugita S (2012) Young mare volcanism in the Orientale region contemporary with the Procellarum KREEP Terrain (PKT) volcanism peak period ~2 billion years ago. Geophys Res Lett 39:L11203

Choudhary RK, Bindu KR, Harshit K, Karkara R, Ambili KM, Pant TK, Shenoy D, Kumar C, Reddy N, Rajendran TK, Nazer M (2020) Dual Frequency Radio Science experiment onboard Chandrayaan-2: a radio occultation technique to study temporal and spatial variations in the surface-bound ionosphere of the Moon. Curr Sci 118:210–218

Chowdhury AR, Banerjee A, Joshi SR, Dutta M, Kumar A, Bhattacharya S, Amitabh SU, Rehman SU, Bhati S, Karelia JC, Biswas A (2020a) Imaging infrared spectrometer onboard Chandrayaan-2 orbiter. Curr Sci 118:368–375

Chowdhury AR, Pate VD, Joshi SR, Arya AS, Kumar A, Paul S, Shah D, Soni P, Karelia JC, Sampat M, Sharma S (2020b) Terrain mapping camera-2 onboard Chandrayaan-2 orbiter. Curr Sci 118:566–572

Chowdhury AR, Saxena M, Kumar A, Joshi SR, Amitabh AD, Dagar A, Mittal M, Kirkire S, Desai J, Shah D, Karelia JC (2020c) Orbiter high resolution camera onboard Chandrayaan-2 orbiter. Curr Sci 117:560–565

Clark RN (2009) Detection of adsorbed water and hydroxyl on the Moon. Science 326:562–564

Clark PE (2018) Cubesats in cislunar space. Small Satellite Conf 2018, https://core.ac.uk/download/pdf/220135796.pdf

Clark RN, Pieters CM, Green RO, Boardman JW, Petro NE (2011) Thermal removal from near-infrared imaging spectroscopy data of the Moon. J Geophys Res 116:E00G16

Clark PE, Malphrus B, Brown K, Fite N, Schabert J, McNeil S, Brambora C, Young J, Patel D, Hurford T, Folta D, Mason P (2019) Lunar Ice Cube: ongoing development of first generation deep space CubeSat mission with compact broadband IR spectrometer. Proc SPIE 11131, CubeSats SmallSats Rem Sens III 1113108

Cohen B, Hayne PO, Greenhagen BT, Paige DA, Camacha JM, Crabtree K, Paine C, Sellar RG (2017) Payload design for the Lunar Flashlight Mission. Lunar Planet Sci Conf 48:1709

Cohen B, Hayne PO, Greenhagen BT, Paige DA, Seybold C, Baker J (2020) Lunar flashlight: Illuminating the lunar south pole. IEEE Aerosp Electron Syst Mag 35:46–52

Colaprete A, Schultz P, Heldmann J, Wooden D, Shirley M, Ennico K, Hermalyn B, Marshall W, Ricco A, Elphic RC, Goldstein D, Summy D, Bart GD, Asphaug E, Korycansky D, Landis D, Sollitt L (2010) Detection of water in the LCROSS ejecta plume. Science 330:463–468

Colaprete A, Elphic RC, Heldmann J, Ennico K (2012) An overview of the Lunar Crater Observation and Sensing Satellite (LCROSS). Space Sci Rev 167:3–22
Colaprete A, Vargo K, Shirley M, Landis D, Wooden D, Karcz J, Hermalyn B, Cook A (2014) An overview of the LADEE ultraviolet-visible spectrometer. Space Sci Rev 63–91
Colaprete A, Sarantos M, Wooden DH, Stubbs TJ, Cook AM, Shirley M (2016) How surface composition and meteoroid impacts mediate sodium and potassium in the lunar exosphere. Science 351:249–252
Coombs CR, Hawke BR (1992) A search for intact lava tubes on the Moon: Possible lunar base habitats. 2nd Confe on Lunar Bases and Space Activities of the 21st Century, NASA Conf Publ NASA CP-3166 1:219–229
Cosgrove D, Frey S, Folta D, Woodard M, Woodfork M, Marchese J, Owens B, Gandhi S, Bester M (2010) Navigating THEMIS to the ARTEMIS Low-Energy Lunar Transfer Trajectory, Proc AIAA 2010 SpaceOps Conf, Huntsville, AL. AIAA 2010–2352
Crawford IA (2017) Why we should build a Moon Village. Astron Geophys 58:6.18–6.21
Crawford IA, Joy KH (2014) Lunar exploration: Opening a window into the history and evolution of the Earth–Moon system. Philos Trans R Soc A (Origin of the Moon) 372:20130315
Crawford IA, Anand M, Cockell CS, Falcke H, Green DA, Jaumann R, Wieczorek MA (2012) Back to the Moon: the scientific rationale for resuming lunar surface exploration. Planet Space Sci 74:3–14
Crawford IA, Anand M, Barber S, Cowley A, Crites S, Fa W, Flahaut J, Gaddis LR, Greenhagen B, Haruyama J, Hurley D, McLeod CL, Morse A, Neal CR, Sargeant H, Sefton-Nash E, Tartèse R (2023) Lunar resources. Rev Mineral Geochem 89:829–868
Cully CM, Ergun RE, Stevens K, Nammari A, Westfall J (2008) The THEMIS digital fields board. Space Sci Rev 141:343–355
Das TP, Thampi SV, Dhanya MB, Naik N, Sreelatha P, Pradeepkumar P, Padmanabhan GP, Sundar B, Vajja DP, Nandi A, Thampi RS (2020) Chandra's Atmospheric Composition Explorer-2 onboard Chandrayaan-2 to study the lunar neutral exosphere. Curr Sci 118:202–209
Denevi BW, Robinson MS, Boyd AK, Sato H, Hapke BW, Hawke BR (2014) Characterization of space weathering from Lunar Reconnaissance Orbiter Camera ultraviolet observations of the Moon. J Geophys Res Planets 119:976–997
Djachkova MV, Litvak ML, Mitrofanov IG, Sanin AB (2017) Selection of Luna-25 landing sites in the south polar region of the Moon. Solar Syst Res 51:185–195
Ehlmann B, Klima RL, Bennett L, Blaney D, Bowles N, Calcutt S, Cannella M, Dickson J, Donaldson Hanna K, Edwards CS, Evans R, Frazier W, Green R, Helou G, House MA, Howe C, Morotta B, Miura J, Pieters C, Sampson M, Scire E, Schindhelm R, Seybold C, Shirley K, Thomson D, Troelzsh J, Warren T, Weinberg J (2020) Directly measuring the distribution of surface hydroxyl water on the moon with Lunar Trailblazer: A pioneering smallsat for lunar water and lunar geology. Lunar Planet Sci Conf 51:1956
Elardo SM, Pieters CM, Dhingra D, Donaldson Hanna KL, Glotch TD, Greenhagen BT, Gross J, Head JW, Jolliff BL, Klima RL, Magna T, McCubbin FM, Ohtake M (2023) The evolution of the lunar crust. Rev Mineral Geochem 89:293–338
Eliason E, Isbell C, Lee E, Becker T, Gaddis L, McEwen A, Robinson M (1999) Mission to the Moon: The Clementine UVVIS Global Lunar Mosaic, PDS Volumes USA_NASA_PDS_CL_4001-4078, https://pds-imaging.jpl.nasa.gov/data/clem1-l-u-5-dim-uvvis-v1.0/cl_4040/document/volinfo.htm
Elphic RC, Delory GT, Hine BP, Mahaffy PR, Horányi M, Colaprete A, Benna M, Noble SK (2014) The Lunar Atmosphere and Dust Environment Explorer mission. Space Sci Rev 185:3–25
Ennico K, Shirley M, Colaprete A, Osetinsky L (2012) The Lunar Crater Observation and Sensing Satellite (LCROSS) payload development and performance inflight. Space Sci Rev 167:23–69
Fa W, Eke VR (2018) Unravelling the mystery of lunar anomalous craters using radar and infrared observations. J Geophys Res Planets 123:2119–2137
Fa W, Jin YQ (2010a) Global inventory of helium-3 in lunar regolith estimated by multi-channel microwave radiometer on Chang'E-1. Chin Sci Bull 55:4005–4009
Fa W, Jin YQ (2010b) Analysis of microwave brightness temperature of lunar surface and inversion of regolith layer thickness: primary results from Chang-E 1 multi-channel radiometer observation. Icarus 207:605–615
Fa W, Zhu M-H, Liu T, Plescia JB (2015) Regolith stratigraphy at the Chang'E-3 landing site as seen by lunar penetrating radar. Geophys Res Lett 42:10,179–10,187
Fang T, Fa W (2014) High frequency thermal emission from the lunar surface and near surface temperature of the Moon from Chang'E-2 microwave radiometer. Icarus 232:34–53
Fang GY, Zhou B, Ji YC, Zhang QY, Shen SX, Li YX, Guan HF, Tang CJ, Gao YZ, Lu W, Ye SB, Han HD, Zheng J, Wang SZ (2014) Lunar penetrating radar onboard the Chang'E-3 mission. Res Astron Astrophys 14:1607–1622
Feldman WC, Barraclough BL, Fuller KR, Lawrence DJ, Maurice S, Miller MC, Prettyman TH, Binder AB (1999) The Lunar Prospector gamma-ray and neutron spectrometers. Nucl Instrum Methods Phys Res A 422:562–566
Feldman WC, Maurice S, Lawrence DJ, Little RC, Lawson SL, Gasnault O, Wiens RC, Barraclough BL, Elphic RC, Prettyman TH, Steinberg J, Binder AB (2001) Evidence for water ice near the lunar poles. J Geophys Res 106(E10):23231–23251

Feng JQ, Liu J-J, He F, Yan W, Ren X, Tan X, He L-P, Chen B, W Zuo, Wen W-B, Su Y, Zou Y-L, Li C-L (2014) Data processing and initial results from the CE3 extreme ultraviolet camera. Res Astron Astrophys 14:1664–1673

Foing BH, Heather DJ, Almeida M and the SMART-1 science technology working team (2001) The science goals of ESA's SMART-1 Mission to the Moon. Earth Moon Planets 85/86:523–531

Foing BH, Racca GD, Marini A, Evrard,E, Stagnaro L, Almeida M, Koschny D, Frew D, Zender J, Heather J, Grande M, Huovelin J, Keller HU, Nathues A, Josset J, Malkki A, Schmidt W, Noci G, Birkl R, Iess L, Sodnik Z, McManamon P (2006) SMART-1 mission to the Moon: Status, first results and goals. Adv Space Res 37:6–13

Folta D, Woodard M, Howell K, Patterson C, Schlei W (2011) Applications of multi-body dynamical environments: The ARTEMIS transfer trajectory design. Acta Astronaut 73:237–249

Folta DC, Pavlak TA, Haapala AF, Howell KC, Woodard MA (2014) Earth–Moon libration point orbit stationkeeping: Theory, modeling, and operations. Acta Astronaut 94:421–433

Fu X, Li C, Zhang G, Zou Y, Liu J, Ren X, Tan X, Zhang X, Zuo W, Wen W, Peng W, Cui X, Zhang C, Wang H, Peng W (2014) Data processing for the active particle-induced X-ray Spectrometer and initial scientific results from Chang'E-3 mission. Res Astron Astrophys 14:1595–1606

Gaffney AM, Gross J, Borg LE, Donaldson Hanna KL, Draper DS, Dygert N, Elkins-Tanton LT, Prissel KB, Prissel TB, Steenstra ES, van Westrenen W (2023) Magmatic evolution I: Initial differentiation of the Moon. Rev Mineral Geochem 89:103–145

Garrick-Bethell I, Weiss BP, Shuster DL, Tikoo SM, Tremblay MM (2017) Further evidence for early lunar magnetism from troctolite 76535. J Geophys Res Planets 122:76–93

Gaza R, Hussein H, Murrow D, Hopkins J, Waterman G, Milstein O, Berger T, Przybyla B, Aeckerlein J, Marsalek K, Matthiae D, Rutczynska A (2018) Matroshka AstroRad Radiation Experiment (MARE) on the Deep Space Gateway, Deep Space Gateway Science Workshop 2018, abstract # 3042

Gillet K, Margerin L, Calvet M, Monnereau M (2017) Scattering attenuation profile of the Moon: Implications for shallow moonquakes and the structure of the megaregolith. Phys Earth Planet Int 262:28–40

Gillis JJ, Spudis PD (2000) Geology of the Smythii and Marginis region of the Moon using integrated remotely sensed data. J Geophys Res 105(E2):4217–4233

Gillis JJ, Jolliff BL, Korotev RL (2004) Lunar surface geochemistry: Global concentrations of Th, K, and FeO as derived from lunar prospector and Clementine data. Geochim Cosmochim Acta 68:3791–3805

Gladstone GR, Stern SA, Retherford KD, Black RK, Slater DC, Davis MW, Versteeg MH, Persson KB, Parker JW, Kaufmann DE, Egan AF, Greathouse TK, Feldman PD, Hurley D, Pryor WR, Hendrix AR (2010) LAMP: The Lyman Alpha Mapping Project on NASA's Lunar Reconnaissance Orbiter mission. Space Sci Rev 150:161–181

Glotch TD, Lucey PG, Bandfield JL, Greenhagen BT, Thomas IR, Elphic R, Bowles NE, Wyatt MB, Allen CC, Donaldson Hanna KL, Paige DA (2010) Highly silicic compositions on the Moon. Science 329:1510–1513

Goldstein DB, Nerem RS, Barker ES, Austin JV (1999) Impacting lunar prospector in a cold trap to detect water ice. Geophys Res Lett 26:1653–1656

Goswami JN, Annadurai M (2009) Chandrayaan-1: India's first planetary science mission to the Moon. Curr Sci 96:486–491

Goossens S, Matsumoto K, Rowlands DD, Lemoine FG, Noda H, Araki H (2011) Orbit determination of the SELENE satellites using multi-satellite data types and evaluation of SELENE gravity field models. J Geodesy 85:487–504

Goossens S, Lemoine FG, Sabaka TJ, Nicholas JB, Mazarico E, Rowlands DD, Loomis BD, Chinn DS, Neumann GA, Smith DE, Zuber MT (2016) A global degree and order 1200 model of the lunar gravity field using GRAIL Mission Data. 47th Lunar Planet Sci Conf, abstract # 1484

Goossens SK, Mazarico E, Gaddis L, Archinal B, Hare T, Speyerer E, Ishihara Y, Haruyama J, Iwata T, Namiki N (2018) Improving the geometry of Kaguya Extended Mission data through refined orbit solutions. 49th Lunar Planet Sci Conf, abstract # 1645

Goossens S, Mazarico E, Ishihara Y, Archinal BA, Gaddis L (2020) Improving the geometry of Kaguya extended mission data through refined orbit determination using laser altimetry. Icarus 226:113454

Goswami JN, Thyagarajan K, Annadurai M (2006) Chandrayaan-1: Indian Mission to Moon. 37th Lunar Planet Sci Conf, abstract # 1704

Grande M, Kellett BJ, Howe C, Perry CH, Swinyard B, Dunkin SK, Huovelin J, Alha L, D'Uston LC, Maurice S, Gasnault O, Couturier-Doux S, Barabash S, Joy KH, Crawford I, Lawrence D, Fernandes V, Casanova I, Wieczorek M, Thomas N, Mall U, Foing B, Hughes D, Alleyne H, Russell S, Grady M, Lundin R, Baker D, Murray CD, Guest J, Christou A (2007) The D-CIXS X-Ray spectrometer on the SMART-1 mission to the Moon—First results. Planet Space Sci 55:494–502

Greeley R, Kadel SD, Williams DA, Gaddis LR, Head JW, McEwen AS, Murchie SL, Nagel E, Neukum G, Pieters CM, Sunshine JM, Wagner R, Belton MJS (1993) Galileo Imaging observations of lunar maria and related deposits. J Geophys Res 98(E9):17183–17205

Halekas JS, Angelopoulos V, Sibeck DG, Khurana KK, Russell CT, Delory GT, Farrell WM, McFadden JP, Bonnell JW, Larson D, Ergun RE, Plaschke F, Glassmeier KH (2010) First results from ARTEMIS, a new two-spacecraft lunar mission: Counter-streaming plasma populations in the lunar wake. *In:* Russell C, Angelopoulos V (eds) The ARTEMIS Mission. Springer, New York, NY

Halekas JS, Delory GT, Farrell WM, Angelopoulos V, McFadden JP, Bonnell JW, Fillingim MO, Plaschke F (2011) First remote measurements of lunar surface charging from ARTEMIS: Evidence for nonmonotonic sheath potentials above the dayside surface. J Geophys Res 116:A07103

Halekas JS, Poppe AR, Delory GT, Sarantos M, Farrell WM, Angelopoulos V, McFadden JP (2012) Lunar pickup ions observed by ARTEMIS: Spatial and temporal distribution and constraints on species and source locations. J Geophys Res 117:E06006

Halekas JS, Poppe AR, Delory GT, Sarantos M, McFadden JP (2013) Using ARTEMIS pickup ion observations to place constraints on the lunar atmosphere. J Geophys Res Planets 118:81–88

Halekas JS, Poppe AR, McFadden JP, Angelopoulos V, Glassmeier K-H, Brain DA (2014) Evidence for small-scale collisionless shocks at the Moon from ARTEMIS. Geophys Res Lett 41:7436–7443

Halekas JS, Benna M, Mahaffy PR, Elphic RC, Poppe AR, Delory GT (2015) Detections of lunar exospheric ions by the LADEE neutral mass spectrometer. Geophys Res Lett 42:5162–5169

Hapke B, Danielson GE, Klaasen K, Wilson L (1975) Photometric observations of Mercury from Mariner 10. J Geophys Res 80:2431–2443

Harada Y, Machida S, Halekas JS, Poppe AR, McFadden JP (2013) ARTEMIS observations of lunar dayside plasma in the terrestrial magnetotail lobe. J Geophys Res Space Physics 118:3042–3054

Harada Y, Goossens S, Matsumoto K, Yan J, Ping J, Noda H, Haruyama J (2014) Strong tidal heating in an ultralow-viscosity zone at the core–mantle boundary of the Moon. Nat Geosci 7:569–572

Harada Y, Halekas JS, Poppe AR, Tsugawa Y, Kurita S, McFadden JP (2015) Statistical characterization of the foremoon particle and wave morphology: ARTEMIS observations. J Geophys Res Space Phys 120:4907–4921

Harada Y, Poppe AR, Halekas JS, Chamberlin PC, Mcfadden JP (2017) Photoemission and electrostatic potentials on the dayside lunar surface in the terrestrial magnetotail lobes. Geophys Res Lett 44:5276–5282

Hardgrove C, Prettyman TH, Starr R, Colaprete T, Drake D, Heffern L and the LunaH-map team (2020) Improved hydrogen maps of the lunar south pole by the Lunar Polar Hydrogen Mapper (LunaH-Map) cubesat mission. 51st Lunar Planet Sci Conf, abstract # 2711

Hareyama M, Ishihara Y, Demura H, Hirata N, Honda C, Kamata S, Karouji Y, Kimura J, Morota T, Nagaoka H, Nakamura R, Yamamoto S, Ohtake M (2017) Global classification map of absorption spectrum of lunar reflectance observed by Spectral Profiler/Kaguya. Lunar Planet Sci Conf 48:1706

Haruyama J, Matsunaga T, Ohtake M, Morota T, Honda C, Yokota Y, Torii M, Ogawa Y, and the LISM Working Group (2008) Global lunar-surface mapping experiment using the lunar imager/spectrometer on SELENE. Earth Planets Space 60:243–255

Haruyama J, Ohtake M, Matsunaga T, Morota T, Honda C, Yokota Y, Abe M, Ogawa Y, Miyamoto H, Iwasaki A, Pieters CM, Asada N, Demura H, Hirata N, Terazono J, Sasaki S, Saiki K, Yamaji A, Torii M, Josset J-L (2009a) Long-lived volcanism on the lunar farside revealed by SELENE Terrain Camera. Science 323:905–908

Haruyama J, Hioki K, Shirao M, Morota T, Hiesinger H, van der Bogert CH, Miyamoto H, Iwasaki A, Yokota Y, Ohtake M, Matsunaga T, Hara S, Nakanotani S, Pieters CM (2009b) Possible lunar lava tube skylight observed by SELENE cameras. Geophys Res Lett 36:L21206

Haruyama J, Hara S, Hioki K, Iwasaki A, Morota T, Ohtake M, Matsunaga T, Araki H, Matsumoto K, Ishihara Y, Noda H, Sasaki S, Goossens S, Iwata T (2012) Lunar global Digital Terrain Model dataset produced from SELENE (Kaguya) Terrain Camera stereo observations. Lunar Planet Sci Conf 43:1200

Haruyama J, Yamamoto S, Yokota Y, Ohtake M, Matsunaga T (2013) An explanation of bright areas inside Shackleton crater and the lunar South Pole other than water-ice deposits. Geophys Res Lett 40:3814–3818

Haruyama J, Ohtake M, Matsunaga T, Otake H, Ishihara Y, Masuda K, Yokota Y, Yamamoto S (2014) Data products of SELENE (Kaguya) Terrain Camera for future lunar missions. Lunar Planet Sci Conf 45:1304

Hashimoto T, Yamada T, Kikuchi J, Otsuki M, Ikenaga T (2017) Nano Moon Lander: OMOTENASHI. 31st Int Symp Space Tech Sci 20017-f-053

Haugaard Z, Ohn D, Philabaum C, Rodriguez K, Shepard M, Laura J, Hare T (2017) Improved access to Kaguya hyperspectral data. Planet Data Workshop 3:7102

Hauri EH, Weinreich T, Saal AE, Rutherford MC, Van Orman JA (2011) High pre-eruptive water contents preserved in lunar melt inclusions. Science 333:213–215

Hauri EH, Saal AE, Rutherford MJ, Van Orman JA (2015) Water in the Moon's interior: truth and consequences. Earth Planet Sci Lett 409:252–264

Hauri EH, Saal AE, Nakajima M, Anand M, Rutherford MJ, Van Orman JA, Le Voyer M (2017) Origin and evolution of water in the Moon's interior. Annu Rev Earth Planet Sci 45:89–111

Hayashi Y, Ogawa Y, Hirata N, Terazono J, Demura H, Matsunaga T, Ohtake M, Otake H (2016) "GEKKO" for hyperspectral data distribution: A new method for utilizing the advantages of a web map service. Lunar Planet Sci Conf, abstract 47:1920

Hayne PO, Hendrix A, Sefton-Nash E, Siegler MA, Lucey PG, Retherford KD, Williams J-P, Greenhagen BT, Paige DA (2015) Evidence for exposed water ice in the Moon's south polar regions from Lunar Reconnaissance Orbiter ultraviolet albedo and temperature measurements. Icarus 255:58–69

He Z, Wang B, Lü G, Li C, Yuan L, Xu R, Liu B, Chen K, Wang J (2014) Operating principles and detection characteristics of the visible and near-infrared imaging spectrometer in the Chang'E-3. Res Astron Astrophys 14:1567–1577

He H, Shen C, Wang H, Zhang X, Chen B, Yan J, Jorgensen AM, He F, Yan Y, Zhu X, Huang Y, Xu R (2016) Response of plasmaspheric configuration to substorms revealed by Chang'E 3. Sci Rep 6:32362

He Q, Li Y, Baziotis I, Qian Y, Xiao L, Wang Z, Zhang Z, Luo B, Neal CR, Day JMD, Pan F, She Z, Wu X, Hu Z, Zong K, Wang L (2022) Detailed petrogenesis of the unsampled Oceanus Procellarum: the case of the Chang'e-5 mare basalts. Icarus 383:115082

Heffels A, Knapmeyer M, Oberst J, Haase I (2017) Re-evaluation of Apollo 17 lunar seismic profiling experiment data. Planet Space Sci 135:43–54

Heiken GH, Vaniman DT, French BM (1991) Lunar Sourcebook—A User's Guide to the Moon, Cambridge University Press, Cambridge, UK

Hendrix AR, Hurley DM, Farrell WM, Greenhagen BT, Hayne PO, Retherford KD, Vilas F, Cahill JTS, Poston MJ, Liu Y (2019) Diurnally migrating lunar water: evidence from ultraviolet data. Geophys Res Lett 46:2417–2424

Hiesinger H, van der Bogert CH, Michael G, Schmedemann N, Iqbal W, Robbins SJ, Ivanov B, Williams J-P, Zanetti M, Plescia J, Ostrach LR, Head III JW (2023) The lunar cratering chronology. Rev Mineral Geochem 89:401–451

Hood LL, Zakharian A, Halekas J, Mitchell DL, Lin RP, Acuna MH, Binder A (2001) Initial mapping and interpretation of lunar crustal magnetic anomalies using Lunar Prospector magnetometer data. J Geophys Res 106(E11):27825–27839

Horányi M, Sternovsky Z, Lankton M, Dumont C, Gagnard S, Gathright D, Grün E, Hansen D, James D, Kempf S, Lamprecht B, Srama R, Szalay JR, Wright G (2014) The Lunar Dust Experiment (LDEX) Onboard the Lunar Atmosphere and Dust Environment Explorer (LADEE) mission. Space Sci Rev 185:93–113

Horányi M, Szalay JR, Kempf S, Schmidt J, Grün E, Srama R, Sternovsky Z (2015) A permanent, asymmetric dust cloud around the Moon. Nature 522:324–326

Hörz F (1986) Lava tubes: Potential shelters for habitats. *In:* Lunar Bases and Space Activities of the 21st Century, Mendell WW (ed), Lunar Planet Inst, Houston, TX, p 405– 412

Howard SK, Halekas JS, Farrell W, McFadden JP, Glassmeier K (2017) Identifying ultra low frequency waves in the lunar plasma environment using trajectory analysis and resonance conditions. J Geophys Res Space Phys 122:9983–9993

Hu S, He H, Ji J, Lin Y, Hui Y, Anand M, Tartèse R, Yan Y, Hao J, Li R, Gu R, Gui Q, He H, Ouyang Z (2021) A dry lunar mantle reservoir for young mare basalts of Chang'e-5. Nature 600:49–53

Huang J, Ji J, Ye P, Wang X, Yan J, Meng L, Wang S, Li C, Li Y, Qiao D, Zhao W, Zhao Y, Zhang T, Liu P, Jiang Y, Rao W, Li S, Huang C, Ip WH, Hu S, Zhu M, Yu L, Zou Y, Tang X, Li J, Zhao H, Huang H, Jiang X, Bai J (2013) The ginger-shaped asteroid 4179 Toutatis: New observations from a successful flyby of Chang'E-2. Sci Rep 3:3411

Huang J, Xiao Z, Flahaut J, Martinot M, Head J, Xiao X, Xie M, Xiao L (2018) Geological characteristics of Von Kármán crater, northwestern South Pole-Aitken basin: Chang'E-4 landing site region. J Geophys Res Planets 123:1684–1700

Hurley DM, Cook JC, Benna M, Halekas JS, Feldman PD, Retherford KD, Hodges RR, Grava C, Mahaffy P, Gladstone GR, Greathouse T, Kaufmann DE, Elphic RC, Stern SA (2015) Understanding temporal and spatial variability of the lunar helium atmosphere using simultaneous observations from LRO, LADEE, and ARTEMIS. Icarus 273:45–52

Hurley DM, Siegler MA, Cahill JTS, Colaprete A, Costello E, Deutsch AN, Elphic RC, Fa W, Grava C, Hayne PO, Heldmann J, Hendrix AR, Jordan AP, Killen RM, Klima RL, Kramer G, Li S, Liu Y, Lucey PG, Mazarico E, Pendleton Y, Poston M, Prem P, Retherford KD, Schaible M (2023) Surface volatiles on the Moon. Rev Mineral Geochem 89:787-827

International Space Exploration Coordination Group (ISECG) (2018a) The Global Exploration Roadmap, 3rd Edition, https://www.globalspaceexploration.org/wordpress/wp-content/isecg/GER_2018_small_mobile.pdf

International Space Exploration Coordination Group (ISECG) (2018b) Scientific opportunities enabled by human exploration beyond low-Earth orbit, an ISECG White Paper, https://www.globalspaceexploration.org/wordpress/wp-content/isecg/ISECG%20SWP_FINAL-web_2017-12.pdf

International Space Exploration Coordination Group (ISECG) (2020) Global Exploration Roadmap Supplement August 2020. https://www.globalspaceexploration.org/wp-content/uploads/2020/08/GER_2020_supplement.pdf

Isbell C, Gaddis L, Garcia P, Hare T, Bailen M (2014) Kaguya terrain camera mosaics. Lunar Planet Sci Conf 45:2268

Jaumann R, Hiesinger H, Anand M, Crawford IA, Wagner R, Sohl F, Jolliff BL, Scholten F, Knapmeyer M, Hoffmann H, Hussmann H, Grott M, Hempel S, Köhler U, Krohn K, Schmitz N, Carpenter J, Wieczoreki M, Spohn T, Robinson MS, Oberst J (2012) Geology, geochemistry and geophysics of the Moon: status and current understanding. Planet Space Sci 74:15–41

Jeong M, Choi Y-C, Moon B, Kim J (2020) Optical performance of wide-angle polarimetric camera (POLCAM). Lunar Planet Sci Conf 51:1706

Jia Y, Zou Y, Ping J, Xue C, Yan J, Ning Y (2018) The scientific objectives and payloads of Chang'E-4 mission. Planet Space Sci 162:207–215

Jolliff BL, Gillis JJ, Haskin LA, Korotev R, Wieczorek MA (2000) Major lunar crustal terranes: Surface expressions and crust-mantle origins. J Geophys Res 105:4197–4216

Jolliff BL, Wieczorek MA, Shearer C, Neal CR (eds) (2006) New Views of the Moon. Reviews in Mineralogy and Geochemistry. Vol 60. Mineralogical Society of America

Jolliff BL, Wiseman SA, Lawrence SJ, Tran TN, Robinson MS, Sato H, Hawke BR, Scholten F, Oberst J, Hiesinger H, van der Bogert CH, Greenhagen BT, Glotch TD, Paige DA (2011) Non-mare silicic volcanism on the lunar farside at Compton–Belkovich. Nat Geosci 4:566–571

Jones, EM, Glover K (2017) Apollo Lunar Surface Journal, a living journal, https://www.hq.nasa.gov/alsj/

Kato M, Sasaki S, Tanaka K, Iijima Y, Takizawa Y (2008) The Japanese lunar mission SELENE: Science goals and present status. Adv Space Res 42:294–300

Kato M, Sasaki S, Takizawa Y and the Kaguya project team (2010) The Kaguya mission overview. Space Sci Rev 154:3–19

Keller JW, Petro NE, Vondrak RR, the LRO Team (2016) The Lunar Reconnaissance Orbiter Mission-—Six years of science and exploration of the Moon. Icarus 273:2–24

Kirchoff MR, Chapman CR, Marchi S, Curtis KM, Enke B, Bottke WF (2013) Ages of large lunar impact craters and implications for bombardment during the Moon's middle age. Icarus 225:325–341

Klima R, Cahill J, Hagerty J, Lawrence D (2013) Remote detection of magmatic water in Bullialdus crater on the Moon. Nat Geosci 6:737–741

Kobayashi T, Kim JH, Lee SR, Araki H, Ono T (2010) Simultaneous observation of Lunar Radar Sounder and Laser Altimeter of Kaguya for lunar regolith layer thickness estimate. IEEE Geosci Rem Sens Lett 7:435–439

Korean National Committee for COSPAR (2020) COSPAR 2020: National Report Republic of Korea. https://cosparhq.cnes.fr/assets/uploads/2021/01/South-Korea_2020_compressed.pdf

Krüger H, Strub P, Srama R, Kobayashi M, Arai T, Kimura H, Hirai T, Moragas-Klostermeyer G, Altobelli N, Sterken V, Agarwal J, Sommer M, Grün E (2019) Modelling DESTINY+ interplanetary and interstellar dust measurements en route to the active asteroid (3200) Phaethon. Planet Space Sci 172:22–42

Kumar YA (2009) The Moon Impact Probe on Chandrayaan-1. Curr Sci 96:540–543

Kumar ASK, Chowdury AR (2005) Terrain mapping camera for Chandrayaan-1. J Earth Syst Sci 114:717–720

Kumar ASK, Kiran S, Chauhan P, Kaur P, Rajasekhar RP, Bhattacharya S, Singh RD, Arya AS, Saran S, Gopala Krishna B (2015) Chandrayaan-1 Lunar Science Atlas. Space Applications Centre, Ahmedabad, India, https://vedas.sac.gov.in/vedas/downloads/atlas/Planetary/lunar_science_atlas_version_2015.pdf

Lawrence DJ, Feldman WC, Barraclough BL, Binder AB, Elphic RC, Maurice S, Thomsen DR (1998) Global Elemental of the Moon: The Lunar Prospector gamma-ray spectrometer. Science 281:1484–1489

Lawrence DJ, Feldman WC, Barraclough BL, Elphic RC, Maurice S, Binder A, Miller MC, Prettyman TH (1999) High resolution measurements of absolute thorium abundances on the lunar surface. Geophys Res Lett 26:2681–2684

Lawrence DJ, Feldman WC, Barraclough BL, Elphic RC, Prettyman TH, Maurice S, Binder AB, Miller M (2000) Thorium abundances on the lunar surface. J Geophys Res 105(E8):20307–20331

Lawrence DJ, Feldman WC, Elphic RC, Little RC, Prettyman TH, Maurice S, Lucey PG, Binder AB (2002) Iron abundances on the lunar surface as measured by the Lunar Prospector gamma-ray and neutron spectrometers. J Geophys Res 107(E12):13-1–13-26

Lawrence DJ, Elphic RC, Feldman WC, Prettyman TH, Gasnault O, Maurice S (2003) Small area thorium features on the lunar surface. J Geophys Res 108(E9):5102

Lawrence DJ, Maurice S, Feldman WC (2004) Gamma-ray measurements from Lunar Prospector: Time series data reduction for the gamma-ray spectrometer. J Geophys Res Planets 109(E7):E07S05

Lawson SL, Jakosky BM, Park H-S, Mellon MT (2000) Brightness temperatures of the lunar surface: Calibration and global analysis of the Clementine long-wave infrared camera data. J Geophys Res Planets 109(E7):E07S05

Le Contel O, Roux A, Robert P, Coillot C, Bouabdellah A, de la Porte B, Alison D, Ruocco S, Angelopoulos V, Bromund K, Chaston CC, Cully C, Auster HU, Glassmeier KH, Baumjohann W, Carlson CW, McFadden JP, Larson D (2008) First results of the THEMIS search coil magnetometers. Space Sci Rev 141:509–534

Lemelin M, Lucey PG, LR Gaddis, T Hare, Ohtake M (2016) Global map products from the Kaguya Multiband Imager at 512 ppd: Minerals, FeO and OMAT. 47th LPSC, abstract # 2994

Lemelin M, Lucey PG, LR Gaddis, T Hare, M Ohtake (2019) The compositions of the lunar crust and upper mantle: Spectral analysis of the inner rings of lunar impact basins. Planet Space Sci 165:230–243

Lemoine FG, Goossens S, Sabaka TJ, Nicholas JB, Mazarico E, Rowlands DD, Loomis BD, Chinn DS, Neumann GA, Smith DE, Zuber MT (2014) GRGM900C: A degree 900 lunar gravity model from GRAIL primary and extended mission data. Geophys Res Lett 41:3382–3389

Li C, Liu J, Ren X, Mou L, Zou Y, Zhang H, L C, Liu J, Zuo W, Su Y, Wen W, Bian W, Zhao B, Yang J, Zou X, Wang M, Xu C, Kong D, Wang X, Wang F, Geng L, Zhang Z, Zheng L, Zhu X, Li J, Ouyang Z (2010a) The global image of the Moon obtained by the Chang'E-1: Data processing and lunar cartography. Sci Chin Earth Sci 53:1091–1102 (in Chinese)

Li C, Ren X, Liu J, Zou X, Mu L, Wang J, Shu R, Zou Y, Zhang H, Lü C, Liu J, Zuo W, Su Y, Wen W, Bian W, Wang M, Xu C, Kong D, Wang X, Wang F, Geng L, Zhang Z, Zheng L, Zhu X, Li J, Liu J (2010b) Laser altimetry data of Chang'E-1 and the global lunar DEM model. Sci Chin Earth Sci 53:1582–1593 (in Chinese)

Li C, Liu J, Ren X, Zuo W, Tan X, Wen W, Li H, Mu L, Su Y, Zhang H, Yan J, Ouyang Z (2015) The Chang'E 3 mission overview. Space Sci Rev 190:85–101

Li S, Lucey PG, Milliken R, Hayne P, Fisher E, Williams JP, Hurley DM, Elphic RM (2018) Direct evidence of surface exposed water ice in the lunar polar regions. Proc Nat Acad Sci 115:8907–8912

Li C, Liu D, Liu, B, Ren X, Liu J, He Z, Zuo W, Zeng X, Xu R, Tan X, Zhang X, Chen W, Shu R, Wen W, Su Y, Zhang H, Ouyang Z (2019) Chang-E-4 initial spectroscopic identification of lunar far-side mantle-derived materials. Nature 569:378–382

Li C, Su Y, Pettinelli E, Xing S, Ding C, Liu J, Ren X, Lauro SE, Soldoveri F, Zeng X, Gao X, Chen W, Dai S, Liu D, Zhang G, Zuo W, Wen W, Zhang Z, Zhang X, Zhang H (2020) The Moon's farside shallow subsurface structure unveiled by Chang'E-4 Lunar Penetrating Radar. Sci Adv 6:eaay6898

Li Q-L, Zhou Q, Liu Y, Xiao Z, Li J-H, Ma H-X, Tang G-Q, Guo S, Tang X, Yuan J-Y, Li J, Wu F-Y, Ouyang Z, Li C, Li X-H (2021) Two-billion-year-old volcanism on the Moon from Chang'e-5 basalts. Nature 600:84–88

Lian Y, Chen S, Meng Z, Zhang F, Zhang Y (2014) Dielectric constant of lunar soil derived from Chang' E-2 passive microwave radiometer measurements. Earth Science, J China Univ Geosci 11:1644–1650 (in Chinese)

Lian Y, Chen S, Meng Z, Zhang Y (2015) Distribution of microwave radiation brightness temperatures on the lunar surface based on Chang'E-2 MRM Data. Geomatics Inf Sci Wuhan Univ 40:732–737 (in Chinese)

Lin RP, Mitchell DL, Curtis DW, Anderson KA, Carlson CW, McFadden J, Acuna MH, Hood LL, Binder A (1998) Lunar surface magnetic fields and their interaction with the solar wind: Results from Lunar Prospector. Science 281:1480–1484

Lin H, Li S, Xu R, Liu Y, Wu X, Yang W, Wei Y, Lin Y, He Z, Hui H, He H, Hu S, Zhang C, Li C, Lv G, Yuan L, Zou Y, Wang C (2022) In situ detection of water on the Moon by the Chang'E-5 lander. Sci Adv 8:eabl9174

Ling Z, Jiang Z, Liu J, Zhang W, Zhang G, Liu B, Li C, Ren X, Mu L, Liu J (2011) Preliminary results of TiO_2 mapping using imaging interferometer data from Chang'E-1. Chin Sci Bull 56:376–379

Ling Z, Jolliff B, Wang A, Li C, Liu J, Zhang J, Li B, Sun L, Chen J, Xiao L, Liu J, Ren X, Peng W, Wang H, Cui X, He X, Wang J (2015) Correlated compositional and mineralogical investigations at the Chang'e-3 landing site. Nat Commun 6:8880

Ling Z, Changqing L, Jolliff BL, Zhang J, Li B, Sun L, Chen J, Liu J (2017) Spectral and mineralogical analysis of the Chang'E-5 candidate landing site in northern Oceanus Procellarum. 48th Lunar Planet Sci Conf, abstract # 2079

Liu B, Li C, Zhang G, Xu R, Liu J, Ren X, Tan X, Zhang X, Zuo W, Wen W (2014) Data processing and preliminary results of the Chang'E-3 VIS/NIR Imaging Spectrometer in-situ analysis. Res Astronom Astrophys 14:1578–1594

Lognonné P, Le Feuvre M, Johnson CL, Weber RC (2009) Moon meteoritic seismic hum: Steady state prediction. J Geophys Res 114:E12003

Lucey P (2004) Mineral maps of the Moon. Geophys Res Lett 3:L08701

Lucey PG, Spudis PD, Zuber M, Smith D, Malaret E (1994) Topographic–compositional units on the Moon and the Early evolution of the lunar crust. Science 266:1855–1858

Lucey P, Taylor GJ, Malaret E (1995) Abundance and distribution of iron on the Moon, Science 268:1150–1153

Lucey PG, Blewett DT, Hawke BR (1998) Mapping the FeO and TiO_2 content of the lunar surface with multispectral imagery. J Geophys Res 103(E2):3679–3699

Lucey PG, DT Blewett, BL Jolliff (2000) Lunar iron and titanium abundance algorithms based on final processing of Clementine ultraviolet-visible images. J Geophys Res 105(E8):20297–20306

Lucey P, Korotev RL, Gillis JJ, Taylor LA, Lawrence D, Campbell BA, Elphic R, Feldmann B, Hood LL, Hunten D, Mendillo M, Noble S, Papike JJ, Reedy RC, Lawson S, Prettyman T, Gasault O, Maurice S (2006) Understanding the lunar surface and space–Moon interactions. Rev Min Geochem 60:83–219

Ludlam M, Angelopoulos V, Taylor E, Snare RC, Means JD, Ge Y, Narvaez P, Auster HU, Le Contel O, Larson D, Moreau T (2008) The THEMIS magnetic cleanliness program. Space Sci Rev 141:171–184

Lunar Exploration Analysis Group (LEAG) (2016a) The lunar exploration roadmap: Exploring the Moon in the 21st century: Themes, goals, objectives, investigations, and priorities, https://www.lpi.usra.edu/leag/LER-2016.pdf

Lunar Exploration Analysis Group (LEAG) (2016b) Lunar Human Exploration Strategic Knowledge Gap Special Action Team Review, held by telecon from 16 February to 1 April 2016, https://www.nasa.gov/sites/default/files/atoms/files/leag-gap-review-sat-2016-v2.pdf

Lunar Exploration Analysis Group (LEAG) (2017) Lunar Exploration Analysis Group - International Space Exploration Coordination Group Volatiles Special Action Team 2. https://www.lpi.usra.edu/leag/reports/V-SAT-2-Final-Report.pdf

Lunar Exploration Analysis Group (LEAG) (2018a) Advancing Science of the Moon: Report of the Lunar Exploration Analysis Group Special Action Team. https://www.lpi.usra.edu/leag/reports/ASM-SAT-Report-final.pdf

Lunar Exploration Analysis Group (LEAG) (2018b) Next Steps on the Moon, Report of the Specific Action Team, meeting held 9–10 August 2017, Houston, Texas, https://www.lpi.usra.edu/leag/reports/NEXT_SAT_REPORT%20(1).pdf

Mahaffy PR, Richard Hodges R, Benna M, King T, Arvey R, Barciniak M, Bendt M, Carigan D, Errigo T, Harpold DN, Holmes V, Johnson CS, Kellogg J, Kimvilakani P, Lefavor M, Hengemihle J, Jaeger F, Lyness E, Maurer J, Nguyen D, Nolan TJ, Noreiga F, Noriega M, Patel K, Prats B, Quinones O, Raaen E, Tan F, Weidner E, Woronowicz M, Gundersen C, Battel S, Block BP, Arnett K, Miller R, Cooper C, Edmonson C (2014) The neutral mass spectrometer on the Lunar Atmosphere and Dust Environment Explorer mission. Space Sci Rev 185:27–61

Mall U, Banaszkiewicz M, Brønstad K, McKenna-Lawlor S, Nathues A, Søraas F, Vilenius E, Ullaland K (2009) Near infrared spectrometer SIR-2 on Chandrayaan-1. Curr Sci 96:506–511

Matsunaga T, Ohtake M, Haruyama J, Ogawa Y, Nakamura R, Yokota Y, Morota T, Honda C, Torii M, Abe M, Nimura T, Hiroi T, Arai T, Saiki K, Takeda H, Hirata N, Kodama S, Sugihara T, Demura H, Asada N, Terazono J, Otake H (2008) Discoveries on the lithology of lunar crater central peaks by SELENE Spectral Profiler. Geophys Res Lett 35:L23201

Matsunaga T, Yokota Y, Yamamoto S, Nakamura R, Ohtake M, Haruyama J (2011) Lunar global spectral reflectance data set by Kaguya Spectral Profiler. Lunar Planet Sci Conf 42:2000

Matsuyama I, Nimmo F, Keane JT, Chan NH, Taylor GJ, Wieczorek MA, Kiefer WS, Williams JG (2016) GRAIL, LLR, and LOLA constraints on the interior structure of the Moon. Geophys Res Lett 43:8365–8375

Mazarico E, Neumann GA, Smith DE, Zuber MT, Torrence MH (2011) Illumination conditions of the lunar polar regions using LOLA topography. Icarus 211:1066–1081

McCubbin FM, Jolliff BJ, Nekvasil H, Carpenter PK, Zeigler RA, Steele A, Elardo SM, Lindsley DH (2011) Fluorine and chlorine abundances in lunar apatite: Implications for heterogeneous distributions of magmatic volatiles in the lunar interior. Geochim Cosmochim Acta 75:5073–5093

McCubbin FM, Vander Kaaden KE, Tartèse R, Klima RL, Liu Y, Mortimer JI, Barnes JJ, Shearer CK, Treiman AH, Lawrence DJ, Elardo SM, Hurley DM, Boyce JW, Anand M (2015) Volatiles (H, C, N, F, S, Cl) in the lunar mantle, crust, and regolith: distribution, processes, sources, and significance. Am Mineral 100:1668–1707

McCubbin FM, Barnes JJ, Ni P, Hui H, Klima RL, Burney D, Day JMD, Magna T, Boyce JW, Tartèse R, Vander Kaaden KE, Steenstra E, Elardo SM, Zeigler RA, Anand M, Liu Y (2023) Endogenous lunar volatiles. Rev Mineral Geochem 89:729-786

McEwen AS, Robinson MS (1997) Mapping of the Moon by Clementine. Adv Space Res 19:1523–1533

McEwen AS, Gaddis LR, Neukum G, Hoffman H, Pieters CM, Head JW (1993) Galileo observations of Post-Imbrium lunar craters during the first Earth–Moon flyby. J Geophys Res 98(E9):17207–17231

McFadden JP, Carlson CW, Larson D, Angelopoulos V, Ludlam M, Abiad R, Elliott B, Turin P, Marckwordt M (2008a) The THEMIS ESA plasma instrument and in-flight calibration. *In*: Burch JL, Angelopoulos V (eds) The THEMIS Mission. Springer, New York, NY

McFadden JP, Carlson CW, Larson D, Bonnell J, Mozer F, Angelopoulos V, Glassmeier K-H, Auster U (2008b) THEMIS ESA first science results and performance issues. *In:* Burch JL, Angelopoulos V (eds) The THEMIS Mission. Springer, New York, NY

Milliken RE, Li S (2017) Remote detection of widespread indigenous water in lunar pyroclastic deposits. Nat Geosci 10:561–565

Melosh HJ, Freed AM, Johnson BC, Blair DM, Andrews-Hanna JC, Neumann GA, Phillips RJ, Smith DE, Solomon SC, Wieczorek MA, Zuber MT (2013) The origin of lunar mascon basins. Science 340:1552–1555

Mitrofanov IG, Sanin AB, Boynton WV, Chin G, Garvin JB, Golovin D, Evans L, Harshman K, Kozyrev AS, Litvak ML, Malakhov A, Mazarico E, McClanahan T, Milikh G, Mokrousov M, Nandikotkur G, Neumann GA, Nuzhdin I, Sagdeev R, Shevchenko V, Shvetsov V, Smith DE, Starr R, Tretyakov VI, Trombka J, Usikov D, Varenikov A, Vostrukhin A, Zuber MT (2010a) Lunar Exploration Neutron Detector for the NASA Lunar Reconnaissance Orbiter. Space Sci Rev 150:183–207

Mitrofanov IG, Sanin AB, Boynton WV, Chin G, Garvin JB, Golovin D, Evans LG, Harshman K, Kozyrev AS, Litvak ML, Malakhov A, Mazarico E, McClanahan T, Milikh G, Mokrousov M, Nandikotkur G, Neumann GA, Nuzhdin I, Sagdeev R, Shevchenko V, Shvetsov V, Smith DE, Starr R, Tretyakov VI, Trombka J, Usikov D, Varenikov A, Vostrukhin A, Zuber MT (2010b) Hydrogen mapping of the lunar south pole using the LRO neutron detector experiment LEND. Science 330:483–486

Mitrofanov IG, Zelenyi LM, Tret'yakov VI (2012) Upgraded program of Russian lunar landers: studying of lunar poles. Proc. Ann Meeting Lunar Exploration Analysis Group, abstract # 3025

Morbidelli A, Marchi S, Bottke WF, Kring DA (2012) A sawtooth-like timeline for the first billion years of lunar bombardment. Earth Planet Sci Lett 355–356:144–151

Morota T, Haruyama J, Ohtake M, Matsunaga T, Honda C, Yokota Y, Kimura J, Ogawa Y, Hirata N, Demura H, Iwasaki A, Sugihara T, Saiki K, Nakamura R, Kobayashi S, Ishihara Y, Takeda H, Hiesinger H (2011) Timing and characteristics of the latest mare eruption on the Moon. Earth Planet Sci Lett 302:255–266

Murphy TW Jr, Adelberger EG, Battat JBR, Hoyle CD, Johnson NH, McMillan RJ, Michelsen EL, Stubbs CW, Swanson HE (2011) Laser ranging to the lost Lunokhod 1 retroreflector. Icarus 211:1103–1108

Mylswamy A, Krishnan A, Alex TK, Rama Murali GK (2012) Chandrayaan-2: India's first soft-landing mission to the Moon. *In:* 39th COSPAR Scientific Assembly A2.1–16–12, 1311

Nakamura R, Yamamoto S, Matsunaga T, Ishihara Y, Morota T, Hiroi T, Takeda H, Ogawa Y, Yikota Y, Hirata N, Ohtake M, Saiki K (2012) Compositional evidence for an impact origin of the Moon's Procellarum basin. Nat Geosci 5:775–778

Namiki N, Iwata T, Matsumoto K, Hanada H, Noda H, Goossens S, Ogawa M, Nobuyuki K, Asari K, Tsuruta S, Ishihara Y, Liu Q, Kikuchi F, Ishiwaka T, Sasaki S, Aoshima C, Kurosawa K, Sugita S, Takano T (2009) Farside gravity field of the Moon from four-way doppler measurements of SELENE (Kaguya). Science 323:900–904

National Research Council (NRC) (2007) The Scientific Context for Exploration of the Moon, National Research Council, National Academies Press, Washington DC, https://www.nap.edu/catalog/11954/the-scientific-context-for-exploration-of-the-moon

Narendranath S, Athiray PS, Sreekumar P, Kellett BJ, Alha L, Howe CJ, Joy KH, Grande M, Huovelin J, Crawford IA, Unnikrishnan U, Lalita S, Subramaniam S, Weider SZ, Nittler LR, Gasnault O, Rothery D, Fernandes VA, Bhandari N, Goswami JN, Wiezoreck MA, and the C1XS team (2011) Lunar X-ray fluorescence observations by the Chandrayaan-1 X-ray Spectrometer (C1XS): Results from a lunar highland region. Icarus 214:53–66

Narendranath S, Athiray PS, Sreekumar P, Radhakrishna V, Tyagi A, Kellett BJ (2014) Mapping lunar surface chemistry: New prospects with the Chandrayaan-2 Large Area Soft X-ray Spectrometer (CLASS). Adv Space Res 54:1993–1999

National Aeronautics and Space Administration (NASA) (2004) The Vision for Space Exploration. NP-2004-01-334-HQ, NASA, Washington DC, https://www.nasa.gov/pdf/55583main_vision_space_exploration2.pdf

National Aeronautics and Space Administration (NASA) (2018) National Space Exploration Campaign Report, https://www.nasa.gov/sites/default/files/atoms/files/nationalspaceexplorationcampaign.pdf

National Aeronautics and Space Administration (NASA) (2020) NASA's Lunar Exploration Program Overview, https://www.nasa.gov/sites/default/files/atoms/files/artemis_plan-20200921.pdf

Nozette S (1994) The Clementine mission to the Moon: Scientific overview. Science 266:1835–1839

Nozette S, Spudis PD, Robinson M, Bussey DBJ, Lichtenberg C, Bonner R (2001) Integration of lunar polar remote-sensing data sets: Evidence for ice at the lunar south pole. J Geophys Res 106(E19):23253–23266

Nozette S, Spudis P, Bussey DBJ, Jensen R, Raney K, Winters H, Lichtenberg CL, Marinelli W, Crusan J, Gates M, Robinson M (2010) The Lunar Reconnaissance Orbiter Miniature Radio Frequency (Mini-RF) technology demonstration. Space Sci Rev 150:285–302

Ogawa Y, Matsunaga T, Nakamura R, Saiki K, Ohtake M, Hiroi T, Takeda H, Arai T, Yokota Y, Yamamoto S, Hirata N, Sugihara T, Sasaki S, Haruyama J, Morota T, Honda C, Demura H, Kitazato K, Terazono J, Asada N (2011) The widespread occurrence of high-calcium pyroxene in bright-ray craters on the Moon and implications for lunar crust composition. Geophys Res Lett 38:L17202-1–L17202-6

Ohtake M, Haruyama J, Matsunaga T, Yokota Y, Morota T, Honda C, and the LISM team (2008) Performance and scientific objectives of the SELENE (KAGUYA) multiband imager. Earth Planets Space 60:257–264

Ohtake M, Matsunaga T, Haruyama J, Yokota Y, Morota T, Honda C, Ogawa Y, Torii M, Miyamoto H, Arai T, Hirata N, Iwasaki A, Nakamura R, Hiroi T, Sugihara T, Takeda H, Otake H, Pieters CM, Saiki K, Kitazato K, Abe M, Asada N, Demura H, Yamaguchi Y, Sasaki S, Kodama S, Terazono J, Shirao M, Yamaji A, Minami S (2009) The global distribution of pure anorthosite on the Moon. Nature 461:236–240

Ohtake M, Takeda H, Matsunaga T, Yokota Y, Haruyama J, Morota T, Saiki K (2012) Asymmetric crustal growth on the Moon indicated by primitive farside highland materials. Nat Geosci 5:384–388

Ohtake M, Pieters C, Isaacson P, Besse S, Yokota Y, Matsunaga T, Boardman J, Yamamoto S, Haruyama J, Staid M, Mall U, Green R (2013) One Moon, many measurements III: Spectral reflectance. Icarus 226:364–374

Ohtake M, Hoshino T, Karouji Y, Shiraishi J (2018) Overview of a Japanese lunar polar mission. New Views of the Moon 2 – Asia 2018, abstract # 6018

Ohtake M, Saiki K, Nakauchi Y, Shiraishi H, Ishihara Y, Sato H, Honda C, Maeda T, Sakai S, Sawai S, Fukuda S, Kushiki K (2019) Geology of the crater Theophilus on the Moon: Landing site of the Smart Lander for Investigating the Moon. 50th Lunar Planet Sci Conf, abstract # 2342

Ono T, Kumamoto A, Nakagawa H, Yamaguchi Y, Oshigami S, Yamaji A, Kobayashi T, Kasahara Y, Oya H (2009) Lunar radar sounder observations of subsurface layers under the nearside maria of the Moon. Science 323:909–912

Oshigami S, Yamaguchi Y, Yamaji A, Ono T, Kumamoto A, Kobayashi T, Nakagawa H (2009) Distribution of the subsurface reflectors of the western nearside maria observed from Kaguya with Lunar Radar Sounder. Geophys Res Lett 36:L18202

Oshigami S, Watanabe S, Yamaguchi Y, Yamaji A, Kobayashi T, Kumamoto A, Ishiyama K, Ono T (2014) Mare volcanism: Reinterpretation based on Kaguya Lunar Radar Sounder data. J Geophys Res Planets 119:1037–1045

Ouyang Z, Li C, Zou Y, Zhang H, Lu C, Liu J, Liu J, Zuo W, Su Y, Wen W, Bian W, Zhao B, Wang J, Yang J, Chang J, Wang H, Zhang X, Wang S, Wang M, Ren X, Mu L, Kong D, Wang X, Wang F, Geng L, Zhang Z, Zheng L, Zhu X, Zheng Y, Li J, Zoi X, Xu C, Shi S, Gao Y, Gao G (2010) Primary scientific results of Chang'E 1 lunar mission. Sci China Earth Sci 53:1565–1581

Paige DA, Foote MC, Greenhagen BT, Schofield JT, Calcutt S, Vasavada AR, Preston DJ, Taylor FW, Allen CC, Snook KJ, Jakosky BM, Murray BC, Soderblom LA, Jau B, Loring S, Bulharowski J, Bowles NE, Thomas IR, Sullivan MT, Avis C, De Jong EM, Hartford W, McCleese DJ (2010a) The Lunar Reconnaissance Orbiter diviner lunar radiometer experiment. Space Sci Rev 150:125–160

Paige DA, Siegler MA, Zhang JA, Hayne PO, Foote EJ, Bennett KA, Vasavada AR, Greenhagen BT, Schofield JT, McCleese DJ, Foote MC, DeJong E, Bills BG, Hartford W, Murray BC, Allen CC, Snook K, Soderblom LA, Calcutt S, Taylor FW, Bowles NE, Bandfield JL, Elphic R, Ghent R, Glotch TD, Wyatt MG, Lucey PG (2010b) Diviner Lunar Radiometer observations of cold traps in the Moon's south polar region. Science 330:479–482

Patterson GW, Stickle AM, Turner FS, Jensen JR, Bussey DBJ, Spudis P, Espiritu RC, Schulze RC, Yocky DA, Wahl DE, Zimmerman M, Cahill JTS, Nolan M, Carter L, Neish CD, Raney RK, Thomson BJ, Kirk R, Thompson TW, Tise BL, Erteza IA, Jakowatz CV (2017) Bistatic observations of the Moon using Mini-RF on LRO and the Arecibo Observatory. Icarus 283:2–19

Petro NE, Keller JW, Cohen BA, McClanahan TP (2019) Ten years of the Lunar Reconnaissance Orbiter: Advancing lunar science and context for future lunar exploration. 50th Lunar Planet Sci Conf, abstract # 2780

Pieters CM, Boardman J, Buratti B, Chatterjee A, Clark R, Glavich T, Green R, Head J III, Isaacson P, Malaret E, McCord T, Mustard J, Petro N, Runyon C, Staid M, Sunshine J, Taylor L, Tompkins S, Varanasi P, White M (2009a) The Moon Mineralogy Mapper (M3) on Chandrayaan-1. Curr Sci 96:500–505

Pieters CM, Goswami JN, Clark RN, Annadurai M, Boardman J, Buratti B, Combe J-P, Dyar MD, Green R, Head JW, Hibbitts C, Hicks M, Isaacson P, Klima R, Kramer G, Kumar S, Livo E, Lundeen S, Malaret E, McCord T, Mustard J, Nettles J, Petro N, Runyon C, Staid M, Sunshine J, Taylor LA, Tompkins S, Varanasi P (2009b) Character and spatial distribution of OH/H_2O on the surface of the Moon seen by M^3 on Chandrayaan-1. Science 326:568–572

Pieters CM, Besse S, Boardman J, Buratti B, Cheek L, Clark RN, Combe JP, Dhingra D, Goswami JN, Green RO, Head JW, Isaacson P, Klima R, Kramer G, Lundeen S, Malaret E, McCord T, Mustard J, Nettles J, Petro N, Runyon C, Staid M, Sunshine J, Taylor L, Thaisen K, Tompkins S, Whitten J (2011) Mg-spinel lithology: A new rock type on the lunar farside, J Geophys Res Planets 116:E00G08

Pieters C, Boardman J, Ohtake M, Matsunaga T, Haruyama J, Green R, Mall U, Staid M, Isaacson P, Yokota Y, Yamamoto S, Besse S, Sunshine J (2013) One moon, many measurements I: radiance values. Icarus 226:951–963

Planetary Data System (PDS) (2009) Mission Information, Chandrayaan-1, https://pds-imaging.jpl.nasa.gov/data/m3/CH1M3_0001/CATALOG/MISSION.CAT

Plescia JB, Cahill J, Greenhagen B, Hayne P, Mahanti P, Robinson MS, Spudis PD, Siegler M, Stickle A, Williams JP, Zanetti M, Zellner N (2023) Lunar surface processes. Rev Mineral Geochem 89:651–690

Poppe AR, Samad R, Halekas JS, Sarantos M, Delory GT, Farrell WM, Angelopoulos V, McFadden JP (2012) ARTEMIS observations of lunar pick-up ions in the terrestrial magnetotail lobes. Geophys Res Lett 39:L17104

Poppe AR, Fatemi S, Halekas JS, Holmström M, Delory GT (2014) ARTEMIS observations of extreme diamagnetic fields in the lunar wake. Geophys Res Lett 41:3766–3773

Poppe AR, Fillingim MO, Halekas JS, Raeder J, Angelopoulos V (2016) ARTEMIS observations of terrestrial ionospheric molecular ion outflow at the Moon. Geophys Res Lett 43:6749–6758

Poppe AR, Halekas JS, Lue C, Fatemi S (2017a) ARTEMIS observations of the solar wind proton scattering function from lunar crustal magnetic anomalies. J Geophys Res 122:771–783

Poppe AR, Farrell W, Halekas JS (2017b) Formation timescales of amorphous rims on lunar grains derived from ARTEMIS observations. J Geophys Res 122:37–46

Prettyman TH, Feldman WC, Lawrence DJ, McKinney GW, Binder AB, Elphic RC, Gasnault OM, Maurice S, Moore KR (2002) Library least squares analysis of Lunar Prospector gamma-ray spectra. 33rd Lunar Planet Sci Conf, abstract # 2012

Prettyman TH, Hagerty JJ, Elphic RC, Feldman WC, Lawrence DJ, McKinney GW, Vaniman DT (2006) Elemental composition of the lunar surface: Analysis of gamma ray spectroscopy data from Lunar Prospector. J Geophys Res Planets 111:E12007

Putrevu D, Trivedi S, Das A, Pandey D, Mehrotra P, Garg SK, Reddy V, Gangele S, Patel H, Sharma D, Sijwali R (2020) L-and S-band polarimetric synthetic aperture radar on Chandrayaan-2 mission. Curr Sci 118:226–233

Qi H, Li Y, Bazotis J, Qian Y, Xiao L, Wang Z, Zhang W, Luo B, Neal CR, Day JMD, Pan F, She Z, Wu X, Hu Z, Zong K, Wang L (2022) Detailed petrogenesis of the unsampled Oceanus Procellarum: The case of the Chang'e-5 mare basalts. Icarus 383:115082

Qian Y, Xiao L, Wang Q, Head JW, Yang R, Kang Y, van der Bogert CH, Hiesinger H, Lai X, Wang G, Pang Y, Zhang N, Yuan Y, He Q, Huang J, Zhao J, Wang J, Zhao S (2021a) China's Chang'e-5 landing site: Geology, stratigraphy, and provenance of materials. Earth Planet Sci Lett 561:116855

Qian Y, Xiao L, Head JW, van der Bogert CH, Hiesinger H, Wilson L (2021b) Young lunar mare basalts in the Chang'e-5 sample return region, northern Oceanus Procellarum. Earth Planet Sci Lett 555:116702

Qin S, Huang Y, Li P, Shan Q, Fan M, Hu X, Wang G (2019) Orbit and tracking data evaluation of Chang'E-4 relay satellite. Adv Space Res 64:836–846

Radhakrishna V, Tyagi A, Narendranath S, Vadodariya K, Yadav R, Singh B, Balaji G, Satya N, Shetty A, Kumar HS, Kumar S (2020) Chandrayaan-2 large area soft x-ray spectrometer. Curr Sci 118:219–225

Rajmon D, Spudis P (2004) Distribution and stratigraphy of basaltic units in Maria Tranquillitatis and Fecunditatis: A Clementine perspective. Meteor Planet Sci 39:1699–1720

Ren X, Li C, Liu J, Wang F, Yang J, Liu E, Xue B, Zhao R (2014) A method and results of color calibration for the Chang'E-3 terrain camera and panoramic camera. Res Astron Astrophys 14:1557–1566

Robinson MS, Jolliff B (2002) Apollo 17 landing site: Topography, photometric corrections and heterogeneity of the surrounding highland massifs. J Geophys Res 107(E11):5110

Robinson MS, Brylow SM, Tschimmel M, Humm D, Lawrence SJ, Thomas PC, Denevi BW, Bowman-Cisneros E, Zerr J, Ravine MA, Caplinger MA, Ghaemi FT, Schaffner JA, Malin MC, Mahanti P, Bartels A, Anderson J, Tran TN, Eliason EM, McEwen AS, Turtle E, Jolliff BL, Hiesinger H (2010) Lunar Reconnaissance Orbiter Camera (LROC) instrument overview. Space Sci Rev 150:81–124

Robinson MS, Ashley JW, Boyd AK, Wagner RV, Speyerer EJ, Hawke BR, Hiesinger H, van der Bogert CH (2012) Confirmation of sublunarean voids and thin layering in mare deposits. Planet Space Sci 69:18–27

Robinson MS, Boyd AK, Denevi BW, Lawrence SJ, McEwen AS, Moser DE, Povilaitis RZ, Stelling RW, Suggs RM, Thompson SD, Wagner RV (2015) New crater on the Moon and a swarm of secondaries. Icarus 252:229–235

Robinson MS, Mahanti P, Carter LM, Denevi DW, Estes NM, Ravine MA, Speyerer EJ, Wagner RV (2017) ShadowCam—seeing in the dark. EPSC Abstracts 11:EPSC2017-506

Robinson MS, Mahanti P, Brylow SM, Bussey DBJ, Carte LM, Denevi BW, Estes NM, Humm DC, Mazarico E, Ravine MA, Schaffner JA, Speyerer EJ, Wagner RV (2022) ShadowCam: Seeing in the Moon's shadows. Lunar Planet Sci Conf 53:1659

Roux A, Le Contel O, Coillot C, Bouabdellah A, de la Porte B, Alison D, Ruocco S, Vassal MC (2008) The search coil magnetometer for THEMIS. Space Sci Rev 141:265–275

Russell CT (1992) The Galileo Mission. Space Sci Rev 60:1–4

Russell CT, Rowe K, Joy S, Aharonson O, Amrusi S, Grosz A, Wieczorek M, Weiss B, Head JW, Garrick-Bethell I (2019) SILMAG: A fluxgate magnetometer on board the SpaceIL lunar lander, 50th Lunar Planet Sci Conf, abstract # 1728

Saal AE, Hauri EH, Lo Cascio M, Van Orman JA, Rutherford MC, Cooper RF (2008) Volatile content of lunar volcanic glasses and the presence of water in the Moon's interior. Nature 454:192–196

Sanin AB, Mitrofanov IG, Litvak ML, Bakhtin BN, Bodnarik JG, Boynton WV, Chin G, Evans LG, Harshman K, Fedosov F, Golovin DV, Kozyrev AS, Livengood TA, Malakhov AV, McClanahan TP, Mokrousov MI, Starr RD, Sagdeev RZ, Tret'yakov VI, Vostrukhin AA (2017) Hydrogen distribution in the lunar polar regions. Icarus 283:20–30

Sato H, Robinson MS, Hapke B, Denevi BW, Boyd AK (2014) Resolved Hapke parameter maps of the Moon. J Geophys Res Planets 119:1775–1805

Sato H, Robinson MS, Lawrence SL, Denevi BW, Hapke B, Jolliff BL, Hiesinger H (2017) Lunar mare TiO_2 abundances estimated from UV/Vis reflectance. Icarus 296:216–238

Schmitt HH, Petro NE, Wells RA, Robinson MS, Weiss BP, Mercer CM (2017) Revisiting the field geology of Taurus-Littrow. Icarus 298:2–33

Schwadron NA, Baker T, Blake B, Case AW, Cooper JF , Golightly M, Jordan A, Joyce C, Kasper J, Kozarev K, Mislinski J, Mazur J, Posner A, Rother O, Smith S, Spence HE, Townsend LW, Wilson J, Zeitlin C (2012) Lunar radiation environment and space weathering from the Cosmic Ray Telescope for the Effects of Radiation (CRaTER). J Geophys Res Planets 117:E00H13

Schwadron NA, Smith S, Spence HE (2013) The CRaTER special issue of Space Weather: Building the observational foundation to deduce biological effects of space radiation. Space Weather 11:47–48

Sefton-Nash E, Fisackerly R, Trautner R, Martin DJP, Carpenter JD, Houdou B (2019) Targeting lunar volatiles with ESA's Prospect payload on Luna 27. Tenth Moscow Solar Syst Symp 129–131

Shearer C, Neal CR, Glotch TD, Prissel TC, Bell AS, Assis Fernandes V, Gaddis LR, Jolliff BL, Laneuville M, Magna T, Simon J (2023) Magmatic evolution II: A new view of post-differentiation magmatism. Rev Mineral Geochem 89:147–205

Shin J, Jin H, Lee H, Lee S, Lee S, Lee M, Jeong B, Lee J-K, Son D, Kim K-H, Garrick-Bethell I, Kim E (2019) KMAG: The magnetometer of the Korean Pathfinder Lunar Orbiter (KPLO) mission. Lunar Planet Sci Conf 50:2276

Sibeck DG, Angelopoulos V, Delory G, Eastwood J, Farrell W, Grimm R, Halekas J, Hasegawa H, Hellinger P, Khurana K, Lillis R, Øieroset M, Phan T, Raeder J, Russell C, Schriver D, Slavin J, Travnicek P, Weygand J (2011) ARTEMIS science objectives and mission phases. Space Sci Rev 165:59–91

Sinha RK, Sivaprahasam V, Bhatt M, Kumari N, Srivastava N, Varatharajan I, Ray D, Wöhler C, Bhardwaj A (2020) Geological characterization of Chandrayaan-2 landing site in the southern high latitudes of the Moon. Icarus 1:113449

Sivakumar V, Kumar B, Srivastava SK, Gopala Krishna B, Srivastava PK, Kumar ASK (2012) DEM Generation for Lunar Surface using Chandrayaan-1 TMC Triplet Data. J Ind Soc Rem Sens 40:551–564

Smith DE, Zuber MT, Neumann G, Lemoine FG (1997) Topography of the Moon from the Clementine LIDAR. J Geophys Res 102:1591–1611

Smith DE, Zuber MT, Jackson GB, Cavanaugh JF, Neumann GA, Riris H, Sun X, Zellar RS, Coltharp C, Connelly J, Katz RB, Kleyner I, Liiva P, Matuszeski A, Mazarico EM, McGarry JF, Novo-Gradac A-M, Ott MN, Peters C, Ramos-Izquierdo LA, Ramsey L, Rowlands DD, Schmidt S, Scott VS III, Shaw GB, Smith JC, Swinski J-P, Torrence MH, Unger G, Yu AW, Zagwodzki TW (2010a) The Lunar Orbiter Laser Altimeter investigation on the Lunar Reconnaissance Orbiter mission. Space Sci Rev 150:209–241

Smith DE, Zuber MT, Neumann GA, Lemoine FG, Mazarico E, Torrence MH, McGarry JF, Rowlands DD, Head JW, Duxbury TH, Aharonson O, Lucey PG, Robinson M, Barnouin OS, Cavanaugh JF, Sun X, Liiva P, Mao DD, Smith JC, Bartels AE (2010b) Initial observations from the Lunar Orbiter Laser Altimeter (LOLA). Geophys Res Lett 37:L18204

Song Y-J, Kim Y-R, Bae J, Park J-I, Hong S, Lee D, Kim D-K (2021) Overview of the flight dynamics subsystem for Korea Pathfinder lunar orbiter mission. Aerospace 8:222

Sorensen TC, Spudis PD (2005) The Clementine mission—A 10-year perspective. J Earth Syst Sci 114:645–668

Spence HE, Case AW, Golightly MJ, Heine T, Larsen BA; Blake JB, Caranza P, Crain WR, George J, Lalic M, Lin A, Looper MD, Mazur JE, Salvaggio D, Kasper J. C, Stubbs TJ, Doucette M, Ford P, Foster R, Goeke R, Gordon D, Klatt B, O'Connor J, Smith M, Onsager T, Zeitlin C, Townsend LW, Charara Y (2010) CRaTER: The Cosmic Ray Telescope for the Effects of Radiation experiment on the Lunar Reconnaissance Orbiter mission. Space Sci Rev 150:243–284

Speyerer EJ, Robinson MS (2013) Persistently illuminated regions at the lunar poles: Ideal sites for future exploration. Icarus 222:122–136

Speyerer EJ, Povilaitis RZ, Robinson MS, Thomas PC, Wagner RV (2016) Quantifying crater production and regolith overturn on the Moon with temporal imaging. Nature 538:215–218
Spudis PD (2001) The case for renewed human exploration of the Moon. Earth Moon Planets 87:159–171
Spudis PD, Reisse RA, Gillis JJ (1994) Ancient multiring basins on the Moon revealed by Clementine laser altimetry. Science 266:1848–1851
Spudis PD, Nozette S, Bussey B, Raney K, Winters H, Lichtenberg CL, Marinelli WM, Crusan JC, Gates MM (2009) Mini-SAR: An imaging radar experiment for the Chandrayaan-1 mission to the Moon. Curr Sci 96:533–539
Spudis PD, Bussey DBJ, Butler B, Carter L, Chakraborty M, Gillis-Davis J, Goswami J, Heggy E, Kirk R, Neish C, Nozette S, Patterson W, Robinson M, Raney RK, Thompson T, Thomson BJ, Ustinov E (2010a) Results of the Mini-SAR Imaging Radar, Chandrayaan-1 Mission to the Moon. 41st Lunar Planet Sci Conf #1224
Spudis PD, Bussey DBJ, Baloga SM, Butler BJ, Carl D, Carter LM, Chakraborty M, Elphic RC, Gillis-Davis JJ, Goswami JN, Heggy E, Hillyard M, Jensen R, Kirk RL, LaVallee D, McKerracher P, Neish CD, Nozette S, Nylund S, Palsetia M, Patterson W, Robinson MS, Raney RK, Schulze RC, Sequeira H, Skura J, Thompson T, Thomson BJ, Ustinov EA, Winters HL (2010b) Initial results for the north pole of the Moon from Mini-SAR, Chandrayaan-1 mission. Geophys Res Lett 37:L06204
Sridharan R, Ahmed SM, Das TP, Sreelatha P, Pradeepkumar P, Naik N, Gogulapati S (2010a) The sunlit lunar atmosphere: a comprehensive study by CHACE on the Moon impact probe of Chandrayaan-1. Planet Space Sci 58:1567–1577
Sridharan R, Ahmed SM, Das TP, Sreelatha P, Pradeepkumar P, Naik N, Gogulapati S (2010b) 'Direct' evidence of water (H_2O) in the sunlit lunar ambience from CHACE on MIP of Chandrayaan I. Planet Space Sci 58:947–950
Sridharan R, Das TP, Ahmed SM, Supriya G, Bhardwaj A, Kamalakar JA (2013) Spatial heterogeneity in the radiogenic activity of the lunar interior: inferences from CHACE and LLRI on Chandrayaan-1. Adv Space Res 51:168–178
Sridharan R, Ahmed SM, Das TP, Sreelatha P, Kumar PP, Naik N, Supriya G (2015) Corrigendum to "The Sunlit lunar atmosphere: A Comprehensive study by CHACE on the Moon Impact Probe of Chandrayaan-1" [Planet. Space Sci. 58 (2010) 1567–1577]. Planet Space Sci 111:167–168
Stone TC (2008) Radiometric calibration stability and inter-calibration of solar-band instruments in orbit using the Moon. Proc SPIE 7081(Earth Observing Systems XIII) 70810X:1–8
Stooke P, Foing B (2017) Crash scene investigation reveals resting place of SMART-1 impact, Press Release, European Planetary Science Congress, Sept 22, 2017, http://www.europlanet-eu.org/crash-scene-investigation-reveals-resting-place-of-smart-1-impact/, see also http://www.planetary.org/blogs/guest-blogs/2017/0207-finding-spacecraft-impacts-on-the-moon.html
Su Y, Fang G, Feng J, Xing S, Ji Y, Zhou B, Gao Y, Li H, Dai S, Xiao Y, Li C (2014) Data processing and initial results of Chang'E-3 lunar penetrating radar. Res Astron Astrophys 14:1623–1632
Sun L, Ling Z, Zhang J, Li B, Chen J, Wu Z, Liu J (2016) Lunar iron and optical maturity mapping: Results from partial least squares modeling of Chang'E-1 IIM data. Icarus 280:183–198
Sunshine JM, Farnham TL, Feaga LM, Groussin O, Merlin F, Milliken RE, A'Hearn MF (2009) Temporal and spatial variability of lunar hydration as observed by the Deep Impact spacecraft. Science 326:565–568
Sweetser TH, Broschart SB, Angelopoulos V, Whiffen GJ, Folta DC, Chung M-K, Hatch SJ, Woodard MA (2011) ARTEMIS mission design. Space Sci Rev 165:27–57
Swinyard BM, Joy KH, Kellett BJ, Crawford IA, Grande M, Howe CJ, Fernandes VA, Gasnault O, Lawrence DJ, Russell SS, Wieczorek MA, Foing BH, the SMART-1 Team (2009) X-ray fluorescence observations of the moon by SMART-1/D-CIXS and the first detection of Ti Kα from the lunar surface. Planet Space Sci 57:744–750
Tan X, Liu J, Li C, Feng J, Ren X, Wang F, Yan W, Zuo W, Wang X, Zhang Z (2014) Scientific data products and the data pre-processing subsystem of the Chang'E-3 mission. Res Astron Astrophys 14:1682–1694
Tao J, Ergun RE, Newman D, Halekas J, Andersson L, Angelopoulos V, Bonnell JW, McFadden JP, Cully C, Auster H-U, Glassmeier K-H, Larson D, Baumjohann W, Golman MV (2012) Kinetic Instabilities in the Lunar Wake: ARTEMIS Observations. J Geophys Res 117:A03106
Tartèse R, Anand M, Barnes JJ, Starkey NA, Franchi IA, Sano Y (2013) The abundance, distribution, and isotopic composition of hydrogen in the Moon as revealed by basaltic lunar samples: Implications for the volatile inventory of the Moon. Geochim Cosmochim Acta 122:58–74
Taylor SR (1975) Lunar Science: A Post-Apollo View, Pergamon Press, New York
Taylor GJ, Wieczorek MA (2014) Lunar bulk chemical composition: a post-Gravity Recovery and Interior Laboratory reassessment. Philos Trans R Soc A 372:20130242
Tian HC, Wang H, Chen Y, Yang W, Zhou Q, Zhang C, Lin HL, Huang C, Wu ST, Jia LH, Xu L (2021) Non-KREEP origin for Chang'e-5 basalts in the Procellarum KREEP Terrane. Nature 600:59–63
Tsunakawa H, F Takahashi, H Shimizu, H Shibuya, M Matsushima (2015) Surface vector mapping of magnetic anomalies over the Moon using Kaguya and Lunar Prospector observations. J Geophys Res Planets 120:1160–1185
Uemoto K, Ohtake M, Haruyama J, Matsunaga T, Yamamoto S, Nakamura R, Yokota Y, Ishihara Y, Iwata T (2017) Evidence of impact meltsheet differentiation of the lunar SouthPole-Aitken basin. J Geophys Res Planets 122:1672–1686
Uesugi K (1993) Space odyssey of an angel: summary of the Hiten's three year mission. Adv Astronaut Sci 84:607–621
Vadawale SV, Shanmugam M, Acharya YB, Patel AR, Goyal SK, Shah B, Hait AK, Patinge A, Subrahmanyam D (2014) Solar X-ray Monitor (XSM) on-board Chandrayaan-2 orbiter. Adv Space Res 54:2021–2028

Vaniman D, Dietrich J, Taylor GJ, Heiken G (1991) Exploration, samples, and recent concepts of the Moon. *In:* Lunar Sourcebook: A User's Guide to the Moon. Heiken GH, Vaniman D, French BM (eds) Cambridge University Press

Vanitha M, Veeramuthuvel P, Kalpana K, Nagesh G (2020) Chandrayaan-2: The second Indian mission to the Moon. 51st Lunar Planet Sci Conf #1994

Vondrak R, Keller J, Chin G, Garvin J (2010) Lunar Reconnaissance Orbiter (LRO): Observations for lunar exploration and science. Space Sci Rev 150:7–22

Wagner RV, Robinson MS (2014) Distribution, formation mechanisms, and significance of lunar pits. Icarus 237:52–60

Wagner RV, Nelson DM, Plescia JB, Robinson MS, Speyerer EJ, Mazarico E (2017) Coordinates of anthropogenic features on the Moon. Icarus 283:92–103

Wang XM, Niu RQ (2012) Lunar titanium abundance characterization using Chang'E-1 IIM data. Sci China Phys Mech Astron 55:170–178

Wang X, Zhu P (2013) Refinement of lunar TiO_2, analysis with multispectral features of Chang'E-1 IIM data. Astrophys Space Sci 343:33–44

Wang FF, Liu JJ, Li CL, Ren X, Mu LL, Yan W, Wang WR, Xiao JT, Tan X, Zhang XX, Zou XD, Gao XY (2014) A new lunar absolute control point: established by images from the landing camera on Chang'E-3. Res Astron Astrophys 14:1543–1556

Wang J, Wu C, Qiu YL, Meng XM, Cai HB, Cao L, Deng JS, Han XH, Wei JY (2015) An unprecedented constraint on water content in the sunlit lunar exosphere seen by Lunar-based ultraviolet telescope of Chang'E-3 mission. J Planet Space Sci 109:123–128

Wang X, Zhang X, Wu K (2016) Thorium distribution on the lunar surface observed by Chang'E-2 gamma-ray spectrometer. Astrophys Space Sci 361:1–11

Wang J, Di K, Chen M, Duan J, Kong J, Xie J, Liu Z, Wan W, Rong Z, Liu B, Peng M, Wang Y (2021) Localization of the Chang'e-5 lander using radio-tracking and image-based methods. Remote Sens 13:590

Watters TR, Robinson MS, Beyer RA, Banks ME, Bell JF III, Pritchard ME, Hiesinger H, van der Bogert C, Thomas PC, Turtle EP, Williams NR (2010) Evidence of recent thrust faulting on the Moon revealed by the Lunar Reconnaissance Orbiter Camera. Science 329:936–940

Watters TR, Robinson MS, Banks ME, Tran T, Denevi BW (2012) Recent extensional tectonics on the Moon revealed by the Lunar Reconnaissance Orbiter Camera. Nat Geosci 5:181–185

Weber RC, Lin P-Y, Garnero EJ, Williams Q, Lognonné P (2011) Seismic detection of the lunar core. Science 331:309–312

Weider SZ, Kellett BJ, Swinyard BM, Crawford IA, Joy KH, Grande M, Howe CJ, Sreekumar P, Huovelin J, Narendranath S, Alha L, Anand M, Athiray PS, Ahandari N, Carter J, Cook AC, d'Uston LC, Fernandes VA, Gasnault O, Goswami JN, Gow JPD, Holland AD, Koschny D, Lawrence DJ, Maddison BJ, Maurice S, McKay DJ, Okada T, Pieters C. Rothery D, Russell SS, Shrivastava A, Smith DR, Wieczorek M (2012) The Chandrayaan-1 X-ray Spectrometer: first results. Planet Space Sci 60:217–228

Weider SZ, Crawford IA, Joy KH, Kellett BJ, Swinyard BM, Howe CJ (2014) Western Oceanus Procellarum as seen by C1XS on Chandrayaan-1. Icarus 229:254–262

Weiss BP, Tikoo SM (2014) The lunar dynamo. Science 346:1198–1208

Wen WB, Wang F, Li CL, Wang J, Cao L, Liu JJ, Tan X, Xiao Y, Fu Q, Su Y, Zuo W (2014) Data processing and initial results from the CE-3 extreme ultraviolet camera. Res Astron Astrophys 14:1674–1681

Wieczorek MA, Phillips RJ (2000) The 'Procellarum KREEP Terrane': implications for mare volcanism and lunar evolution. J Geophys Res 105(E8):20,417–20,430

Wieczorek MA, Neumann GA, Nimmo F, Kiefer WS, Taylor GJ, Melosh HJ, Phillips RJ, Solomon SC. Andrews-Hanna JC, Asmar SW, Konopliv AS (2013) The crust of the Moon as seen by GRAIL. Science 339:671–675

Wieczorek MA, Weiss BP, Breuer D, Cébron D, Fuller M, Garrick-Bethell I, Gattacceca J, Halekas JS, Hemingway DJ, Hood LL, Laneuville M, Nimmo F, Oran R, Purucker ME, Rückriemen T, Soderlund KM, Tikoo1 SM (2023) Lunar magnetism. Rev Mineral Geochem 89:207–241

Williams JG, Boggs DH (2015) Tides on the Moon: Theory and determination of dissipation. J Geophys Res Planets 120:689–724

Williams JG, Konopliv A, Boggs DH, Park RS, Yuan D-H, Lemoine FG, Goossens S, Mazarico E, Nimmo F, Weber RC, Asmar SW, Melosh HJ, Neumann GA, Phillips RJ, Smith DE, Solomon SC, Watkins MM, Wieczorek MA, Andrews-Hanna JC, Head JW III, Kiefer WS, Matsuyama I, McGovern RJ, Taylor GJ, Zuber MT (2014) Lunar interior properties from the GRAIL mission. J Geophys Res Planets 119:1546–1578

Williams J-P, Paige DA, Greenhagen BT, Sefton-Nash E (2017) The global surface temperatures of the Moon as measured by the Diviner Lunar Radiometer Experiment. Icarus 283:300–325

Wilson JT, Eke VR, Massey RJ, Elphic RC, Jolliff BL, Lawrence DJ, Llewellin EW, McElwaine JN, Teodoro LFA (2015) Evidence for explosive silicic volcanism on the Moon from the extended distribution of thorium near the Compton–Belkovich volcanic complex. J Geophys Res Planets 120:92–108

Wooden DH, Cook AM, Colaprete A, Glenar DA, Stubbs TJ, Shirley M (2016) Evidence for a dynamic nanodust cloud enveloping the Moon. Nature Geosci 9:665–668

Wörner J, Foing B (2016) The Moon Village concept and initiative, Annual Meeting of the Lunar Exploration Analysis Group, abstract # 5084

Wu Y (2012) Major elements and Mg# of the Moon: Results from Chang'E-1 Interference Imaging Spectrometer (IIM) data. Geochim Cosmochim Acta 93:214–234

Wu Y, Xue B, Zhao B, Lucey P, Chen J, Xu X, Li C, Ouyang Z (2012) Global estimates of lunar iron and titanium contents from the Chang' E-1 IIM data. J Geophys Res Planets 117:E02001
Wu B, Hu H, Guo J (2014) Integration of Chang'E-2 imagery and LRO laser altimeter data with a combined block adjustment for precision lunar topographic modeling. Earth Planet Sci Lett 391:1–15
Xiao L (2014) China's touch on the Moon. Nat Geosci 7:391–392
Xiao L, Zhu P, Fang G, Xiao Z, Zou Y, Zhao J, Zhao N, Yuan Y, Qiao L, Zhang X, Zhang H, Wang J, Huang J, Huang Q, He Q, Zhou B, Ji Y, Zhang Q, Shen S, Li Y, Gao Y (2015) A young multilayered terrane of the northern Mare Imbrium revealed by Chang'E-3 mission. Science 347:1226–1229
Xiao Y, Su Y, Dai S, Fen J, Xing S, Din C, Li C (2019) Ground experiments of Chang'e-5 lunar regolith penetrating radar. Adv Space Res 63:3404–3419
Xu X, Angelopoulos V, Wang Y, Zuo P, Wong H-C, Cui J (2017) The energetic particle environment of the lunar nearside: SEP influence. Astrophys J 849:151
Xu L, Zou Y, Wu J (2018) Preliminary imagines for the planning and its scientific objectives of China's lunar research station. 49th Lunar Planet Sci Conf, abstract # 1856
Yamamoto S, Nakamura R, Matsunaga T, Ogawa Y, Ishihara Y, Morota T, Hirata N, Ohtake M, Hiroi T, Yokota Y, Haruyama J (2010) Possible mantle origin of olivine around lunar impact basins detected by SELENE. Nat Geosci 3:533–536
Yamamoto S, Nakamura R, Matsunaga T, Ogawa Y, Ishihara Y, Morota T, Hirata N, Ohtake M, Hiroi T, Yokota Y, Haruyama J (2012) Olivine-rich exposures in the South Pole-Aitken basin. Icarus 218:331–344
Yamashita N, Gasnault O, Forni O, d'Uston C, Reedy RC, Karouji Y, Kobayashi S, Hareyama M, Nagaoka H, Hasebe N, Kim KJ (2012) The global distribution of calcium on the Moon: implications for high-Ca pyroxene in the eastern mare region. Earth Planet Sci Lett 353–354:93–98
Yan B, Xiong SQ, Wu Y, Wang Z, Dong L, Gan F, Yang S, Wang R (2012) Mapping lunar global chemical composition from Chang'E-1 IIM data. Planet Space Sci 67:119–129
Ye PJ, Huang JC, Zhang TX (2013) Technical achievements of Chang'E-2 satellite and prospects for deep space exploration in China. Scientia Sinica Tech 43:467–477
Zhang H, Khurana KK, Zong Q-G, Wan WX, Pu ZY, Kivelson MG, Angelopoulos V, Cao X, Wang YF, Shi QQ, Liu WL, Tian AM, Tang CL (2012) Outward expansion of the lunar wake: ARTEMIS observations. Geophys Res Lett 39:L18104
Zhang J, Yang W, Hu S, Lin Y, Fang G, Li C, Peng W, Zhu S, He Z, Zhou B, Lin H, Yang J, Liy E, Xu Y, Wang J, Yao Z, Zou Y, Yan J, Ouyang Z (2015a) Volcanic history of the Imbrium basin: A close-up view from the lunar rover Yutu. Proc Nat Acad Sciences 112:5342–5347
Zhang H, Yang Y, Yuan Y, Jin W, Lucey PG, Zhu MH, Kaydash VG, Shkuratov YG, Di K, Wan W, Xu B (2015b) In situ optical measurements of Chang'E-3 landing site in Mare Imbrium: 1. Mineral abundances inferred from spectral reflectance. Geophys Res Lett 42:6945–6950
Zhang ZB, Zuo W, Zeng XG, Gao XY, Xin R (2019) The scientific data and its archiving from Chang'E 4 mission. 4th Planet Data Workshop, abstract # 7032
Zhao W, Wang C (2019) China's lunar and deep space exploration: touching the Moon and exploring the universe. Nat Sci Rev 6:1274–1278
Zhao B, Li C, Huang J (2012) Analysis on in-orbit CCD stereo camera images of Chang'E-2 lunar satellite. Spacecraft Engin 21:1–7
Zheng Y, Ouyang ZY, Li C, Liu J, Zou Y (2008a) China's lunar exploration program: present and future. Planet Space Sci 56:881–886
Zheng Y, Ouyang Z, Blewett DT (2008b) Implanted helium-3 abundance distribution on the Moon. Lunar Planet Sci Conf 39:1049
Zheng YC, Tsang KT, Chan KL, Zou YL, Zhang F, Ouyang ZY (2012) First microwave map of the Moon with Chang'E-1 data: The role of local time in global imaging. Icarus 219:194–210
Zhou X-Z, Angelopoulos V, Poppe AR, Halekas JS (2013) ARTEMIS observations of lunar pickup ions: Mass constraints on ion species. J Geophys Res Planets 118:1766–1774
Zhou C, Jia Y, Liu J, Li H, Fan Y, Zhang Z, Liu Y, Jiang Y, Zhou B, He Z, Yang J, Hu Y, Liu Z, Qin L, Lv B, Fu Z, Yan J, Wang C, Zou Y (2022) Scientific objectives and payloads of the lunar sample return mission—Chang'E-5. Adv Space Res 69:823–836
Zhu MH, Chang J, Ma T, Ip W-H, Fa WZ, Wu J, Cai MS, Gong YZ, Hu Y, Xu AA, Tang Z (2013) Potassium map from Chang'E-2 constraints the impact of Crisium and Orientale basin on the Moon. Sci Rep 3:1611
Zhu MH, Fa W, Ip WH, Huang J, Liu T, Meng L, Qiao D (2014a) Morphology of asteroid (4179) Toutatis as imaged by Chang'E-2 spacecraft. Geophys Res Lett 41:328–333
Zhu MH, Chang J, Fa WZ, Ip WH, Ma T, Xie MG, Xu AA, Tang ZS (2014b) Thorium on the lunar highlands surface: Insights from Chang'E-2 Gamma-Ray Spectrometer. 45th Lunar Planet Sci Conf, abstract # 1237
Zhu MH, Chang J, Xie M, Fritz J, Fernandes VA, Ip W-H, Ma T, Xu A (2015) The uniform K distribution of the mare deposits in the Orientale Basin: Insights from Chang'E-2 gamma-ray spectrometer. Earth Planet Sci Lett 418:172–180

Zou Y, Liyan Z, Jianzhong L, Lingli M, Xin R, Guangliang Z, Jin C, Jun Y, Nan Z, Hongbo Z, Chang L (2011) Data analysis of Chang'E-1 gamma-ray spectrometer and global distribution of U, K, and Th elemental abundances. J Geol 85:1299–1309

Zou X, Li C, Liu J, Wang W, Li H, Ping J (2014) The preliminary analysis of the 4179 Toutatis snapshots of the Chang'E-2 flyby. Icarus 229:348–354

Zuo W, Li C, Zhoubin Z (2014) Scientific data and their release of Chang'E-1 and Chang'E-2. Chin J Geochem 33:24–44

Zuo W, Li CL, Zhang ZB, Zeng XG, Zou YL, Zhang GL (2016) Scientific data and its release of Chang'E-3 mission. 47th Lunar Planet Sci Conf, abstract #1353

Zuber MT, Smith DE, Zellar S, Neumann GA, Sun X, Katz R, Kleyner I, Matuszeski A, McGarry JF, Ott MN, Ramos-Izquierdo LA (2010) The Lunar Reconnaissance Orbiter laser ranging investigation. Space Sci Rev 150:63–80

Zuber MT, Head JW, Smith DE, Neumann GA, Mazarico E, Torrence MH, Aharonson O, Tye AR, Fassett CI, Rosenburg MA, Melosh HJ (2012) Constraints on the volatile distribution within Shackleton crater at the lunar south pole. Nature 486:378–381

Zuber MT, Smith DE, Lehman DH, Hoffman TL, Asmar SW, Watkins MM (2013a) Gravity Recovery and Interior Laboratory (GRAIL): Mapping the lunar interior from crust to core. Space Sci Rev 178:3–24

Zuber MT, Smith DE, Watkins MM, Asmar SW, Konopliv AS, Lemoine FG, Melosh HJ, Neumann GA, Phillips RJ, Solomon SC, Wieczorek MA, Williams JG, Goossens SJ, Kruisinga G, Mazarico E, Park RS, Yuan DN (2013b) Gravity field of the Moon from the Gravity Recovery and Interior Laboratory (GRAIL) mission. Science 339:668–671

APPENDIX—RECENT DEVELOPMENTS

- ISRO, the Indian Space Research Organization, indicated a launch in 2023 for Chandrayaan-3.
- NASA is moving forward with planned launches for Artemis 1, 2 and 3, with the uncrewed Artemis 1 mission launching toward the end of 2022. This mission carried 3 CubeSats for lunar exploration—LunaH-Map, Lunar Ice Cube, LunIR. A fourth lunar CubeSat, Lunar Flashlight, launched in 2022 on the Hakuto-R mission. Artemis 2 and 3, the first crewed and first landed human missions in the series, respectively, are planned for later in the decade.
- In April 2022 the European Space Agency (ESA) announced via press release that it will no longer be collaborating with Russia on the Luna 27 and 28 mission. The PROSPECT payload will instead be deployed on a forthcoming NASA CLPS mission.
- CNSA, the Chinese National Space Administration, has announced plans for launch dates in 2025 for Chang'E-6 and 2026 for Chang'E 7.

ELECTRONIC ANNEX

Figures and tables referred to by the prefix "EA" are in an electronic annex available at https://apenninus.u-aizu.ac.jp/NVM2-EA.html